Self-Assembly of Poly(*N*-isopropylacrylamide) Microgel Thin Films

A Thesis
Presented to
The Academic Faculty

by

Michael J. Serpe

In Partial Fulfillment
of the Requirements for the Degree
Doctor of Philosophy in the
School of Chemistry and Biochemistry

Georgia Institute of Technology
August 2004

Self-Assembly of Poly(*N*-isopropylacrylamide) Microgel Thin Films

Approved by:

Dr. L. Andrew Lyon, Advisor

Dr. Jiri Janata

Dr. Peter J. Ludovice

Dr. Boris Mizaikoff

Dr. Thomas Orlando

August 24, 2004

ACKNOWLEDGEMENTS

There are numerous people that have to be thanked for helping me through this stage of my life, most of which cannot be mentioned in this short space. I would like to thank my advisor Dr. L. Andrew Lyon for giving me the opportunity to work in his lab. He always offered great conversations about science and was always available (with an open door) for discussions about my research and future life plans. Throughout the four years in his lab, Andrew always gave me the freedom to pursue the research I was interested in and exhibited patience, knowledge, and a great enthusiasm for Chemistry and science in general. His excitement about science and chemistry has been transferred to me and for that I thank him. I would like to thank the Lyon group especially Jongseong Kim, Satish Nayak, and Clint Jones. The friendships we have made from this experience are very valuable to me and I look forward to our continued friendship on the personal and professional level. I would like to thank all of my family members who supported me throughout the years especially my brother and sister, Carl and Suzanne, and my mother and father, Michele and Carl. Last, but certainly not least, I would like to thank my wife, Shannon, for everything she has sacrificed for me to make it this far in my career. I promise to spend the rest of my life supporting you in every venture you wish to pursue. For the past 10 years of friendship/marriage she has shown me extreme patience as well as offered unconditional love and support when I needed it most. She always offered me great advice and encouragement and still encourages me to pursue all of my interests. I thank God everyday for giving me such a special person, she is one of a kind.

TABLE OF CONTENTS

LIST OF TABLES

LIST OF FIGURES

LIST OF SCHEMES

LIST OF ABBREVIATIONS

NIPAm	*N*-isopropylacrylamide
BIS	*N,N'*-Methylene(bisacrylamide)
AAc	Acrylic Acid
pNIPAm	Poly(*N*-isopropylacrylamide)
VPT	Volume Phase Transition
LCST	Lower Critical Solution Temperature
pNIPAm-co-AAc	Poly(*N*-isopropylacrylamide-*co*-acrylic acid)
VPTT	Volume Phase Transition Temperature
RBF	Round Bottom Flask
SDS	Sodium Dodecyl Sulfate
APS	Ammonium Persulfate
RI	Refractive Index
LbL	Layer-by-Layer
PAA	Poly(acrylic acid)
PAH	Poly(allylamine hydrochloride)
PSS	Poly(sodium 4-styrenesulfonate)
MW	Molecular Weight
PCS	Photon Correlation Spectroscopy
APTMS	3-Aminopropyltrimethoxysilane
AFA	4-Aminofluorescein
QCI	Quartz Crystal Impedance

SPR	Surface Plasmon Resonance Spectroscopy
scLbL	Spin Coating Layer-by-Layer
MEA	2-Mercaptoethylamine
MPTMS	3-Mercaptopropyltrimethoxysilane
cryo-SEM	Cryo-Scanning Electron Microscopy
FITC	Fluorescein-5-Isothiocyanate
DX	Doxorubicin
QCM	Quartz Crystal Microgravimetry
DIC	Differential Image Contrast
SEM	Scanning Electron Microscope
TEM	Transmission Electron Microscopy
AOPTMS	3-Acryloxypropyltrimethoxysilane
PI	2,2'-Diethoxyacetophenone
EtOH	Ethanol

SUMMARY

This dissertation describes the assembly of poly(*N*-isopropylacrylamide-*co*-acrylic acid) (pNIPAm-co-AAc) microgel films in a disordered (Chapters 3-7) and an ordered fashion (Chapter 8). Chapter 3 details the interactions between pNIPAm-co-AAc microgels and poly(allylamine hydrochloride) (PAH) in aqueous solution. Chapter 4 describes the use of the electrostatic interactions between pNIPAm-co-AAc microgels and PAH to construct thin films. Chapter 5 describes the pH tunable interactions between PAH and pNIPAm-co-AAc microgels in assembled thin films. In Chapter 6 the assembled thin films are used as controlled delivery platforms for the chemotherapeutic drug agent doxorubicin. Chapter 7 details the use of a monolayer of pNIPAm-co-AAc microgels as microlens elements that function in air and solution and have dynamically tunable focal lengths in response to temperature and pH. The last chapter of this dissertation is devoted to the assembly of anionic microgels into ordered crystalline arrays in the absence of polyelectrolyte interactions. These crystals were polymerized into stable structures and were shown to have temperature tunable diffraction properties.

CHAPTER 1

HYDROGEL MATERIALS

1.1 Introduction

This chapter is intended as a general introduction to hydrogel materials with the focus being on the synthesis and behavior of responsive hydrogel microparticles (microgels), composed mainly of the monomer *N*-isopropylacrylamide (NIPAm).

Hydrogel materials are defined as crosslinked polymeric networks that are able to swell with large amounts of water, sometimes up to thousands of times their weight in the dry state.[1-4] These materials can be split into two general categories: physical and chemical gels. Physical gels are polymeric networks held together by polymer chain entanglement and/or by attractive forces present between the network polymers.[1,3,5,6] Attractive forces can be due to a variety of interactions, typically electrostatic or hydrophobic in nature. Environmentally stable physical gel networks are synthesized by mixing appropriate polymeric components together in the proper ratio. Although these networks have structural integrity they can be easily dissolved by exposure to chemical species, i.e. acid/base or salt, that weaken the interactions between the polymers holding the network together.

In contrast to physical gels, chemical gels are polymeric network structures held together by covalent crosslinks between the network polymers.[1,7,8] This structure is achieved by reacting simple hydrophilic monomers in the presence of a monomer containing two or more polymerizable groups (crosslinker). This network structure is inherently more stable than physical gels under a variety of conditions and is for all

intensive purposes a permanent structure. Chemical gels have found numerous uses such as contact lenses,[9,10] membranes,[11] and drug delivery platforms.[1,12-17]

Hydrogels, whether stabilized by physical or chemical interactions, can be classified as responsive or non-responsive. Non-responsive hydrogels are water swollen materials that are able to retain their integrity upon exposure to various stimuli unless a stimulus is able to completely break up the polymeric network, as is the case for physical gels.[1,2,18,19] Responsive hydrogels are a more interesting class of material, which undergo solvation changes in response to the application of an external stimulus.[7,14,16,20,21] In general, the responsivity of a hydrogel arises from competing solvation mechanisms where under one condition the network polymer chains are fully solvent swollen but upon introduction of an external stimulus the favorable polymer-solvent interactions are disrupted and polymer-polymer interactions begin to dominate, causing the polymer network to aggregate and deswell therefore expelling its entrained solvent.[22-25]

Hydrogels can still be further classified, based on size, as a macrogel or microgel. Macrogels are hydrogels that are typically on the millimeter (or larger) length scale.[26-31] Microgels can be defined as colloidally stable analogues of macrogels, which are on micro/nano length scale.[32-40] Macrogels and microgels can commonly be synthesized from the same starting materials and can be physical or chemical in nature as well as responsive or non-responsive. For all investigations presented in this dissertation responsive, chemically crosslinked microgels mainly composed of *N*-isopropylacrylamide (NIPAm) were used. The structure of NIPAm can be seen in Figure 1-1.

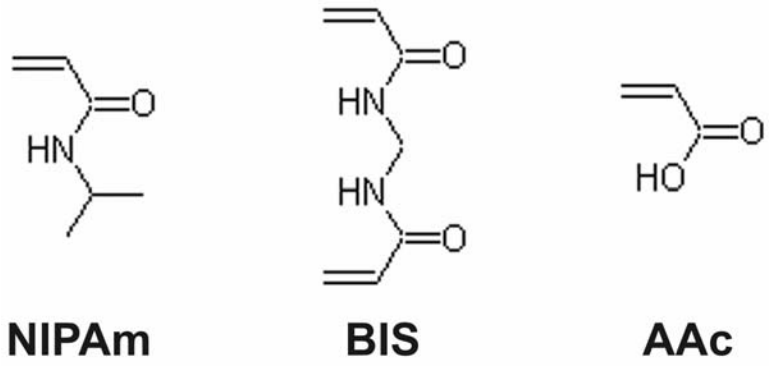

Figure 1-1. Chemical structures for *N*-isopropylacrylamide (NIPAm), *N,N'*-Methylene(bisacrylamide) (BIS), and acrylic acid (AAc).

1.2 Poly(N-isopropylacrylamide) Based Hydrogels

1.2.1 Basic Characteristics

As stated above, hydrogels are crosslinked (whether physically or chemically), polymeric materials that are highly water swollen, typically >90% water by volume. Responsive hydrogels can be synthesized by incorporation of functional monomers into the network structure during polymerization. The most commonly studied structures are thermoresponsive and are usually composed of poly(alkylacrylamides)[32,41,42] with poly(*N*-isopropylacrylamide) (pNIPAm) being the most common.[7,21,26,32,42,43] PNIPAm linear and network structures posses the ability to respond to changes in temperature by undergoing reversible swelling/deswelling transitions. This temperature dependent deswelling is known as a volume phase transition (VPT) and occurs at ~31 ºC, which is the lower critical solution temperature (LCST) for pNIPAm.[23,25,44,45] This differential solvation behavior is due to the unique interactions of pNIPAm with water molecules in a temperature dependent fashion where the interactions between the water molecules and polymer are weakened, while the polymer-polymer interactions are strengthened, at high

temperature, as depicted in Figure 1-2. Numerous other monomers/moieties are available that can be added to the hydrogel structure in order to render the structure responsive to numerous other stimuli such as electrical current,[46-49] magnetic field,[50-53] pH,[39,40,54] a host of biomolecules,[11,55-59] and the list goes on and on. Hydrogel structures can also be easily rendered multifunctional by the polymerization of two or more functional monomers into the network structure.[39,40] Performing this copolymerization results in a hydrogel that changes its solvation state in response to multiple stimuli where the energetics involved in responsivity are dictated by the component of the network that has the strongest interaction with water. Hydrogel swelling/deswelling behavior has been described previously by numerous theories including Flory-Huggins theory.[60-62] A discussion of theory is not included in this dissertation because it is a very broad topic of discussion that is beyond the scope of my thesis work.

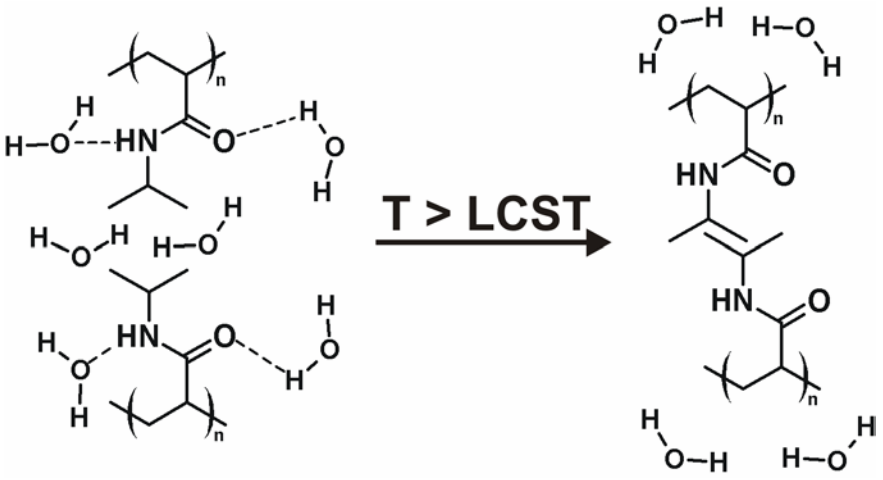

Figure 1-2. Molecular level view of the water dissociation process for pNIPAm structures. At temperatures below the LCST of pNIPAm water is a good solvent for pNIPAm but as the temperature of the solution is increased the polymer becomes a better solvent for itself resulting in an entropy driven expulsion of water.

1.3 Poly(*N*-isopropylacrylamide) Macrogels

As mentioned above, covalently crosslinked macrogels have been made to respond to multiple stimuli for various applications with the most studied structures to date being thermoresponsive macrogels composed of pNIPAm. These materials typically have size dimensions on the millimeter scale and respond by swelling/deswelling, in a reversible fashion, at ~31 ºC. The deswelling transition is characterized by the gel going from a transparent to opaque state.[7,63,64] Deswelling kinetics have been studied extensively for these systems and are known to be highly correlated to the gel dimensions, where the deswelling rate is inversely proportional to the square of the smallest dimension of the hydrogel.[63,65,66] As a result, macrogels on the millimeter, or larger, length scale can take hours or even days to completely deswell. One reason for the size dependent deswelling kinetics is simply due to the fact that the as the material deswells, the water inside the material has a harder time being expelled.[32,65,67]

Thermoresponsive macrogels have been studied by our group and others in regards to deswelling mechanism/kinetics,[16,68] and macrogel composition[27,69,70] using techniques such as surface plasmon resonance spectroscopy,[71-74] quartz crystal microbalance,[75,76] light scattering/turbidimetry,[68,69] differential scanning calorimetry,[70] and microscopy.[27]

1.4 Poly(*N*-isopropylacrylamide) Microgels

As mentioned in the introduction, thermoresponsive pNIPAm based microgels were used for all investigations presented in this dissertation. Microgels can be defined as colloidally stable hydrogels with dimensions on the micro/nano scale.[32] Because of their dimensions the kinetics of temperature induced deswelling are much faster than that seen for macrogels with deswelling rates for microgels being on the order of microseconds.[67] Similar to macrogels, microgels contain up to 99% water by volume in their swollen state, with collapsed microgels containing ~20% or less water by volume.[32] Figure 1-3 shows this temperature induced deswelling for some typical pNIPAm microgels in aqueous solution as a function of temperature. The microgels decrease in radius with increasing temperature indicating a transition from highly water swollen to deswollen, as can be observed by the increase in light scattering intensity in the deswollen state. The position of the VPT can easily be manipulated by incorporation of various functional co-monomers into the microgel network. In this dissertation, acrylic acid (AAc) was used exclusively to modify the thermoresponsivity of pNIPAm microgels.[39] Figure 1-4 shows the temperature induced deswelling for some typical poly(*N*-isopropylacrylamide-*co*-acrylic acid) (pNIPAm-co-AAc) microgels, which nicely illustrates the ability to tune the volume phase transition temperature (VPTT) of the microgels. Specifically, this figure

shows that microgels at acidic (~3.0) pH values have an average R_h of ~300 nm. Since the AAc groups are almost fully protonated at this pH (pK_a of AAc is ~ 4.25), the microgels undergo a continuous VPT over a ~6 ºC range, with a LCST of ~31ºC. This thermoresponsivity is hindered upon exposure to a pH 6.5 solution. At this pH it is observed that the microgels have an average R_h of ~550 nm. The swelling of the microgels at this pH is expected due to deprotonation of the majority of the AAc groups, which introduces charge-charge repulsion and increased osmotic pressure in the network. Furthermore, as the microgels are heated in pH 6.5 solution, they are unable to deswell to the same minimum R_h observed at pH 3.0, and the VPT temperature is much higher, again due to the charged nature of the microgel network.

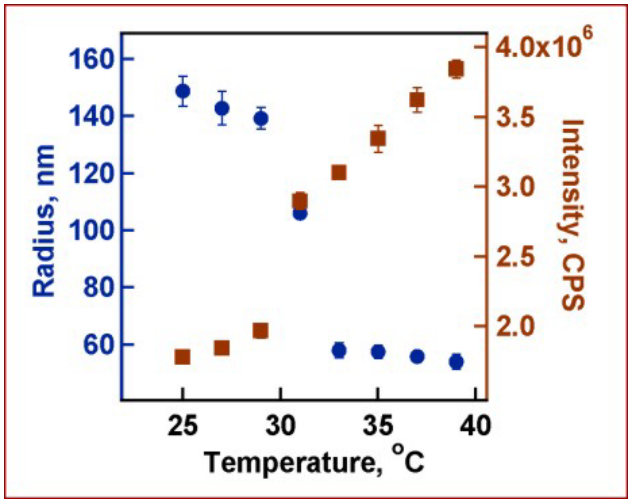

Figure 1-3. Typical temperature dependent deswelling behavior from pNIPAm microgels. As the temperature is increased the microgels undergo a deswelling transition, going from solvent swollen to deswollen (circles). As a result, the scattered light intensity (squares) drastically increases due to the increase of the refractive index contrast between the deswollen microgels and the water.

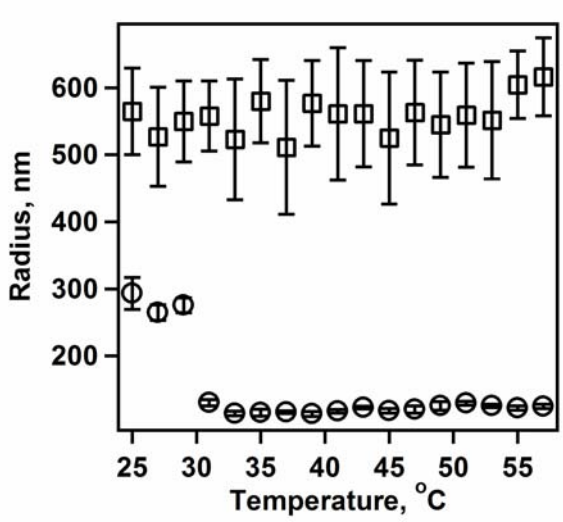

Figure 1-4. Typical temperature dependent deswelling behavior from pNIPAm-co-AAc microgels. At pH 3.0 (circles) as the temperature is increased the microgels undergo a deswelling transition, which is hindered due to Coulombic repulsion at pH 6.5 (squares).

1.4.1 Microgel Synthesis

PNIPAm microgels can be synthesized following a number of routes where for these studies we exclusively used standard temperature induced free-radical precipitation polymerization.[36,37,39,77-79] This method of synthesis takes advantage of the water solubility of the precursor monomers and the different solubility of the polymerized form of the monomers. Precipitation polymerization is performed in a three-neck round bottom flask (RBF) containing water that is rigorously purged with N_2. Purging is necessary to remove any dissolved O_2 from the reaction mixture, which acts as a free radical scavenger capable of preventing the polymerization reaction from occurring. The main monomer NIPAm and the crosslinker *N,N'*-Methylene(bisacrylamide) (BIS) are added to the RBF along with some concentration of the surfactant sodium dodecyl sulfate (SDS), at a concentration well below the critical micelle concentration. SDS acts as a microgel

stabilizer in these reactions. This solution is allowed to stir and heat to 70 ºC for 1 hr. After 1 hr any comonomers can be added to the reaction mixture prior to initiation. For all studies contained in this dissertation AAc was used as a comonomer. The chemical structures for the common monomers used in this dissertation are shown in Figure 1-1. The reaction can be initiated, following addition of the desired comonomer(s), by adding the free-radical initiator ammonium persulfate (APS). Addition of APS at this temperature results in its cleavage producing free radical fragments in solution, which are able to react with the solubilized monomer and crosslinker. If the reaction is performed correctly, i.e. fast addition of APS and fast initiation, growing pNIPAm chains form in a homogenous fashion that, upon reaching a certain critical chain length, collapse upon themselves forming precursor particles. Precursor particles serve as nuclei for microgel growth eventually reaching a stable structure with a diameter partially dictated by the amount of SDS present in the reaction mixture. For example, high SDS concentrations result in small microgels while low SDS concentrations result in large microgels. Figure 1-5 shows a schematic of the various stages of microgel growth. As was also mentioned in the introduction, numerous comonomers are available that can be added to the reaction mixture to add multiple functionalities to microgels.[32]

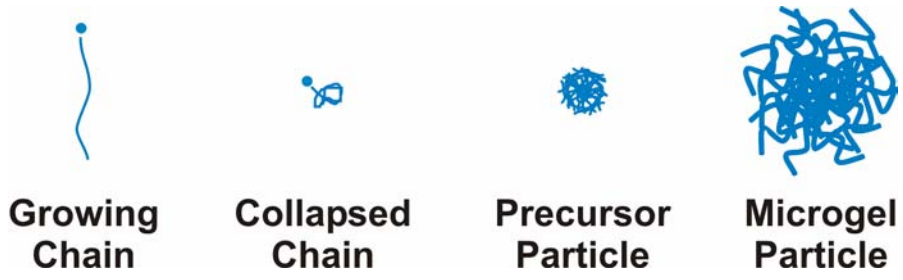

Figure 1-5. Growth of a microgel during free-radical precipitation polymerization involves pNIPAm chain growth, which collapse upon reaching a critical chain length. The collapsed chains then serve as precursor particles for growth resulting in a stable microgel.

Our group has also devised synthetic techniques for adding hydrogel shells to previously synthesized core microgels.[36,37,40,79,80] These core/shell microgels are synthesized by adding previously synthesized microgels to a reaction mixture, at the same conditions as above, containing any water soluble monomers/crosslinkers one would like to add to the core microgel, along with SDS for stabilization. This reaction is believed to proceed by the collapsed core microgels acting as nuclei for growth of additional polymer onto its periphery. This synthetic procedure has been demonstrated on numerous occasions to synthesize microgels with multiple functionalities in a spatially defined fashion. For a majority of the studies presented in this dissertation core microgels were used so discussion of core/shell fundamentals will only be discussed where necessary.

1.4.2 Microgel Solution Characteristics

PNIPAm microgels respond to increases/decreases in temperature by decreasing/increasing their size, respectively, as seen in Figure 1-3 and 1-4. This transition is also highly reversible. A dilute, aqueous solution of microgels, under ambient conditions, appears clear and for the most part colorless to the eye due to the fact that microgels are generally >90% water by volume and therefore highly refractive index (RI) matched with the surrounding water. If the temperature of the system is increased to above the LCST of pNIPAm the microgel network structure deswells in an entropically driven phase transition. As a result of this deswelling event the microgel network structure becomes very dense by expelling most of its water from the network thereby increasing the refractive index (RI) contrast between the microgel and water giving rise to a more turbid solution, as seen in the above figures.

1.4.3 Microgel Characterization

Microgel particles can be characterized using a number techniques with laser light scattering being used almost exclusively in this dissertation. Laser light scattering can be performed in two different modes to give different, but complementary, information about the microgel particles. These two techniques are known as static and dynamic light scattering and differ in the information they provide and how the experiments are performed but have in common a laser light source and some sort of photodiode, typically an avalanche photodiode, for detection of scattered light.[81,82] Since static light scattering techniques were not readily available at the time of experimentation for this dissertation no such measurements are included and hence static light scattering will only be briefly mentioned. Static light scattering monitors light scattered from a dilute solution

of microgels as a function of angle between the incoming light and detector. Among other things, this technique is able to report molar mass as well as conformation/shape of microgels.

Dynamic light scattering was used exclusively in this dissertation for determining the size of pNIPAm-co-AAc microgels and their response to solution temperature and pH changes. Dynamic light scattering is a well known technique that is able to report the radius of a particle, in a dilute solution, by monitoring fluctuations in the scattered light intensity as a function of time. The scattered light intensity fluctuations over time can then be plotted as an autocorrelation function. The decay of this autocorrelation function can then be fit using a regularization algorithm (Dynamics Software Version 5.25.44) and related to the microgel diffusion coefficient, making the assumption of Brownian motion. From the diffusion coefficient the radius of the particles can be calculated using the Stokes-Einstein equation.

This chapter described the basic behavior of hydrogel materials and how they are synthesized, characterized, and applied to various technologies. This dissertation is mainly focused on assembling thin films composed of microgels in a Layer-by-Layer (LbL) fashion and studying their resulting behavior, and how they can be used for a few applications. The next chapter will give a basic introduction to the LbL technique for assembling thin, polymeric films.

REFERENCES

(1) Hoffman, A. S. *Adv. Drug Deliv. Rev.* **2002**, *54*, 3-12.

(2) Drury, J. L.; Mooney, D. J. *Biomaterials* **2003**, *24*, 4337-4351.

(3) DeRossi, D.; Kajiwara, K.; Osada, Y.; Yamauchi, A. *Polymer Gels. Fundamentals and Biomedical Applications*; Plenum Press: New York, 1991.

(4) Dhara, D.; Nisha, C. K.; Chatterji, P. R. *J. Macromol. Sci., Pure Appl. Chem.* **1999**, *A36*, 197-210.

(5) Akiyoshi, K.; Kang, E.-C.; Kurumada, S.; Sunamoto, J.; Principi, T.; Winnik, F. M. *Macromolecules* **2000**, *33*, 3244-3249.

(6) Collier, J. H.; Hu, B.-H.; Ruberti, J. W.; Zhang, J.; Shum, P.; Thompson, D. H.; Messersmith, P. B. *J. Am. Chem. Soc.* **2001**, *123*, 9463-9464.

(7) Eddington, D. T.; Beebe, D. J. *Adv. Drug Deliv. Rev.* **2004**, *56*, 199-210.

(8) Hennink, W. E.; van Nostrum, C. F. *Adv. Drug Deliv. Rev.* **2002**, *54*, 13-36.

(9) McMahon, T. T.; Zadnik, K. *Cornea* **2000**, *19*, 730-740.

(10) Opdahl, A.; Koffas, T. S.; Amitay-Sadovsky, E.; Kim, J.; Somorjai, G. A. *J. Phys.-Condes. Matter* **2004**, *16*, R659-R677.

(11) Obaidat, A. A.; Park, K. *Biomaterials* **1997**, *18*, 801-806.

(12) Kikuchi, A.; Okano, T. *Adv. Drug Deliv. Rev.* **2002**, *54*, 53-77.

(13) Kim, S. W.; Bae, Y. H.; Okano, T. *Pharm. Res.* **1992**, *9*, 283-290.

(14) Qiu, Y.; Park, K. *Adv. Drug Deliv. Rev.* **2001**, *53*, 321-339.

(15) Park, T. G. *Biomaterials* **1999**, *20*, 517-521.

(16) Yan, Q.; Hoffman, A. S. *Poly. Commun.* **1995**, *36*, 887-889.

(17) Gupta, P.; Vermani, K.; Garg, S. *Drug Discov. Today* **2002**, *7*, 569-579.

(18) Zaldivar, D.; Peniche, C.; Gallardo, A.; Sanroman, J. *Biomaterials* **1993**, *14*, 1073-1079.

(19) Martin, B. D.; Ampofo, S. A.; Linhardt, R. J.; Dordick, J. S. *Macromolecules* **1992**, *25*, 7081-7085.

(20) Beebe, D. J.; Moore, J. S.; Bauer, J. M.; Yu, Q.; Liu, R. H.; Devadoss, C.; Jo, B. H. *Nature* **2000**, *404*, 588-590.

(21) Wu, X. S.; Hoffman, A. S.; Yager, P. *J. Polym. Sci. Pol. Chem.* **1992**, *30*, 2121-2129.

(22) Wu, C. *Polymer* **1998**, *39*, 4609-4619.

(23) Wu, C.; Wang, X. *Phys. Rev. Lett.* **1998**, *80*, 4092-4094.

(24) Wu, C.; Zhou, S. *J. Macromol. Sci., Phys.* **1997**, *B36*, 345-355.

(25) Wu, C.; Zhou, S. *Macromolecules* **1995**, *28*, 8381-8387.

(26) Chen, J.; Park, H.; Park, K. *Polym. Mater. Sci. Eng.* **1998**, *79*, 236-237.

(27) Chen, J.; Park, H.; Park, K. *J. Biomed. Mater. Res.* **1999**, *44*, 53-62.

(28) Gemeinhart, R. A.; Chen, J.; Park, H.; Park, K. *J. Biomater. Sci., Polym. Ed.* **2000**, *11*, 1371-1380.

(29) Gemeinhart, R. A.; Park, H.; Park, K. *J. Biomed. Mater. Res.* **2000**, *55*, 54-62.

(30) Gemeinhart, R. A.; Park, H.; Park, K. *Polym. Adv. Technol.* **2000**, *11*, 617-625.

(31) Park, K.; Chen, J.; Park, H. *Polym. Drugs Drug Delivery Syst.* **2001**, 145-155.

(32) Pelton, R. *Adv. Colloid. Interface Sci.* **2000**, *85*, 1-33.

(33) Saunders, B. R.; Vincent, B. *Adv. Colloid Interface Sci.* **1999**, *80*, 1-25.

(34) Kawaguchi, H. *Prog. Polym. Sci.* **2000**, *25*, 1171-1210.

(35) Gilanyi, T.; Varga, I.; Meszaros, R.; Filipcsei, G.; Zrinyi, M. *Phys. Chem. Chem. Phys.* **2000**, *2*, 1973-1977.

(36) Gan, D.; Lyon, L. A. *J. Am. Chem. Soc.* **2001**, *123*, 7511-7517.

(37) Gan, D.; Lyon, L. A. *J. Am. Chem. Soc.* **2001**, *123*, 8203-8209.

(38) Gan, D. J.; Lyon, L. A. *Macromolecules* **2002**, *35*, 9634-9639.

(39) Jones, C. D.; Lyon, L. A. *Macromolecules* **2000**, *33*, 8301-8306.

(40) Jones, C. D.; Lyon, L. A. *Macromolecules* **2003**, *36*, 1988-1993.

(41) Shibayama, M.; Tanaka, T. *Adv. Polym. Sci.* **1993**, *109*, 1-62.

(42) Inomata, H.; Goto, S.; Saito, S. *Macromolecules* **1990**, *23*, 4887-4888.

(43) Kaneko, Y.; Nakamura, S.; Sakai, K.; Aoyagi, T.; Kikuchi, A.; Sakurai, Y.; Okano, T. *Macromolecules* **1998**, *31*, 6099-6105.

(44) Wu, C.; Zhou, S. *Macromolecules* **1995**, *28*, 5388-5390.

(45) Hu, T. J.; You, Y. Z.; Pan, C. Y.; Wu, C. *J. Phys. Chem. B* **2002**, *106*, 6659-6662.

(46) Tanaka, T.; Nishio, I.; Sun, S. T.; Uenonishio, S. *Science* **1982**, *218*, 467-469.

(47) Feher, J.; Filipcsei, G.; Szalma, J.; Zrinyi, M. *Colloids Surf., A* **2001**, *183-185*, 505-515.

(48) Murdan, S. *J. Control. Release* **2003**, *92*, 1-17.

(49) Shiga, T. In *Neutron Spin Echo Spectroscopy Viscoelasticity Rheology*, 1997; Vol. 134, pp 131-163.

(50) Roubeau, O.; Colin, A.; Schmitt, W.; Clerac, R. *Angew. Chem.-Int. Edit.* **2004**, *43*, 3283-3286.

(51) Xulu, P. M.; Filipcsei, G.; Zrinyi, M. *Macromolecules* **2000**, *33*, 1716-1719.

(52) Szabo, D.; Szeghy, G.; Zrinyi, M. *Macromolecules* **1998**, *31*, 6541-6548.

(53) Zrinyi, M. *Colloid and Polymer Science* **2000**, *278*, 98-103.

(54) Tanaka, T.; Fillmore, D. J.; Sun, S.-T.; Nishio, I.; Swislow, G.; Shah, A. *Phys. Rev. Lett.* **1980**, *45*, 1636-1639.

(55) Alvarez-Lorenzo, C.; Guney, O.; Oya, T.; Sakai, Y.; Kobayashi, M.; Enoki, T.; Takeoka, Y.; Ishibashi, T.; Kuroda, K.; Tanaka, K.; Wang, G.; Grosberg, A. Y.; Masamune, S.; Tanaka, T. *J. Chem. Phys.* **2001**, *114*, 2812-2816.

(56) Miyata, T.; Asami, N.; Uragami, T. *Nature* **1999**, *399*, 766-769.

(57) Kokufata, E.; Zhang, Y. Q.; Tanaka, T. *Nature* **1991**, *351*, 302-304.

(58) Kataoka, K.; Miyazaki, H.; Bunya, M.; Okano, T.; Sakurai, Y. *J. Am. Chem. Soc.* **1998**, *120*, 12694-12695.

(59) Ogawa, K.; Wang, B.; Kokufuta, E. *Langmuir* **2001**, *17*, 4704-4707.

(60) Hino, T.; Prausnitz, J. M. *Polymer* **1998**, *39*, 3279-3283.

(61) Tanaka, T. *Phys. Rev. Lett.* **1978**, *40*, 820-823.

(62) Flory, P. J. *Principles of Polymer Chemistry*; Cornell University Press: London, 1953.

(63) Li, Y.; Tanaka, T. *J. Chem. Phys.* **1990**, *92*, 1365-1371.

(64) Wang, C.; Li, Y.; Hu, Z. *Macromolecules* **1997**, *30*, 4727-4732.

(65) Tanaka, T.; Fillmore, D. J. *J. Chem. Phys.* **1979**, *70*, 1214 - 1218.

(66) Matsuo, E. S.; Tanaka, T. *J. Chem. Phys.* **1988**, *89*, 1695-1703.

(67) Wang, J.; Gan, D.; Lyon, L. A.; El-Sayed, M. A. *J. Am. Chem. Soc.* **2001**, *123*, 11284-11289.

(68) Tanaka, T.; Sato, E.; Hirokawa, Y.; Hirotsu, S.; Peetermans, J. *Phys. Rev. Lett.* **1985**, *55*, 2455-2458.

(69) Nayak, S.; Debord, S. B.; Lyon, L. A. *Langmuir* **2003**, *19*, 7374-7379.

(70) Cai, W. S.; Gupta, R. B. *J. Appl. Polym. Sci.* **2002**, *83*, 169-178.

(71) Harmon, M. E.; Jakob, T. A. M.; Knoll, W.; Frank, C. W. *Macromolecules* **2002**, *35*, 5999-6004.

(72) Kuckling, D.; Harmon, M. E.; Frank, C. W. *Macromolecules* **2002**, *35*, 6377-6383.

(73) Harmon, M. E.; Kuckling, D.; Pareek, P.; Frank, C. W. *Langmuir* **2003**, *19*, 10947-10956.

(74) Harmon, M. E.; Kuckling, D.; Frank, C. W. *Macromolecules* **2003**, *36*, 162-172.

(75) Plunkett, M. A.; Wang, Z. H.; Rutland, M. W.; Johannsmann, D. *Langmuir* **2003**, *19*, 6837-6844.

(76) Calvo, E. J.; Danilowicz, C.; Etchenique, R. *J. Chem. Soc.-Faraday Trans.* **1995**, *91*, 4083-4091.

(77) Serpe, M. J.; Jones, C. D.; Lyon, L. A. *Langmuir* **2003**, *19*, 8759-8764.

(78) Nayak, S.; Lyon, L. A. *Chem. Mater.* **2004**, *16*, 2623-2627.

(79) Gan, D.; Lyon, L. A. *Macromolecules* **2002**, *35*, 9634-9639.

(80) Jones, C. D.; Lyon, L. A. *Langmuir* **2003**, *19*, 4544-4547.

(81) Pecora, R. *Dynamic Light Scattering*; Plenum Press: New York, 1985.

(82) Chu, B. *Laser light scattering : basic principles and practice*; Academic Press: Boston, 1991.

CHAPTER 2

POLYELECTROLYTE MULTILAYER THIN FILMS

2.1 Introduction

Fabrication and patterning of films on surfaces has been of interest for many years for uses in a multitude of applications such as photonic materials,[1-6] drug delivery systems,[7-9] sensors,[10-14] and chemical resistant surfaces.[15-18] These films are typically composed of multiple components frequently requiring the individual components to be arranged in a spatially defined fashion. Because of these film requirements there are few technologies available to achieve such goals, and the technology that is available is typically complicated and difficult to scale to the coating of large substrate surfaces made of a variety of materials and dimensions. For example, one of the classical methods for fabricating thin films with some control over layer ordering/orientation is the Langmuir-Blodgett technique.[19,20] This technique involves the transfer of a self-assembled, specifically orientated monolayer of molecules from an air-water interface to the surface of a planar substrate. This is accomplished by slowly dipping the substrate into and out of the solution containing the self-assembled molecules. While this technique has the benefit of depositing molecularly thin layers, it has the downfall of requiring special equipment, not easily scalable to deposition on large surfaces and is limited to planar surfaces. This technique has the additional downfall of not being able to deposit layers containing multiple components with various compositions, i.e. nanoparticle modified surfaces.

A breakthrough in thin film deposition technology occurred in the early 1990's when Decher and coworkers discovered a technique for constructing thin films in a

Layer-by-Layer (LbL) fashion.[21-23] In their initial study the authors constructed multilayer thin films by exposing a charged substrate to an aqueous solution containing rod-like molecules that were end-functionalized with charged moieties, which had an opposite charge than that of the substrate.[23] These molecules were shown to adsorb to the surface in self-regulated fashion. Self-regulated meaning that molecules adsorb to the substrate until the charge on the unmodified substrate is reversed, which hinders further molecule adsorption to the substrate by electrostatic repulsion. After rinsing and drying the substrate it was exposed to an aqueous solution containing oppositely charged molecules, which resulted in adsorption of that molecule to the substrate surface, again in a self-regulated fashion, resulting in substrate charge reversal. This substrate can then be sequentially added to each solution until the desired film thickness or composition is reached. Following this initial publication, Decher and coworkers extended this technology to the deposition of polymers containing charged monomer units.[22] These charged polymers, or more frequently called polyelectrolytes, were shown to deposit in a similar fashion as in their original study. The chemical structure of a few frequently used polyelectrolytes can be seen in Figure 2-1. This technique of alternately adsorbing polyelectrolytes to surfaces is currently one of the most common and versatile techniques in use for producing polymeric thin films of various compositions.[24-31] In addition to fabricating films stabilized by electrostatics, thin films have also been constructed using hydrogen bonding,[32-35] and ligand-receptor interactions (coordinate covalent or covalent bonding, biological recognition).[36-40] The use of a variety of interactions to assemble films is possible because adsorption of a molecule, in solution, onto a surface depends mostly on whether the substrate surface is presenting functional groups that have

attractive interactions with the adsorbate molecules. In general, as long as these attractive interactions are present, regardless of the nature of the interactions, molecules will attach to the substrate surface. Another requirement to achieve stable multilayer thin films is that the layers must have multiple attractive interactions with the substrate and the other components of the film. A schematic illustrating these points can be seen in Figure 2-2.

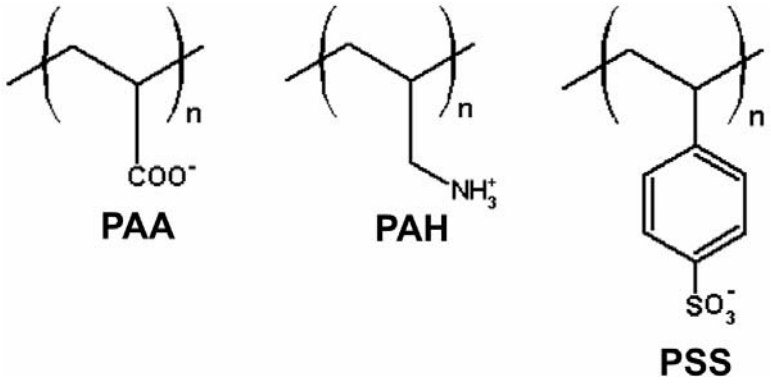

Figure 2-1. Chemical structures for the polyelectrolytes poly(acrylic acid) (PAA), poly(allylamine hydrochloride) (PAH) and poly(sodium 4-styrenesulfonate) (PSS).

This technique has many advantages over other thin film fabrication methods including the ability to scale the deposition to the coating of large substrates, and because this is a solution based technique, substrates of virtually any shape, morphology or composition can be coated as long as multiple attractive interactions are present in the film. This technique also has the benefit of being able to control the order (in one dimension) and composition of the individual layers in the films, which is difficult to achieve using other methods.

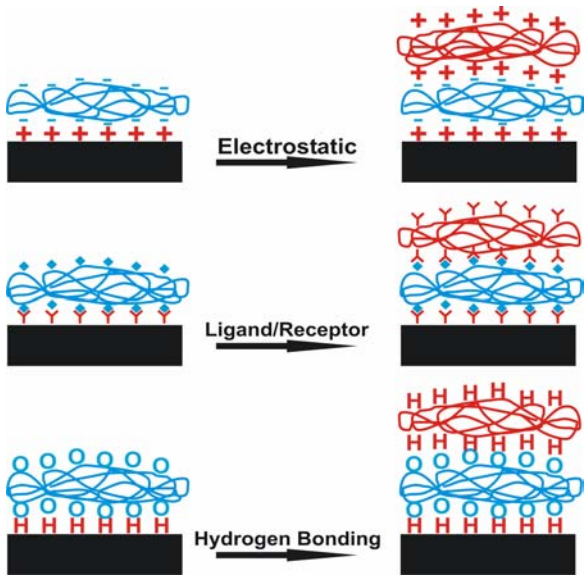

Figure 2-2. Schematic illustrating how layers can be adsorbed to surfaces using various attractive forces.

2.2 LbL assembly of Thin Films

To begin this section it should be pointed out that LbL assembly refers to the technique used to adsorb macromolecules sequentially on to a surface one layer at a time and is not intended to imply that the layers are being deposited in a ordered/stratified fashion normal to the substrate. There are reports of macromolecules being deposited in such a stratified fashion[21,41,42] but for all the studies presented in this dissertation this is not the case.

2.2.1 Passive Polyelectrolyte Adsorption

The majority of LbL processes involve the passive adsorption of macromolecules on surfaces.[21-23] As stated above the surface can be of virtually any size, shape, morphology, or composition, with the most common being planar glass substrates. A general prerequisite for the adsorption of a macromolecule on a surface is that it must

have multiple attractive interactions with the substrate surface. As mentioned above, there are a variety of possible interactions that can be exploited for the deposition of layers but this section will be limited to the discussion of polyelectrolyte adsorption to surfaces.

To begin this process, the substrate surface must be properly conditioned to render it charged. This can be accomplished in a variety of ways depending on the type of substrate being used. For example; if a glass substrate is being used for deposition it can be rendered negatively charged by exposure to a strong oxidizing solution such as piranha solution, or positively charged by covalently attaching positively charged silanes to the surface. Regardless of the initial charge on the substrate, polyelectrolyte deposition is performed in same manner. A charged substrate is exposed to an aqueous polyelectrolyte solution, at the desired pH, ionic strength and concentration (typically on the order of milligrams/mL), and the polyelectrolyte is allowed to adsorb to the substrate surface for ~20 minutes. The 20 minute adsorption time is standard for the adsorption of relatively low molecular weight (MW) polyelectrolytes (~70 000) but can be increased for the deposition of large MW polyelectrolytes and colloidal species.[21] This substrate is then rinsed with water, dried with N_2 gas, and exposed to an aqueous solution of oppositely charged polyelectrolyte. After 20 minutes this substrate is again rinsed with water and dried with N_2 gas and exposed to the original polyelectrolyte solution. This process can be repeated numerous times to achieve a film with the desired properties. A schematic depiction of the deposition process can be seen in Figure 2-3.

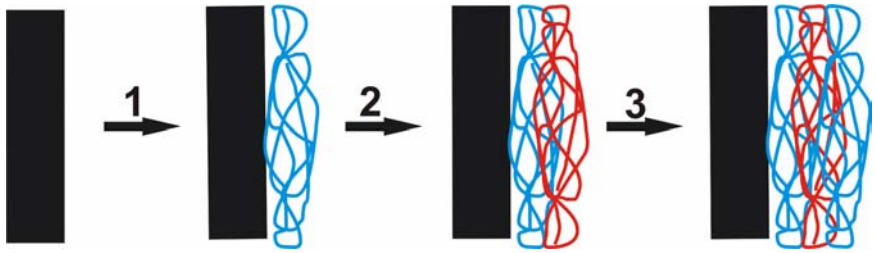

Figure 2-3. Step 1 shows a positively charged substrate that adsorbed polyanion (blue) to its surface followed by rinsing the surface copiously with water and drying. Step 2 shows the polyanion modified surface adsorbing polycation (red) to its surface followed by rinsing with water and drying. Step 3 shows subsequent addition of polyanion to the polycation modified surface. This process can be repeated numerous times to achieve the desired number of layers.

This technique has been used to fabricate films for in vivo repair of blood vessels,[43] preparation of polymeric nanotubes,[44] nanoscale reactors,[45-48] micropatterning,[49-51] membrane synthesis,[52-54] drug delivery,[55,56] photonics,[45,47,57] and bio-composite film assembly.[24-26,39,40,58,59] In addition to the fabrication of the above materials there is a significant amount of research being conducted on fabricating colloid functionalized substrates using LbL assembly. Using this technique a variety of nanoparticles such as: polystyrene,[60,61] Au,[62,63] Fe_3O_4,[64] CdS,[65] ZnS-capped CdSe,[66] and CdTe[67] have been incorporated into thin films. The ability to incorporate a variety of nanoparticles into thin films has opened new doors for achieving photonic bandgap materials,[45,47] conducting films,[62,63] novel recording/memory devices,[64] and patterned electroluminescent materials.[66] This idea of nanoparticle incorporation into thin films via electrostatics is especially important to the work contained in this dissertation.

Another interesting extension of using passive adsorption of polyelectrolytes to coat surfaces is the deposition of polyelectrolyte layers on colloidal micro/nanoparticles.[68,69] This technique is performed using the same basic coating steps

as outlined above: exposure of the surface to the polyelectrolyte solution, washing the surface free of any unbound polyelectrolyte and exposure of the surface to a polyelectrolyte of opposite charge. This process can also be repeated until the desired film properties are achieved. The only modification to the basic LbL scheme is the need to wash the colloids using several centrifugation/resuspension or filtration cycles to separate the unbound polyelectrolyte from the coated colloids. Also, there are some additional factors that must be considered when coating colloidal particles such as aggregation of the particles instead of layer growth. To prevent aggregation, the particles are always added to a polyelectrolyte solution containing a large excess of polyelectrolyte. This technique has also been used to construct polymeric capsules by dissolving out the colloidal core template using chemical degradation. Commonly used colloidal templates are: melamine-formaldehyde particles,[70] $MnCO_3$ particles,[71,72] polystyrene particles[73] and metal nanoparticles.[68,69,74] This technique has been used to produce a variety of capsules containing multiple functional groups for applications mainly in the field of encapsulation and drug delivery.[68]

2.2.2 Spin Coated Polyelectrolyte Layers

This technique allows for the adsorption of polyelectrolytes to surfaces, in a LbL fashion, by taking advantage of a standard spin coater commonly used for the deposition of photoresist onto SiO_2 surfaces for photolithography.[75-78] This polyelectrolyte deposition technique is relatively new and allows for multilayer thin films to be built up in a fraction of the time it takes for traditional passive adsorption of polyelectrolytes onto surfaces. For example, a polyelectrolyte layer can be deposited on a substrate in seconds rather than tens of minutes. This decrease in deposition time is due to the fact that passive

adsorption relies on diffusion of polyelectrolytes to surface while this technique enforces interaction of the polyelectrolyte with the surface due to the mechanical forces operative during spin coating. Deposition of a variety of polyelectrolytic species have been accomplished using this technique where it is proposed that the films deposit in a very dense, layered fashion with minimal interpenetration of the neighboring polyelectrolyte layers, which results in very smooth layers.[78] This technique has also been extended to the deposition of polyelectrolytic colloidal particles.[79] Performing this technique is straightforward and involves attaching an appropriately charged substrate to a vacuum chuck of a spin coater. The substrate is typically set to rotate at ~3 000 RPM. This spinning rate can be increased or decreased depending on the material being deposited and the viscosity of the deposition solution. Polyelectrolyte solution, of a similar concentration to that used for passive adsorption, is then dripped onto the spinning substrate, which is allowed to spin for ~20 sec. Following this step the spinning substrate is rinsed copiously with water and allowed to spin for an additional ~20 sec. The spinning substrate is then exposed to a solution of polyelectrolyte with an opposite charge, allowed to spin for ~20 sec and subsequently rinsed with water. This process can be repeated numerous times until the desired film thickness or properties are achieved. A schematic illustrating the spin coating process can be seen in Figure 2-4.

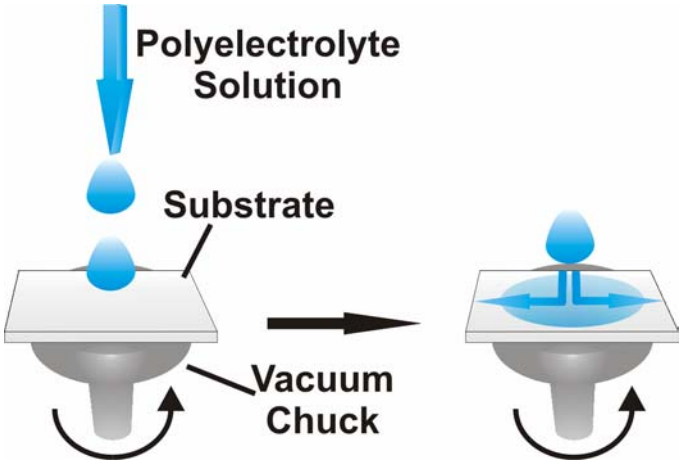

Figure 2-4. Schematic showing how a spin coater is used to add polyelectrolyte layers to surfaces. The desired substrate is added to the vacuum chuck of a spin coater and spun at ~ 3 000 RPM while polyelectrolyte solutions are added to the substrate.

2.2.3 Polyelectrolyte Layer Deposition Characteristics

Regardless of whether a polyelectrolyte thin film is constructed using passive adsorption or spin assisted adsorption the pH and ionic strength of the deposition solution is extremely important to define and control. These solution properties affect the extent of molecular scale ionic interactions between the layers. For example, pH can control the number of ionic interactions between sequentially adsorbed layers, in the case of weak polyacid/base deposition, and ionic strength can be used to control the strength and number of molecular scale ionic interactions by electrostatic screening effects.

Tuning of molecular scale ionic interactions was previously investigated for polyelectrolyte multilayer thin films composed of weak polyacids/bases.[80-84] The results showed that polyelectrolyte layers deposited from a solution at a pH where the polyelectrolyte is not fully charged results in a layer that deposits in a thick, "loopy" conformation, whereas deposition from a solution at a pH that enforces polyelectrolyte

ionization results in thin, more rigid layers.[81] These results can be understood by considering the number of ionic interactions necessary to neutralize the previously adsorbed polyelectrolyte layer and reverse the charge on the surface. Under low polyelectrolyte ionization conditions the layers deposit with fewer sidechain-sidechain interactions, leaving loopy polymer segments, which results in an overall thicker film. Under high polyelectrolyte ionization conditions, the layers interact very strongly with a high number of interactions, resulting in rigid, thin layer.[81,82]

The ionic strength of polyelectrolyte deposition solutions were also shown to play a similar role in the deposition of polyelectrolyte layers as a result of charge screening.[85-89] The generally observed trend was an increase in absorbed layer thickness as a function of increasing salt concentration. This behavior was explained by considering the change in polyelectrolyte macromolecule conformation at high ionic strengths. Specifically, highly charged polyelectrolytes in low ionic strength solutions have significant repulsion between the charged monomeric units on the polyelectrolyte chain and is considered to be in a stretched conformation. As the ionic strength of the deposition solution is increased ionic repulsions are reduced and the polyelectrolyte can take on a more coiled conformation. By consideration of the conformation of the polyelectrolytes in solution it is expected that adsorption of a polyelectrolyte at low ionic strength will result in a thin layer while deposition from a high ionic strength solution will result in a relatively thick layer. Increasing ionic strength also decreases the repulsion between adsorbed polyelectrolyte and the polyelectrolytes in solution. This presumably allows more polyelectrolyte to access the surface and bind, resulting in thicker adsorbed layers. Layer thickness has been shown to scale approximately linearly with ionic strength eventually

reaching a solution ionic strength that completely hinders layer adsorption.[85,86] This is because the charges on the polyelectrolyte are screened so much that ionic attractive forces between polyelectrolyte layers will not be strong.

2.3 Polyelectrolyte Thin Film Behavior

As can be gleaned from the previous section, polyelectrolytes are extremely sensitive to solution properties such as pH and ionic strength. Likewise, it has also been shown that pH and ionic strength dictate polyelectrolyte layer morphology in previously assembled thin films.[34,80,90] These investigations have shown that when a thin film composed of weak polyacids/bases, which were assembled at a pH that promoted a large number of ionic interactions between the layers, was exposed to a pH solution that disrupted the ionic interactions the film became thicker due to breakage of the ionic interactions that held the film together. This results in film swelling and in some cases, disassembly. If the film was subsequently exposed to a pH solution that reinforces the films ionic interactions the film re-rigidifies due to enforced ionic interactions. This pH dependent film morphology is strictly limited to systems assembled from weak polyacids/bases where the degree of polyelectrolyte ionization is easily controlled by solution pH. If a film is assembled from strong polyacids/bases this pH dependent film thickness is not seen. Another interesting characteristic of these thin films is that the acid/base groups on the polyelectrolyte become stronger acids/bases once electrostatically bound in films.[84] This was attributed to the fact that the associated electrostatic groups are more stable than they would be if one charge was compensated by protonation/deprotonation leaving the other charge free. Studies also showed that

polyelectrolyte layer morphology, in preassembled thin films, could be modulated by exposure to high ionic strength solutions.[85] These films were shown to swell as a function of ionic strength due to the weakened ionic interactions between the layers. Films were also shown to disassemble at extreme ionic strength values.

This chapter described how polyelectrolyte multilayers, assembled in a LbL fashion, can be easily assembled following two general approaches: passive or spin assisted polyelectrolyte adsorption. This discussion also points out the versatility of the LbL method, which can be adapted to coat substrate surfaces of a variety of sizes, shapes, and compositions with a multitude of components for various applications. The tunability of polyelectrolyte/multilayer thin film morphology was also discussed with respect to pH and ionic strength.

The focus of this dissertation is the assembly of microgel thin films. First, electrostatic assembly of monolayer and multilayer microgel thin films on surfaces, in a random fashion is discussed. The initial chapters describe polycation interactions with anionic microgels and how these interactions can be used to assemble thermoresponsive microgel thin films. In subsequent chapters, pH dependent film behavior is discussed followed by a discussion of their use as microlens arrays and platforms for controlled release of small molecules. The last chapter in this dissertation is devoted to the assembly of anionic microgels into ordered crystalline arrays in the absence of polyelectrolyte interactions. These crystals were polymerized into stable structures and used as wavelength tunable filters.

REFERENCES

(1) Ozin, G. A.; Yang, S. M. *Adv. Funct. Mater.* **2001**, *11*, 95-104.

(2) Yang, S. M.; Ozin, G. A. *Chem. Commun.* **2000**, 2507-2508.

(3) Hanken, H. G.; Corn, R. M. *Anal. Chem.* **1995**, *67*, 3767-3774.

(4) Ibn-Elhaj, M.; Schadt, M. *Nature* **2001**, *410*, 796-799.

(5) Romanov, S. G.; Maka, T.; Torres, C. M. S.; Muller, M.; Zentel, R. *Synth. Met.* **2001**, *116*, 475-479.

(6) Richter, B.; Kirstein, S. *J. Chem. Phys.* **1999**, *111*, 5191-5200.

(7) Gupta, P.; Vermani, K.; Garg, S. *Drug Discov. Today* **2002**, *7*, 569-579.

(8) Qiu, Y.; Park, K. *Adv. Drug Deliv. Rev.* **2001**, *53*, 321-339.

(9) Peppas, N. A. *Curr. Opin. Colloid Interface Sci.* **1997**, *2*, 531-537.

(10) Malinsky, M. D.; Kelly, K. L.; Schatz, G. C.; Van Duyne, R. P. *J. Am. Chem. Soc.* **2001**, *123*, 1471-1482.

(11) Holtz, J. H.; Asher, S. A. *Nature* **1997**, *389*, 829-832.

(12) Larsson, C.; Rodahl, M.; Hook, F. *Anal. Chem.* **2003**, *75*, 5080-5087.

(13) Nakamura, R.; Muguruma, H.; Ikebukuro, K.; Sasaki, S.; Nagata, R.; Karube, I.; Pedersen, H. *Anal. Chem.* **1997**, *69*, 4649-4652.

(14) Conboy, J. C.; McReynolds, K. D.; Gervay-Hague, J.; Saavedra, S. S. *J. Am. Chem. Soc.* **2002**, *124*, 968-977.

(15) Moller, G.; Harke, M.; Motschmann, H.; Prescher, D. *Langmuir* **1998**, *14*, 4955-4957.

(16) Roberts, C.; Chen, C. S.; Mrksich, M.; Martichonok, V.; Ingber, D. E.; Whitesides, G. M. *J. Am. Chem. Soc.* **1998**, *120*, 6548-6555.

(17) Xia, Y. N.; Kim, E.; Mrksich, M.; Whitesides, G. M. *Chem. Mat.* **1996**, *8*, 601-603.

(18) Deng, L.; Mrksich, M.; Whitesides, G. M. *J. Am. Chem. Soc.* **1996**, *118*, 5136-5137.

(19) Blodgett, K. B. *J. Am. Chem. Soc.* **1934**, *56*, 495.

(20) Blodgett, K. B.; Langmuir, I. *Phys. Rev.* **1937**, *51*, 964-982.

(21) Decher, G. *Science* **1997**, *277*, 1232-1237.

(22) Decher, G.; Hong, J. D.; Schmitt, J. *Thin Solid Films* **1992**, *210*, 831-835.

(23) Decher, G.; Hong, J. D. *Ber. Bunsen-Ges. Phys. Chem. Chem. Phys.* **1991**, *95*, 1430-1434.

(24) Lvov, Y. M.; Price, R. R.; Selinger, J. V.; Singh, A.; Spector, M. S.; Schnur, J. M. *Langmuir* **2000**, *16*, 5932-5935.

(25) Sukhorukov, G. B.; Mohwald, H.; Decher, G.; Lvov, Y. M. *Thin Solid Films* **1996**, *285*, 220-223.

(26) Ai, H.; Fang, M.; Jones, S. A.; Lvov, Y. M. *Biomacromolecules* **2002**, *3*, 560-564.

(27) He, J. A.; Valluzzi, R.; Yang, K.; Dolukhanyan, T.; Sung, C. M.; Kumar, J.; Tripathy, S. K.; Samuelson, L.; Balogh, L.; Tomalia, D. A. *Chem. Mat.* **1999**, *11*, 3268-3274.

(28) Heflin, J. R.; Figura, C.; Marciu, D.; Liu, Y.; Claus, R. O. *Appl. Phys. Lett.* **1999**, *74*, 495-497.

(29) Lenahan, K. M.; Wang, Y. X.; Liu, Y. J.; Claus, R. O.; Heflin, J. R.; Marciu, D.; Figura, C. *Adv. Mater.* **1998**, *10*, 853-855.

(30) Fulda, K. U.; Kampes, A.; Krasemann, L.; Tieke, B. *Thin Solid Films* **1998**, *329*, 752-757.

(31) Lvov, Y.; Ariga, K.; Onda, M.; Ichinose, I.; Kunitake, T. *Langmuir* **1997**, *13*, 6195-6203.

(32) Sukhishvili, S. A.; Granick, S. *J. Am. Chem. Soc.* **2000**, *122*, 9550-9551.

(33) Yang, S. Y.; Mendelsohn, J. D.; Rubner, M. F. *Biomacromolecules* **2003**, *4*, 987-994.

(34) Yang, S. Y.; Rubner, M. F. *J. Am. Chem. Soc.* **2002**, *124*, 2100-2101.

(35) Stockton, W. B.; Rubner, M. F. *Macromolecules* **1997**, *30*, 2717-2725.

(36) Brown, K. R.; Lyon, L. A.; Fox, A. P.; Reiss, B. D.; Natan, M. J. *Chem. Mat.* **2000**, *12*, 314-323.

(37) Musick, M. D.; Pena, D. J.; Botsko, S. L.; McEvoy, T. M.; Richardson, J. N.; Natan, M. J. *Langmuir* **1999**, *15*, 844-850.

(38) Musick, M. D.; Keating, C. D.; Keefe, M. H.; Natan, M. J. *Chem. Mat.* **1997**, *9*, 1499-1501.

(39) Lvov, Y.; Ariga, K.; Ichinose, I.; Kunitake, T. *J. Chem. Soc.-Chem. Commun.* **1995**, 2313-2314.

(40) Decher, G.; Lehr, B.; Lowack, K.; Lvov, Y.; Schmitt, J. *Biosens. Bioelectron.* **1994**, *9*, 677-684.

(41) Baur, J. W.; Rubner, M. F.; Reynolds, J. R.; Kim, S. *Langmuir* **1999**, *15*, 6460-6469.

(42) Hammond, P. T. *Curr. Opin. Colloid Interface Sci.* **1999**, *4*, 430-442.

(43) Groth, T.; Lendlein, A. *Angew. Chem.-Int. Edit.* **2004**, *43*, 926-928.

(44) Liang, Z. J.; Susha, A. S.; Yu, A. M.; Caruso, F. *Adv. Mater.* **2003**, *15*, 1849-1853.

(45) Nolte, A. J.; Rubner, M. F.; Cohen, R. E. *Langmuir* **2004**, *20*, 3304-3310.

(46) Lee, I. S.; Hammond, P. T.; Rubner, M. F. *Chem. Mat.* **2003**, *15*, 4583-4589.

(47) Wang, T. C.; Cohen, R. E.; Rubner, M. F. *Adv. Mater.* **2002**, *14*, 1534-1537.

(48) Joly, S.; Kane, R.; Radzilowski, L.; Wang, T.; Wu, A.; Cohen, R. E.; Thomas, E. L.; Rubner, M. F. *Langmuir* **2000**, *16*, 1354-1359.

(49) Lee, I.; Ahn, J. S.; Hendricks, T. R.; Rubner, M. F.; Hammond, P. T. *Langmuir* **2004**, *20*, 2478-2483.

(50) Berg, M. C.; Yang, S. Y.; Hammond, P. T.; Rubner, M. F. *Langmuir* **2004**, *20*, 1362-1368.

(51) Lee, I.; Zheng, H. P.; Rubner, M. F.; Hammond, P. T. *Adv. Mater.* **2002**, *14*, 572-577.

(52) Liu, X. Y.; Bruening, M. L. *Chem. Mat.* **2004**, *16*, 351-357.

(53) Sullivan, D. M.; Bruening, M. L. *Chem. Mat.* **2003**, *15*, 281-287.

(54) Balachandra, A. M.; Dai, J. H.; Bruening, M. L. *Macromolecules* **2002**, *35*, 3171-3178.

(55) Quinn, J. F.; Caruso, F. *Langmuir* **2004**, *20*, 20-22.

(56) Cho, J.; Caruso, F. *Macromolecules* **2003**, *36*, 2845-2851.

(57) Zhai, L.; Nolte, A. J.; Cohen, R. E.; Rubner, M. F. *Macromolecules* **2004**, *ACS ASAP*.

(58) Caruso, F.; Niikura, K.; Furlong, D. N.; Okahata, Y. *Langmuir* **1997**, *13*, 3427-3433.

(59) Nolan, C. M.; Serpe, M. J.; Lyon, L. A. *Biomacromolecules* **2004**, *ACS ASAP*.

(60) Serizawa, T.; Takeshita, H.; Akashi, M. *Langmuir* **1998**, *14*, 4088-4094.

(61) Serizawa, T.; Kamimura, S.; Akashi, M. *Colloid Surf. A-Physicochem. Eng. Asp.* **2000**, *164*, 237-245.

(62) Schrof, W.; Rozouvan, S.; Van Keuren, E.; Horn, D.; Schmitt, J.; Decher, G. *Adv. Mater.* **1998**, *10*, 338-341.

(63) Schmitt, J.; Decher, G.; Dressick, W. J.; Brandow, S. L.; Geer, R. E.; Shashidhar, R.; Calvert, J. M. *Adv. Mater.* **1997**, *9*, 61-65.

(64) Liu, Y. J.; Wang, A. B.; Claus, R. O. *Appl. Phys. Lett.* **1997**, *71*, 2265-2267.

(65) Hu, K.; Brust, M.; Bard, A. J. *Chem. Mat.* **1998**, *10*, 1160-1165.

(66) Jaffar, S.; Nam, K. T.; Khademhosseini, A.; Xing, J.; Langer, R.; Belcher, A. M. *Nano. Lett.* **2004**, *ACS ASAP*.

(67) Mamedov, A. A.; Belov, A.; Giersig, M.; Mamedova, N. N.; Kotov, N. A. *J. Am. Chem. Soc.* **2001**, *123*, 7738-7739.

(68) Peyratout, C. S.; Dahne, L. *Angew. Chem.-Int. Edit.* **2004**, *43*, 3762-3783.

(69) Donath, E.; Sukhorukov, G. B.; Caruso, F.; Davis, S. A.; Mohwald, H. *Angew. Chem.-Int. Edit.* **1998**, *37*, 2202-2205.

(70) Sukhorukov, G. B.; Shchukin, D. G.; Dong, W. F.; Mohwald, H.; Lulevich, V. V.; Vinogradova, O. I. *Macromol. Chem. Phys.* **2004**, *205*, 530-535.

(71) Shchukin, D. G.; Patel, A. A.; Sukhorukov, G. B.; Lvov, Y. M. *J. Am. Chem. Soc.* **2004**, *126*, 3374-3375.

(72) Shchukin, D. G.; Sukhorukov, G. B.; Mohwald, H. *Angew. Chem.-Int. Edit.* **2003**, *42*, 4472-4475.

(73) Schuetz, P.; Caruso, F. *Chem. Mater.* **2004**, *ACS ASAP*.

(74) Liang, Z. J.; Susha, A.; Caruso, F. *Chem. Mat.* **2003**, *15*, 3176-3183.

(75) Chiarelli, P. A.; Johal, M. S.; Holmes, D. J.; Casson, J. L.; Robinson, J. M.; Wang, H. L. *Langmuir* **2002**, *18*, 168-173.

(76) Cho, J.; Char, K. *Langmuir* **2004**, *20*, 4011-4016.

(77) Lee, S. S.; Lee, K. B.; Hong, J. D. *Langmuir* **2003**, *19*, 7592-7596.

(78) Lee, S. S.; Hong, J. D.; Kim, C. H.; Kim, K.; Koo, J. P.; Lee, K. B. *Macromolecules* **2001**, *34*, 5358-5360.

(79) Jiang, C. Y.; Markutsya, S.; Tsukruk, V. V. *Langmuir* **2004**, *20*, 882-890.

(80) Tanchak, O. M.; Barrett, C. J. *Chem. Mater.* **2004**, *16*, 2734-2739.

(81) Shiratori, S. S.; Rubner, M. F. *Macromolecules* **2000**, *33*, 4213-4219.

(82) Yoo, D.; Shiratori, S. S.; Rubner, M. F. *Macromolecules* **1998**, *31*, 4309-4318.

(83) Xie, A. F.; Granick, S. *J. Am. Chem. Soc.* **2001**, *123*, 3175-3176.

(84) Rmaile, H. H.; Schlenoff, J. B. *Langmuir* **2002**, *18*, 8263-8265.

(85) Dubas, S. T.; Schlenoff, J. B. *Langmuir* **2001**, *17*, 7725-7727.

(86) Dubas, S. T.; Schlenoff, J. B. *Macromolecules* **1999**, *32*, 8153-8160.

(87) Lulevich, V. V.; Vinogradova, O. I. *Langmuir* **2004**, *20*, 2874-2878.

(88) Izumrudov, V.; Sukhishvili, S. A. *Langmuir* **2003**, *19*, 5188-5191.

(89) Kovacevic, D.; van der Burgh, S.; de Keizer, A.; Stuart, M. A. C. *J. Phys. Chem. B* **2003**, *107*, 7998-8002.

(90) Hiller, J.; Rubner, M. F. *Macromolecules* **2003**, *36*, 4078-4083.

CHAPTER 3

POLYELECTROLYTE INTERACTIONS WITH CORE AND CORE/SHELL MICROGELS

3.1 Introduction

As outlined in Chapter 2, polyelectrolyte interactions have been used to construct functional thin films and micro/nano capsules for various applications. This chapter describes how charged poly(*N*-isopropylacrylamide-*co*-acrylic acid) (pNIPAm-co-AAc) core and core/shell microgels and the linear polyelectrolyte poly(allylamine hydrochloride) (PAH) interact in aqueous colloidal dispersions. In particular, how does a porous microgel with anionic charge distributed throughout its structure, interact with the linear polycation PAH. Can the PAH penetrate the microgel and neutralize its internal charges or does the PAH just stick to the periphery of the microgel? Also, is it possible for PAH to penetrate a neutral pNIPAm shell to interact with a charged core?

Charge-charge interactions for similar systems have been exploited to form physically crosslinked hydrogel particles[1] for applications in drug delivery.[2-7] As mentioned in Chapter 2, studies have been completed that exploit charge complexation to fabricate micro/nano capsules by building up polyelectrolyte multilayers on *non-porous* colloidal nanoparticles followed by nanoparticle dissolution.[8-18] Similar to the work presented in this chapter, polyelectrolyte interaction with pNIPAm-co-AAc polymeric thin films were also completed to determine the interaction/effects of various polyelectrolytes on the behavior (swelling and temperature responsivity) of the thin film.[19-21] Polyelectrolytes have also been shown to be useful for gene delivery where

electrostatic interactions between the polyelectrolyte and DNA are used to form nanoparticles which can transfect cells, degrade and deliver their genetic payload.[22-24]

The first part of this chapter describes the interaction of pNIPAm-co-AAc microgels with PAH in aqueous colloidal dispersions. Using photon correlation spectroscopy (PCS), microgel hydrodynamic radius (R_h) was monitored as a function of PAH addition and correlated to the charge of the microgels by monitoring the electrophoretic mobility. Using these complementary techniques it was found that PAH is able to penetrate the microgel network and interact with the acid groups, as noted by a decrease in R_h as a function of PAH addition. It was further shown that microgel stability is dependent on the stoichiometry between NH_2:AAc on the PAH and microgel, respectively. For example, if the microgel solution was titrated with very small aliquots of PAH such that the stoichiometric equivalence point between AAc and NH_2 is approached slowly, the R_h of the microgels decrease until the equivalence point, followed by aggregation at supra-stoichiometric PAH additions. Electrophoretic mobility measurements indicate that the microgel incrementally goes from anionic to neutral to cationic, with the critical aggregation point correlating with an electrophoretic mobility close to zero. This aggregation behavior is attributed to colloidal instability due to a decrease of electrical double layer repulsion and an inhomogeneous charge distribution on the microgel. In contrast, if the microgels are titrated with large aliquots of PAH such that a single addition of PAH traverses the stoichiometric equivalence point, the microgel switches rapidly from anionic to cationic as observed by electrophoretic mobility measurements, and no aggregation is observed. As further evidence of PAH penetration and neutralization of the microgel, deswelling thermodynamics were probed using

temperature programmed PCS to monitor the lower critical solution temperature (LCST) of the dispersion. LCST data shows that microgels at pH 6.5 (greater than the AAc pKa), in the absence of PAH, have a higher LCST than when PAH is present at 1:1 AAc:NH_2 stoichiometry indicating that PAH neutralizes the negative charge inside the microgel network. However, if an excess amount of PAH is added to the microgel solution, the LCST shifts back to higher temperatures presumably due to the presence of a net positive charge in the microgel network.

The second part of this chapter describes the interactions of pNIPAm-co-AAc (core)/pNIPAm (shell) microgels with PAH in aqueous colloidal dispersions. PCS was used to probe microgel R_h and thermoresponsivity as a function of PAH addition. This study showed that PAH is able to interact with the pNIPAm-co-AAc core acid groups through the neutral pNIPAm shell. This behavior was also studied as a function of pNIPAm shell thickness.

3.2 Experimental

Materials All reagents were purchased from Sigma-Aldrich unless otherwise specified. *N*-Isopropylacrylamide (NIPAm) was re-crystallized from hexanes (J.T. Baker) and dried under vacuum prior to use. Acrylic acid (AAc) was distilled under reduced pressure. *N*,*N*'-Methylene(bisacrylamide) (BIS), ammonium persulfate (APS), and sodium dodecyl sulfate (SDS) were used as received. Poly(allylamine hydrochloride) (PAH), MW 70 000, was used as received. All water used throughout this investigation was house distilled, deionized to a resistance of at least 18 MΩ (Barnstead Thermolyne E-Pure system), and then filtered through a 0.2 μm filter for particulate removal.

pNIPAm-co-AAc Core Microgel Synthesis. Microgels were synthesized via aqueous free-radical precipitation polymerization, as previously described.[25,26] The syntheses were carried out by fixing the total monomer concentration constant at 70 mM and the AAc mole percent constant at 10% while varying the BIS mole percent between 2 and 10% and adjusting the NIPAm concentration accordingly. Polymerization was performed in a three-neck, 200 mL round-bottom flask (RBF) containing a magnetic stir bar. To this reactor, 100 mL of a filtered (0.2 μm filter, Pall Gelman Metricel), aqueous solution of NIPAm, BIS, and the surfactant SDS (1 mM) was added. This solution was heated to ~70 °C while degassing with N_2 and stirring vigorously for ~1 hr. After 1 hr, AAc was added to the flask in order to bring the total monomer concentration up to 70 mM. Once the AAc was added, polymerization was immediately initiated by injection of 1.0 mL of a hot (~70°C), APS solution (0.3 mmol). The solution immediately turned turbid indicating successful initiation. This solution was allowed to heat and stir for an additional 5 hours while under a constant flow of N_2 gas. Following synthesis the particles were purified by dialysis against water for ~2 weeks with the water being changed twice per day, using 10 000 MW cut-off dialysis tubing (VWR).

pNIPAm-co-AAc Core/pNIPAm Shell Microgel Synthesis. pNIPAm shells of varying thicknesses were added to the above core particles using "seed and feed" precipitation polymerization. This technique uses previously synthesized core particles in their collapsed state (seed) as hydrophobic nuclei for subsequent polymer addition (feed) in a precipitation polymerization reaction, as previously reported by our group.[25,26] For the particular microgels used in this chapter 7.5 mL of the core particle solution was added to a 100 mL RBF along with 12 mL H_2O. 0.02 mmol SDS was added to the

solution, which was heated to 70 ºC while degassing with N_2 and stirring for 1 h. Shell monomers (NIPAm and BIS) were dissolved in 5 mL H_2O and heated to 70 ºC prior to addition. Following 1 h the shell monomer solution was added to the core solution bringing the total volume of the solution to 24.5 mL. For these syntheses the shell thickness was controlled by varying the shell monomer solution concentration from 20 to 40 mM (after dilution in the reaction solution). This solution was allowed to mix, by stirring, for several minutes. Free radical polymerization was initiated by adding 0.04 mmol APS. Polymerization was allowed to continue for 5 h at 70 ºC. Following synthesis the particles were purified by dialysis against water for ~2 weeks with the water being changed daily, using 10 000 MW cut-off dialysis tubing. It should be noted that 2% BIS was used for all core/shell microgels in this chapter.

Microgel Titrations with PAH Titration of the microgels used in this chapter was accomplished by adding aliquots of 0.0526 monoM (moles/L monomer) PAH solution to a dilute solution of core or core/shell microgels with C_{AAc} ~2.0 x 10^{-5} M, at pH 6.5 (~0.001 ionic strength) contained in a plastic cuvette. Each microgel solution was made immediately before each measurement. The radius and thermoresponsive behavior of the microgels following titration was followed using photon correlation spectroscopy (PCS, Protein Solutions Inc.).

Photon Correlation Spectroscopy The use of PCS as a tool for determining mean particle size and particle size distributions has been described previously[27] and used for these microgel systems in the past.[25,26] Briefly, a diluted microgel solution was added to a plastic cuvette and inserted into the PCS cuvette holder, which was equipped with a Peltier device for sample temperature control. Laser light (783.9 nm) was introduced to

the sample via a single-mode optical fiber and scattered light was collected by a fiber coupled avalanche photodiode detector at 90º. The random intensity fluctuations of the scattered radiation were used to calculate an autocorrelation decay, which can then be related to the particle translational diffusion coefficient (Dynamics Software Version 5.25.44). The average hydrodynamic radius was then calculated using the Stokes-Einstein equation. For equilibrium microgel radius measurements each sample was allowed to equilibrate at 25 ºC for 10 minutes. The reported radius value was an average of 15 individual radius measurements using a 10 sec integration time for each measurement. For thermoresponsivity measurements the microgels were first titrated with a given amount of PAH. The solution was then heated and the microgel size determined every 2 ºC by letting the sample equilibrate at each temperature for 10 minutes. At each temperature 5 consecutive runs were performed where each run was composed of 15 individual radius measurements using a 10 sec integration time for each measurement.

Electrophoretic Mobility Measurements Electrophoretic mobility, (μm/s)/(V/cm), was used as an indicator of microgel charge upon PAH addition using a ZetaPlus instrument (Brookhaven Instruments Corporation). The samples were prepared in the same way they were prepared for PCS analysis and each reported mobility value is the mean value of 10 runs. The software provided by the instrument manufacturer was used to calculate the electrophoretic mobility.

3.3 Results and Discussion

3.3.1 pNIPAm-co-AAc Core Microgel Interaction with PAH

PCS was used to determine the interaction of PAH with pNIPAm-co-AAc microgels by following the average microgel R_h as a function of PAH addition. As shown in Figure 3-1, for titration of 10% AAc/2% BIS microgels, the R_h decreases from ~250 nm to ~100 nm upon the addition of PAH, regardless of the PAH aliquot volume. In the case of 2.0 and 5.0 μL PAH aliquot additions, the microgel R_h increases to ~250 nm upon subsequent PAH addition. This value is important to note because it is approximately the same as the particle R_h at this pH in the absence of PAH. This swelling behavior is most likely due to the microgel network structure becoming internally crosslinked by AAc/NH_2 interactions and saturated with PAH. The saturation of the particle with PAH should in turn produce an excess positive charge in the microgel network, thereby resulting in Coulombic swelling. Another interesting feature of Figure 3-1 is the behavior seen upon adding 0.5 μL PAH aliquots to the system. As the [AAc]/[NH_2] ratio approaches 1, the microgel R_h decreases, as seen in the case of the 2.0 and 5.0 μL PAH aliquot additions. However, in the 0.5 μL PAH aliquot addition case the microgels tend to significantly increase in R_h indicating system aggregation rather than Coulombic swelling. Further evidence of aggregation can be seen from the particle size histograms obtained from PCS in Figure 3-2. From the figure it can be seen that in the case of 0.5 μL PAH aliquot addition the population breadth increases dramatically as a function of PAH addition, which is indicative of aggregation. This behavior was not observed for the 5.0 μL PAH aliquot addition case. One way to explain this behavior is by considering the fact that as the microgels reach the neutralization point, the electrical repulsion between

the microgel particles is decreased and van der Waals attraction may dominate the microgel dispersion in aqueous system. Thus, the energy barrier that prevents particle collisions may be decreased resulting in aggregation of the microgels on the time scale of the experiment.[28,29] However, this mechanism is not the most likely source of aggregation in this system, since neutral pNIPAm microgels of this material have a low Hamaker constant and do not tend to aggregate at temperatures below the LCST. Another way to describe this behavior is to consider the homogeneity (or lack thereof) of absorption of PAH on the microgels. It is most likely the case that the absorption of PAH is extremely inhomogeneous resulting in microgels that have patchy charge distribution. To a first approximation, this should occur due to simple geometrical reasons. During the neutralization of microgels containing a low density of negative charge with a high charge density polyelectrolyte such as PAH, it is unlikely that all sites are neutralized at 1:1 stoichiometry. Due to this patchy charge distribution, when the microgels collide they should have a high tendency to aggregate at the point of slightly suprastoichiometric AAc:NH_2 values.[30,31] Figure 3-3 shows a schematic of the proposed aggregation mechanism.

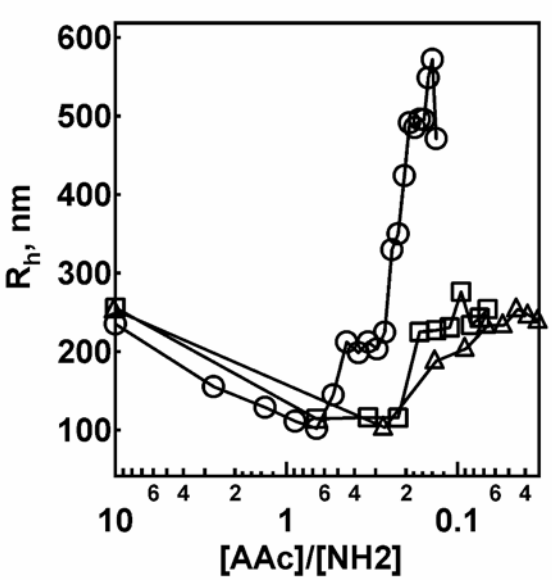

Figure 3-1. Titration plots for 10% AAc, 2% BIS microgels upon the addition of 0.5 (○), 2.0 (□), and 5.0 (△) μL PAH aliquots. The dramatic increase in particle size past the stoichiometric point for microgels titrated with 0.5 μL PAH aliquots is due to particle aggregation.

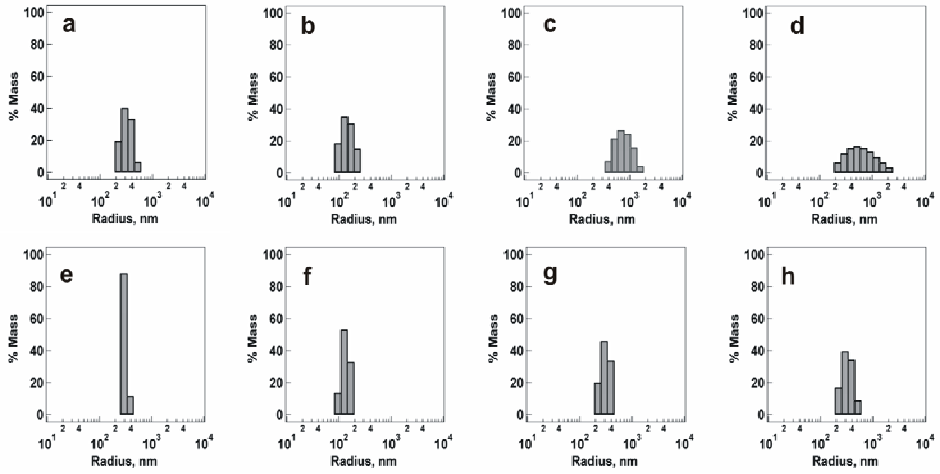

Figure 3-2. Histograms for the 0.5 and 5.0 μL PAH aliquot addition cases for 2% BIS crosslinked microgels. As shown in panels (a-d) for the 0.5 μL PAH aliquot addition as PAH is titrated into the system in small aliquots the system goes from a point of high monodispersity before PAH addition (a) to a point of minimum radius (b) then as more PAH is added to the system the radius distribution significantly increases with a shift to extremely high radii indicative of aggregation (c and d). As shown in panels (e-h) for the 5.0 μL PAH aliquot addition as PAH is titrated into the system in large aliquots the system goes from a point of high monodispersity before PAH addition (e) to a point of minimum radius upon the first addition of PAH (f) to a point of high radius and high monodispersity (g and h) indicative of osmotic/Coulombic swelling. [AAc]/[NH_2] for (b) is .67, (c) .19, (d) .13, (f) .27, (g) .067, (h) .033.

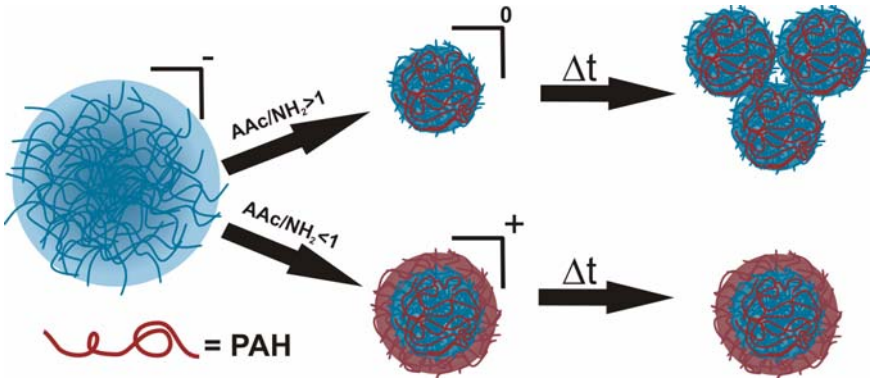

Figure 3-3. PAH is adsorbed to the microgel in a "patchy" fashion in the case of small PAH aliquot addition ($AAc/NH_2>1$) so microgel collisions over time results in aggregation. If PAH is added in larger aliquots ($AAc/NH_2<1$) the microgels are quickly stabilized by positive charge so microgel collisions over time does not result in aggregation.

To determine if microgel crosslink density has an effect on the interactions between PAH and AAc, titration experiments were conducted exactly as outlined above using core microgels containing 10% BIS and 10% AAc. As seen in Figure 3-4, the same qualitative trends are obtained as were seen for the 2% BIS titrations. For the 2.0 and 5.0 μL PAH aliquot additions the microgels are colloidally stable at all stoichiometries, but in the case of the 0.5 μL PAH aliquot addition, the microgels again aggregate. One important difference that must be pointed out between the 10% and 2% BIS microgel titrations is the magnitude of the deswelling upon PAH addition. In the 2% BIS case the magnitude of collapse is much greater than that for the 10% BIS microgels upon PAH addition. This can be understood by taking into account the fact that the 10% BIS microgels have a greater network density than the 2% BIS microgels, thus allowing for a smaller change in equilibrium swelling degree upon the addition of PAH.

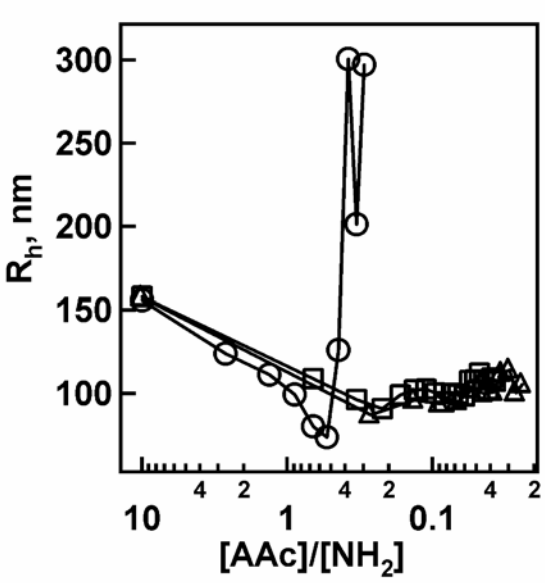

Figure 3-4. Titration plots for of 10% AAc, 10% BIS microgels upon the addition of 0.5 (○), 2.0 (□), and 5.0 (△) μL PAH aliquots. The dramatic increase in particle size past the stoichiometric point for microgels titrated with 0.5 μL PAH aliquots is due to particle aggregation.

Electrophoretic mobility measurements were made for the pNIPAm-co-AAc microgels containing 2% BIS upon addition of 0.5 and 5.0 μL PAH aliquots to verify the above claims of microgel neutralization and charge reversal. To interpret the data it is important to keep in mind that uncharged (no AAc) pNIPAm microgels have approximately zero electrophoretic mobility under the conditions that these experiments were conducted, Figure 3-5. Also, the electrophoretic mobility of a simple PAH solution is not measurable due to the small scattering cross-section of the PAH chains. Figure 3-6 shows that the microgels initially display a negative electrophoretic mobility due to the deprotonated AAc groups on the pNIPAm-co-AAc microgels. As PAH is titrated into the solution in 0.5 μL aliquots, the microgel electrophoretic mobility slowly approaches zero. At ~1:1 AAc:NH_2 the average electrophoretic mobility is approximately zero, as might

be expected for a 1:1 acid:base stoichiometry. As more PAH is added to the system, the electrophoretic mobility then reverses to positive values due to the excess charge present in the microgel. If, on the other hand, the electrophoretic mobility is followed as a function of 5.0 μL PAH aliquot additions, the behavior is very different. This result can be seen in Figure 3-7, where following the first 5.0 μL PAH aliquot the average electrophoretic mobility reverses from a negative to a positive value. In light of these results, the data shown in Figures 3-1 and 3-4 can be understood. If excess amounts of PAH are added to the system (2.0 and 5.0 μL case) the microgel rapidly reverses charge from negative to positive never reaching a point of instability. In contrast, 0.5 μL PAH aliquot additions cause the critical aggregation (neutralization) point to be reached, whereupon the microgels are able to approach one another and aggregate due to the inhomogeneous charge distribution present on the microgels.

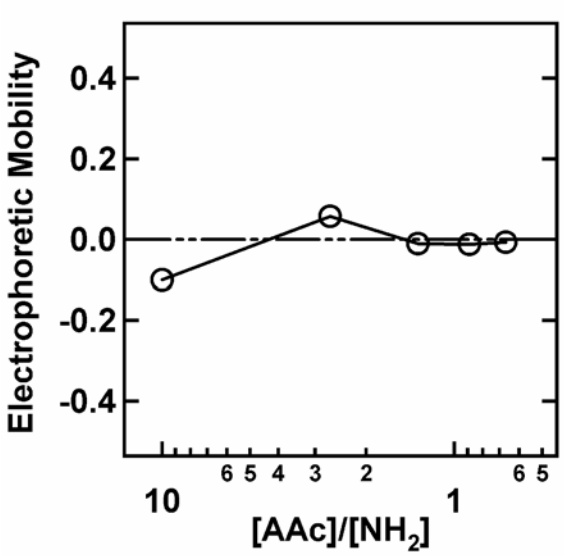

Figure 3-5. Electrophoretic mobility values as a function of PAH addition for 2% BIS, 98% NIPAm microgels at pH 6.5.

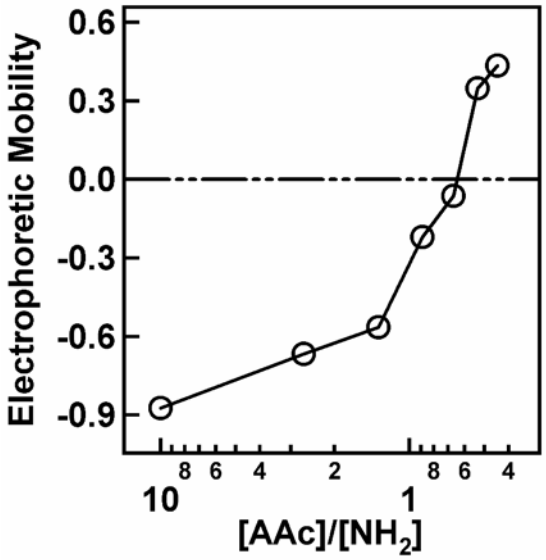

Figure 3-6. Electrophoretic mobility values as a function of PAH addition for 10% AAc, 2% BIS microgels upon 0.5 μL PAH aliquot additions.

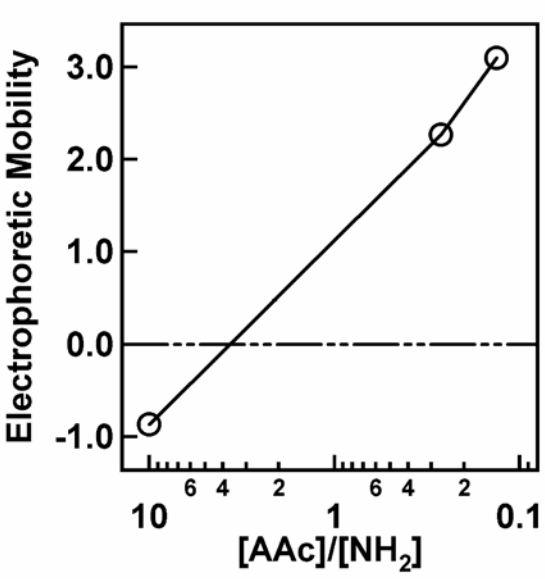

Figure 3-7. Electrophoretic mobility values as a function of PAH addition for 10% AAc, 2% BIS microgels upon 5.0 μL PAH aliquot additions.

To investigate the influence of PAH on the thermal deswelling of pNIPAm-AAc microgels, we determined the particle R_h as a function of temperature at various microgel:PAH stoichiometries (Figure 3-8). This figure shows a series of volume phase transition curves obtained by PCS for pNIPAm-co-AAc microgels at pH 3.0, where the particles are essentially electroneutral, and 6.5, where the particles are anionic due to AAc deprotonation. Figure 3-8 shows that the pNIPAm-co-AAc microgels at pH 3.0 have the characteristic LCST behavior at ~31 ºC while the microgels at pH 6.5 are not thermoresponsive over the temperature range probed.[26,32] However, when pNIPAm-co-AAc microgels at pH 6.5 are titrated with PAH such that AAc:NH_2 is 1:1 the microgel LCST shifts to ~ 31 ºC. This behavior suggests that the microgel structure is becoming fully neutralized due to the AAc-NH_2 interactions, where the NH_2 groups are capable of neutralizing the deprotonated AAc sites inside the microgel network. This observation

also indicates that the microgels are extremely porous allowing for very efficient interactions between AAc and PAH throughout the network, thereby resulting in efficient neutralization of the microgels. It is also interesting to note the microgel R_h following PAH addition. The measured particle R_h is much smaller that the R_h of the native microgel at pH 3.0, illustrating the additional crosslinking present in the systems where PAH is added. Figure 3-8 also shows the effect of the addition of excess PAH to the pNIPAm-co-AAc microgels, where it can be seen that the LCST is not observed over this temperature range. This is most likely an effect of excess PAH present in the microgel. This excess PAH adds positive charge to the microgel structure, resulting in Coulombic repulsion, which can shift the LCST to higher temperatures. Another observation is the microgel R_h in the excess PAH case is larger than that of the AAc:NH_2 ~1:1 complex particle. Conversely, this R_h is not as large as it was at pH 6.5 prior to PAH addition, where the microgel is solvated due to osmotic swelling and charge repulsion. This behavior is most likely due to the physical bonds between AAc:NH_2 in the microgel network restricting the microgel from swelling to its full extent. Although this behavior has been observed by others studying polyelectrolyte interactions with thin films composed of pNIPAm-co-AAc,[19-21] such studies have not previously been reported for microgels.

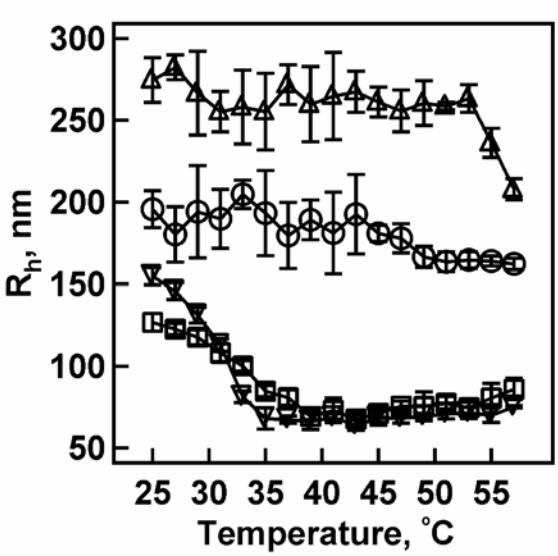

Figure 3-8. Volume phase transition curves for 10% AAc, 2% BIS microgels at pH 6.5 (△), pH 3.0 (▽), pH 6.5 with [AAc]/[NH_2] = 0.9 (□), and pH 6.5 with [AAc]/[NH_2] = 0.26 (○). The LCST for microgels at pH 6.5 with [AAc]/[NH_2] = 0.9 is very close to the LCST observed for pH 3.0, indicating charge neutralization due to AAc/NH_2 complexation. When excess PAH is added, the LCST is no longer observed due to Coulombic repulsion in the cationic network.

3.3.2 pNIPAm-co-AAc Core/pNIPAm Shell Microgel Interaction with PAH

PCS was used to characterize the interactions between PAH and pNIPAm-co-AAc core/pNIPAm shell microgels as a function of shell thickness. We wanted to know if PAH is capable of penetrating the neutral pNIPAm shell in order to complex the charges on the pNIPAm-co-AAc core. If this is possible we wanted to determine the pNIPAm shell thickness dependence. Specifically, can a thick pNIPAm shell hinder PAH interaction with the core?

To answer these questions the average microgel R_h was monitored for pNIPAm-co-AAc core microgels (the same cores used in previous section, 10% AAc, 2% BIS) containing pNIPAm shells made from 20 mM (thin) and 40 mM (thick) monomer solutions. Figure 3-9 shows the results for titration of core/thin shell microgels with PAH.

It can be seen from the figure that, regardless of PAH aliquot volume, the microgel R_h generally decreases from ~240 nm to ~100 nm and then increases to ~150 nm as a function of PAH addition due to PAH crosslinking the core AAc groups. The increase in microgel R_h at high PAH concentration is most likely due to Coulombic swelling in the core of the microgel. It is pointed out that no microgel aggregation is apparent regardless of the PAH aliquot volume. This same general behavior can be seen in Figure 3-10 for PAH addition to core/thick shell microgels. The microgel R_h generally decreases from ~220 nm to ~150 nm upon the addition of PAH again independent of PAH aliquot volume with no microgel aggregation. In this case the microgel was less responsive, i.e. changed less from its initial R_h, than the microgel with a thinner shell. These results can be understood by taking into account recent results from our group that show a core in a core/shell microgel is more compressed as the shell thickness increases resulting in a core that has less volume.[33,34] If this is the case, a core/thin shell microgel should respond to PAH addition more than a core/thick shell microgel. Another interesting point is that the microgels show no aggregation independent of pNIPAm shell thickness and PAH aliquot addition. This is most likely the result of the pNIPAm shell sterically protecting the cores from aggregating at points of instability (neutrality). A schematic summarizing these results can be seen in Figure 3-11.

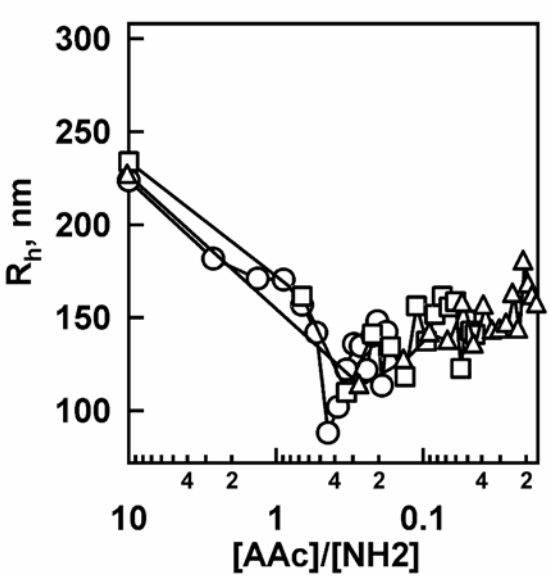

Figure 3-9. Titration plots for 10% AAc, 2% BIS core/thin shell microgels upon the addition of 0.5 (○), 2.0 (□), and 5.0 (△) μL PAH aliquots. The microgels interact with PAH through the pNIPAm shell without aggregation.

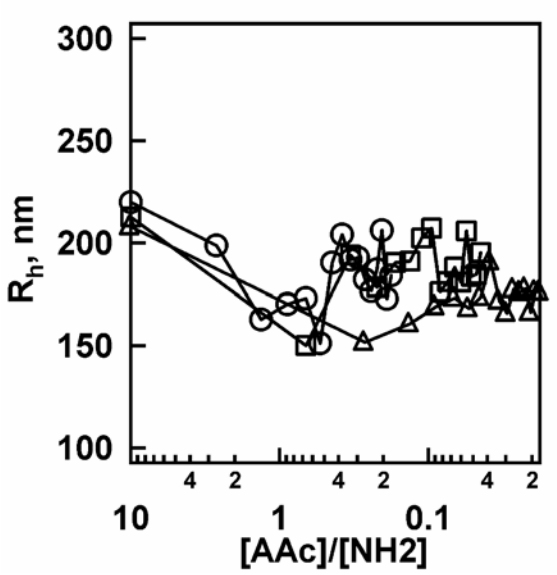

Figure 3-10. Titration plots for 10% AAc, 2% BIS core/thick shell microgels upon the addition of 0.5 (○), 2.0 (□), and 5.0 (△) μL PAH aliquots. Even though a thick pNIPAm shell is present the PAH is still able to interact with the charged core without aggregation.

Figure 3-11. PAH interacts with the charged core, through the neutral pNIPAm shell, crosslinking its structure. Also, the shell component acts to stabilize the microgel from aggregation over time by preventing the charged cores, in their neutral state, from colliding.

To further probe the interactions between PAH and the core/shell microgels, thermal deswelling was monitored using PCS (as in previous section) at various microgel:PAH stoichiometries. Figure 3-12 shows a series of volume phase transition curves obtained by PCS for core/thick shell microgels at pH 3.0, where the particles are essentially electroneutral, and 6.5, where core is anionic due to AAc deprotonation. Figure 3-12 shows that the microgels at pH 3.0 exhibit the characteristic LCST behavior at ~31 ºC while the microgels at pH 6.5 have an LCST but at ~45 ºC. The LCST for the microgels at pH 6.5, as previously explained our group, has been attributed to shell assisted deswelling, i.e. the pNIPAm shell deswelling can force the charged core to collapse.[26,33,34] If the above core/shell microgels at pH 6.5 are titrated with PAH such that AAc:NH_2 is 1:1 the microgel LCST shifts back to ~31 ºC. This behavior suggests that the core is becoming fully neutralized due to the AAc-NH_2 interactions This observation also indicates that core/shell microgels are extremely porous allowing for very efficient interactions between core AAc and PAH even through a pNIPAm protecting shell layer. Figure 3-12 also shows the effect of excess PAH addition to the core/shell microgels, where it can be seen that the LCST is still observed close to ~31 ºC. The LCST is not shifted to high temperature most likely due to shell assisted deswelling; even though the core has excess positive charge the shell can deswell it.

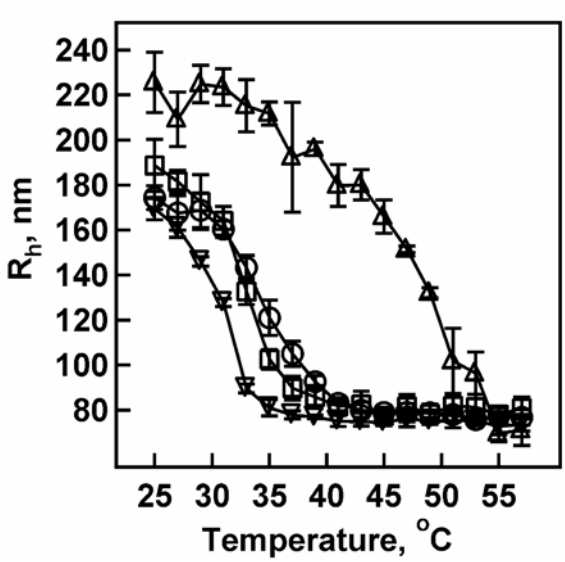

Figure 3-12. Volume phase transition curves for pNIPAm-co-AAc core/thick pNIPAm shell microgels at pH 6.5 (△), pH 3.0 (▽), pH 6.5 with [AAc]/[NH_2] = 0.9 (□), and pH 6.5 with [AAc]/[NH_2] = 0.26 (○). The LCST for microgels at pH 6.5 with [AAc]/[NH_2] = 0.9 is very close to the LCST observed for pH 3.0, indicating charge neutralization due to AAc/NH_2 complexation. When excess PAH is added, the LCST does not significantly shift to high temperature most likely due to the shell forcing the core to deswell even though it has excess positive charge.

3.4 Conclusions

The findings in this chapter indicate that anionic microgels electrostatically bind to polycationic PAH regardless of whether the core is "protected" by a pNIPAm shell. These electrostatic interactions are important to understand if they are to be used for any applications. In the next chapter the electrostatic interactions between anionic microgels and polycationic PAH are exploited to construct thin films in a LbL fashion.

REFERENCES

(1) Mende, M.; Petzold, G.; Buchhammer, H. M. *Colloid Polym. Sci.* **2002**, *280*, 342-351.

(2) Antipov, A. A.; Sukhorukov, G. B.; Donath, E.; Mohwald, H. *J. Phys. Chem. B* **2001**, *105*, 2281-2284.

(3) Chellat, F.; Tabrizian, M.; Dumitriu, S.; Chornet, E.; Rivard, C. H.; Yahia, L. *J. Biomed. Mater. Res.* **2000**, *53*, 592-599.

(4) Kamiya, N.; Klibanov, A. M. *Biotechnol. Bioeng.* **2003**, *82*, 590-594.

(5) Ko, J. A.; Park, H. J.; Hwang, S. J.; Park, J. B.; Lee, J. S. *Int. J. Pharm.* **2002**, *249*, 165-174.

(6) Munjeri, O.; Collett, J. H.; Fell, J. T. *J. Control. Release* **1997**, *46*, 273-278.

(7) Hoffman, A. S. *Adv. Drug Deliv. Rev.* **2002**, *54*, 3-12.

(8) Liang, Z. J.; Susha, A.; Caruso, F. *Chem. Mat.* **2003**, *15*, 3176-3183.

(9) Lulevich, V. V.; Vinogradova, O. I. *Langmuir* **2004**, *20*, 2874-2878.

(10) Shchukin, D. G.; Patel, A. A.; Sukhorukov, G. B.; Lvov, Y. M. *J. Am. Chem. Soc.* **2004**, *126*, 3374-3375.

(11) Sukhorukov, G. B.; Shchukin, D. G.; Dong, W. F.; Mohwald, H.; Lulevich, V. V.; Vinogradova, O. I. *Macromol. Chem. Phys.* **2004**, *205*, 530-535.

(12) Shchukin, D. G.; Sukhorukov, G. B.; Mohwald, H. *Angew. Chem.-Int. Edit.* **2003**, *42*, 4472-4475.

(13) Kato, N.; Schuetz, P.; Fery, A.; Caruso, F. *Macromolecules* **2002**, *35*, 9780-9787.

(14) Cho, J.; Caruso, F. *Macromolecules* **2003**, *36*, 2845-2851.

(15) Pastoriza-Santos, I.; Scholer, B.; Caruso, F. *Adv. Funct. Mater.* **2001**, *11*, 122-128.

(16) Caruso, F.; Yang, W. J.; Trau, D.; Renneberg, R. *Langmuir* **2000**, *16*, 8932-8936.

(17) Gittins, D. I.; Caruso, F. *Adv. Mater.* **2000**, *12*, 1947-1949.

(18) Donath, E.; Sukhorukov, G. B.; Caruso, F.; Davis, S. A.; Mohwald, H. *Angew. Chem.-Int. Edit.* **1998**, *37*, 2202-2205.

(19) Yoo, M. K.; Sung, Y. K.; Lee, Y. M.; Cho, C. S. *Polymer* **2000**, *41*, 5713-5719.

(20) Yoo, M. K.; Sung, Y. K.; Lee, Y. M.; Cho, C. S. *Polymer* **1998**, *39*, 3703-3708.

(21) Yoo, M. K.; Sung, Y. K.; Cho, C. S.; Lee, Y. M. *Polymer* **1997**, *38*, 2759-2765.

(22) Reineke, T. M.; Davis, M. E. *Bioconj. Chem.* **2003**, *14*, 247-254.

(23) Rungsardthong, U.; Ehtezazi, T.; Bailey, L.; Armes, S. P.; Garnett, M. C.; Stolnik, S. *Biomacromolecules* **2003**, *4*, 683-690.

(24) Sergeyev, V. G.; Novoskoltseva, O. A.; Pyshkina, O. A.; Zinchenko, A. A.; Rogacheva, V. B.; Zezin, A. B.; Yoshikawa, K.; Kabanov, V. A. *J. Am. Chem. Soc.* **2002**, *124*, 11324-11333.

(25) Gan, D.; Lyon, L. A. *J. Am. Chem. Soc.* **2001**, *123*, 7511-7517.

(26) Jones, C. D.; Lyon, L. A. *Macromolecules* **2000**, *33*, 8301-8306.

(27) Pecora, R. *Dynamic Light Scattering*; Plenum Press: New York, 1985.

(28) Sato, T.; Ruch, R. *Stabilization of Colloidal Dispersions by Polymer Adsorption*; Marcel Dekker, Inc.: New York, 1980; Vol. 9.

(29) Evans, D. F.; Wennerstrom, H. *The Colloidal Domain: Where Physics, Chemistry, Biology, and Technology Meet, 2nd*; VCH Publishers, Inc.: New York, 1998.

(30) Elimelech, M.; Williams, R. A.; Jia, X.; Gregory, J. *Particle Deposition and Aggregation: Measurement, Modeling and Simulation*; Butterworth-Heinemann Ltd: Oxford, 1997.

(31) Gregory, J. *J. Colloid Interface Sci.* **1973**, *42*, 448-456.

(32) Pelton, R. *Adv. Colloid. Interface Sci.* **2000**, *85*, 1-33.

(33) Jones, C. D.; Lyon, L. A. *Macromolecules* **2003**, *36*, 1988-1993.

(34) Jones, C. D.; Lyon, L. A. *Langmuir* **2003**, *19*, 4544-4547.

CHAPTER 4

LAYER-BY-LAYER DEPOSITION OF THERMORESPONSIVE MICROGEL THIN FILMS

4.1 Introduction

This chapter describes the assembly of thermoresponsive, 4-acrylamidofluorescein (*) modified poly(*N*-isopropylacrylamide-*co*-acrylic acid) (pNIPAm-co-AAc*) microgel thin films using Layer-by-Layer (LbL) assembly.[1-3] PNIPAm-co-AAc* microgels were synthesized and incorporated into thin films by taking advantage of the charge-charge interactions between polyanionic pNIPAm-co-AAc microgels and polycationic poly(allylamine hydrochloride) (PAH), as discussed in Chapter 3. LbL assembly was performed on 3-aminopropyltrimethoxysilane (APTMS) functionalized glass substrates using passive polyelectrolyte adsorption, as described in Chapter 2. Using this method, pNIPAm-co-AAc* microgel thin films were constructed as confirmed by fluorescence microscopy. Experiments were also conducted to investigate the effect of microgel deposition temperature on the resultant film morphology and thermoresponsivity. In addition, the thermoresponsivity of the pNIPAm-co-AAc* microgel thin films was studied with respect to microgel layer number, microgel deposition conditions and pH. This behavior was related to the solution behavior of the microgels where the films exhibited enhanced thermoresponsivity and hindered deswelling at pH's below and above the pK_a of the microgel acrylic acid (AAc) groups, respectively.[4]

4.2 Experimental

Materials All reagents were purchased from Sigma-Aldrich unless otherwise specified. *N*-Isopropylacrylamide (NIPAm) was re-crystallized from hexanes (J.T. Baker) and dried under vacuum prior to use. Acrylic acid (AAc) was distilled under reduced pressure. *N*,*N*'-Methylene(bisacrylamide) (BIS), ammonium persulfate (APS) was used as received. Poly(allylamine hydrochloride) (PAH), MW 70 000, was used as received. 3-Aminopropyltrimethoxysilane (APTMS) was purchased from United Chemical Technologies Inc. and was kept in a desiccator for storage. The oxygen scavenger propyl gallate was used as received (Acros). The glass substrates used were 24 x 50 mm Fisher Finest brand cover glass obtained from Fisher Scientific. Sulfuric acid and 30% hydrogen peroxide (J.T. Baker) were used to make Piranha cleaning solutions. Eight-chamber perfusion gaskets (9 mm diameter chambers, 1 mm deep) were obtained from Molecular Probes. Cuvettes were obtained from VWR. 95% and absolute ethanol was used for various purposes in this investigation. All water used throughout this investigation was first house distilled and then deionized to a resistance of at least 18 MΩ (Barnstead Thermolyne E-Pure system) and then filtered through a 0.2 μm filter for further purification.

Glass Substrate Preparation APTMS functionalized glass cover slips were used as positively charged substrates for alternate layer deposition. Prior to functionalization the glass substrates were cleaned as previously outlined.[5] Glass cover slips were first wiped clean of any dust using a Kimwipe (Kimberly-Clark). Following this step the substrates were immersed in hot Piranha solution, 4:1 H_2SO_4 : H_2O_2, (~70 °C) to remove any organics from the substrate surface (**Caution**: Piranha solutions react violently in the

presence of many organic compounds and should be handled with extreme caution). Next, the substrates were rinsed copiously with H_2O then copiously with 95% ethanol. Following this rinsing procedure the substrates were immersed in an ethanolic (absolute ethanol) 1% APTMS solution for ~2 hrs. After 2 hrs the substrates were removed from the APTMS solution and again rinsed copiously with 95% ethanol. These substrates were stored in 95% ethanol for no longer than 5 days prior to use. Prior to alternate layer deposition, these substrates were rinsed with H_2O and dried under a stream of nitrogen gas.

4-Acrylamidofluorescein (AFA) Monomer Synthesis This monomeric dye was synthesized in a similar manner as previously reported.[6] Acetone was dried overnight with $CaSO_4$ then filtered to remove particulate matter. 4-Aminofluorescein (1.25 g, 3.6 mmol) was suspended in 50 mL of dry acetone in a 50 mL round bottom flask along with a magnetic stir bar. The dark orange suspension was submersed and stirred in an ice bath for 15 min. Acryloyl chloride (0.32 mL, 3.9 mmol) was dissolved in 0.5 mL of dry acetone and this solution was added drop-wise to the suspension at 0 °C over 10 minutes. The stirring solution was allowed to react for 3 hours while warming to ambient temperature. The yellow crystals were then separated from the solution via filtration and washed with cold acetone and diethyl ether. The final product was recrystallized twice from anhydrous THF and dried in vacuo overnight. The substituted phenyl proton resonances of the product were shifted downfield relative to those of the starting fluorescein, as shown previously for AFA.[7] ^{1}H NMR (300 MHz, DMSO-d_6, δ): 5.82 (2d, 1 H), 6.33 (2d, 1 H), 6.4–6.7 (m, 1 H), 7.21 (d, 1 H), 8.39 (d, 1 H), 10.8 (s, 1 H). FAB-MS ($C_{23}H_{15}O_6N$) calcd 401.4, $[M + H]^+$ 402.1. λ_{ex}= 478 nm and λ_{em}= 525 nm.

Microgel Synthesis The same batch of microgels were used as the polyanion in the alternate layer deposition protocol. These microgels had a molar composition of 88.5% NIPAm, 1.4% BIS, 10% AAc, and 0.1% 4-acrylamidofluorescein and were synthesized via aqueous free-radical precipitation polymerization as previously described in Chapter 1, using 140 mM total monomer concentration.[8,9] Polymerization was carried out in a three-neck, 200 mL round-bottom flask to which 100 mL of filtered, aqueous solution of NIPAm and BIS was added. This solution was heated to ~70 °C while degassing with N_2 gas and stirring vigorously for ~1 hr. After 1 hr, AAc and 4-acrylamidofluorescein solutions were added to the round-bottom flask in order to bring the total monomer concentration up to 140 mM. Once the additional monomers were added, the reaction was immediately initiated by injection of 1 mL of a hot (~ 70°C), 2 mM aqueous APS solution. The solution immediately turned turbid indicating successful initiation. This solution was allowed to heat and stir for an additional 4 hours while purging with N_2 gas. Following synthesis the particles were purified by dialysis against water for ~2 weeks with the water being changed twice per day, using 10 000 MW cut-off dialysis tubing (VWR).

Alternate Layer Deposition Alternate layer deposition was performed on APTMS functionalized cover glass following the well known protocol introduced by Decher and co-workers, as discussed in Chapter 2.[1-3] In this case pNIPAm-co-AAc* microgels were used as the polyanion. Since each microgel has a high number of negative charges, surface charge reversal should be possible, although the mechanism of reversal will be different from the traditional linear polyelectrolyte systems. PAH was used as the polycation and has a well-known deposition behavior.

Each cover slip was fitted with an 8-chamber perfusion gasket and exposed to aqueous microgel/PAH solutions. Each chamber on the glass cover slip was used as a separate deposition chamber, which allows for the independent deposition of multiple thicknesses of microgel/PAH films on the same substrate. Each microgel layer deposition was performed in the same manner, as outlined in Figure 4-1. First, the substrate was exposed to a 10% v/v aqueous microgel solution. This microgel solution was allowed to remain in contact with the substrate for ~1 hr. Second, the substrate was rinsed copiously with water and exposed to a 0.0526 monoM (moles/L monomer) PAH solution. The PAH was allowed to remain in contact with the substrate for ~20 min. The substrate was again rinsed copiously with water and exposed to the microgel solution. This process was repeated until the desired number of microgel layers was achieved. For the investigations in this chapter, up to 8 microgel layers were assembled. This same protocol was followed for films assembled at high temperatures (~60°C) where the substrate was heated for 1 hr while microgel deposition took place but was kept at room temperature for PAH deposition.

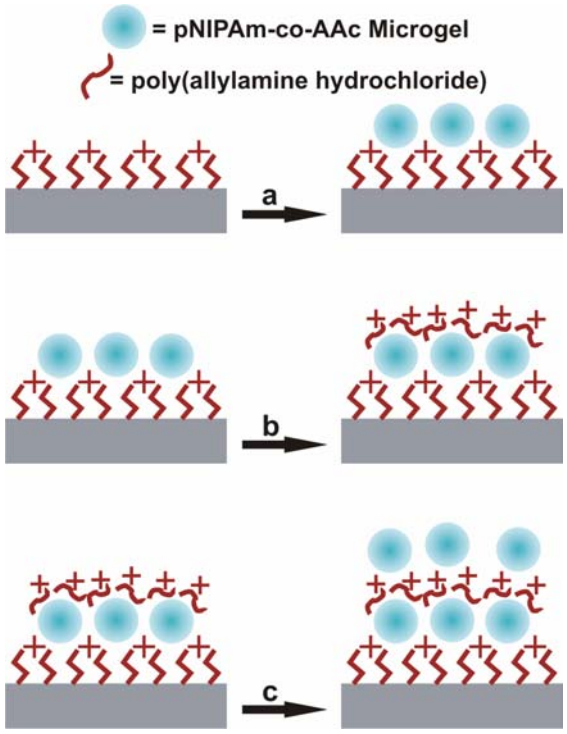

Figure 4-1. Idealized schematic for the alternate layer deposition scheme followed in this study (not meant to imply any order or morphology of the thin film). (a), microgel attachment to APTMS functionalized glass substrate (b), addition of PAH (c), subsequent addition of microgel results in their attachment to the PAH layer. PAH and microgel not drawn to scale.

Photon Correlation Spectroscopy The thermoresponsive behavior of the microgels was confirmed by photon correlation spectroscopy (PCS, Protein Solutions Inc.) prior to their use in thin film fabrication. This technique was explained in Chapter 3 so an explanation of the technique will not be given here. For these measurements, each sample was allowed to equilibrate at each temperature for 3 min. At each temperature 5 consecutive runs were performed where each run was composed of 15 individual radius measurements using a 5 sec integration time for each measurement.

Fluorescence Microscopy Fluorescence microscopy was used to image the films composed of pNIPAm-co-AAc* microgels. An Olympus IX 70 inverted microscope equipped with a mercury arc lamp was used. Images were captured using a Coolsnap CCD camera (RS Photometrics). An Olympus 100x UplanFl 1.30 NA oil immersion objective was used for imaging. Film temperature was controlled using a microscope objective heater (Bioptechs) and a Peltier temperature stage (Physitemp). For experiments requiring multiple images of a single film over time, propyl gallate (~200 μM) was added as an oxygen scavenger to reduce the degree of oxygen-induced photobleaching of AFA.[10]

Film Thermoresponsivity Measurements The thermoresponsivity of the thin films was determined using a Photon Technologies International fluorometer to detect elastic light scattering from the film. For these experiments the glass substrates were cut to the necessary dimensions in order to allow light to pass through the center of the desired microgel thin film. The cut slide was then inserted into a plastic cuvette at a 45° angle with respect to the excitation beam and was oriented properly to eliminate direct reflection of light into the photomultiplier tube. In addition, the slide was inserted into the cuvette so the microgel thin film was backside illuminated. The cuvette was then filled with the desired pH solution, which was either pH 3.0 or pH 6.5 (~0.001 ionic strength), and inserted into the fluorometer. The film was illuminated at λ=550 nm while scattering was monitored at λ=550 nm. The slit widths on the fluorometer were set to ~2 nm bandpass. Films were cycled in temperature between 25°C and 42°C while scattering intensity was monitored. Each film was allowed to equilibrate at each temperature for ~1.5 hrs prior to measurement of the intensity. It should be noted that in each case the

same film was used at pH 3.0 and pH 6.5, where the measurement at pH 3.0 was always conducted first followed by immersion in the pH 6.5 solution. Figure 4-2 shows a schematic of the experiment.

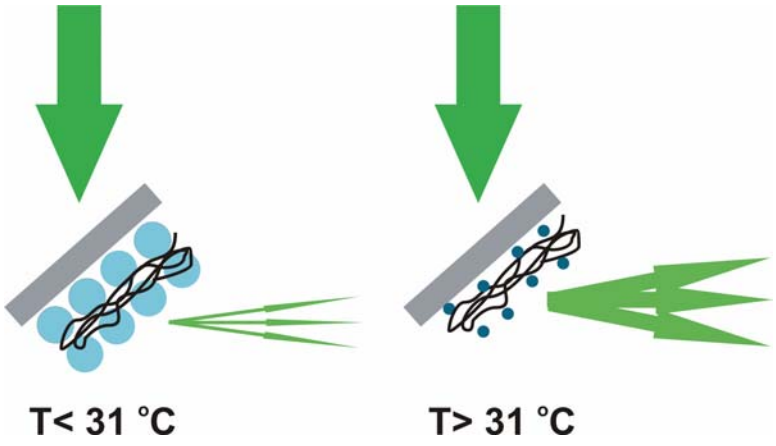

Figure 4-2. Light scattering from films at temperatures below and above the LCST of the microgels that make up the film. At temperatures below ~31 °C the microgel thin films are more swollen with water than the films above ~31 °C, which results in less intense light scattering.

4.3 Results and Discussion

An important feature of these thin films is the presence of thermoresponsive pNIPAm-co-AAc* microgels (polyanion). With the use of pNIPAm-co-AAc* microgels we can construct thin polymeric films with micro-to-nanoscale structure, which collapse in response to temperatures above their lower critical solution temperature (LCST). As discussed in Chapter 1, pNIPAm-*co*-AAc microgels, at pH's<pK_a of the AAc groups, undergo a sharp volume phase transition (VPT) at ~31°C where the water inside the microgels is expelled in an entropically favored transition. At this point the microgel refractive index increases, therefore increasing the refractive index contrast with respect

to water, resulting in an increase in scattered light intensity. Another important feature of pNIPAm-*co*-AAc microgels is the presence of the AAc groups, which imparts pH responsivity to the microgels. At a given temperature, if the pH of the surrounding solution is above the pK_a of the microgel AAc groups, the microgel will swell and the VPT will become hindered due to charge repulsion of the AAc groups inside of the microgel network. The behavior seen for pNIPAm-*co*-AAc microgels is also seen for the pNIPAm-co-AAc* microgels used in this study, as observed in Figure 4-3(a), which shows that the 4-acrylamidofluorescein bound to the microgel is not interfering with the characteristic microgel deswelling behavior. Seen in Figure 4-3(b) is the intensity profile obtained for the microgels via photon correlation spectroscopy.

Microgel thin films were constructed with 1-8 microgel layers at deposition temperatures of ~25 °C and ~60 °C by using the electrostatic interactions between the microgels and PAH, discussed in Chapter 3. Due to the fluorescence of the 4-acrylamidofluorescein bound to the microgels, it was possible to image the films using conventional fluorescence microscopy.

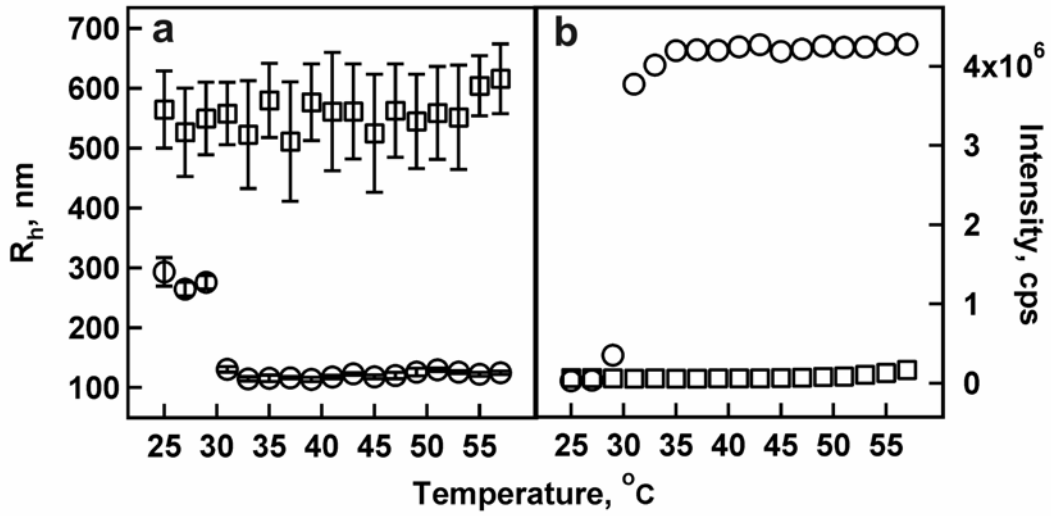

Figure 4-3. Volume phase transition curves (a) taken from photon correlation spectroscopy measurements for pNIPAm-co-AAc* microgels at pH 3.0 (circles) and pH 6.5 (squares). As the pH is increased above the pK_a of the AAc groups, the phase transition of the microgels is suppressed due to Coulombic repulsion. The intensity profile (b) shows the microgels ability to scatter more light when collapsed vs. swollen. Error bars represent one standard deviation about the average of five measurements.

Room Temperature Deposition. Shown in Figure 4-4 is a series of fluorescence microscope images of the films after alternate layer deposition at ~25 °C. From these images it can be seen that 1 microgel layer displays a sparse distribution of particles. This deposition behavior has been previously observed in other particle based alternate layer deposition schemes[11-16] and is related to Coulombic repulsion between particles as would be expected for a Frumkin-type adsorption isotherm with a repulsive particle-particle interaction potential. This is similar to the self-regulation mechanism observed for traditional polyelectrolyte layer deposition, as discussed in Chapter 2. Despite the sparse microgel distribution for the first layer, the addition of more layers appears to produce homogenous films. Microgel layer number 3 shows an increase in particle density with respect to layer 1 with a moderate improvement in the homogeneity of the film. The

increase in particle density for the 3 layer film is interesting because it shows the microgels adsorbing to the surface rather than building up a true multilayer structure in the z-dimension. This result can be explained by considering the possibility of PAH neutralizing and reversing the charge on the microgels bound to the surface therefore removing the repulsive interaction between particles bound to the surface and the particles in solution. This will allow microgels to access the surface and therefore bind to the free charged amine sites.[11-13] This process will proceed until the surface becomes saturated with microgels. Once the surface is saturated with microgels buildup in the z-dimension can proceed. Microgel layer number 5 shows a dramatic increase in particle density and film homogeneity. This film also begins to show signs of multilayer buildup most likely a result of surface charge saturation by the microgels therefore allowing for multilayer buildup in the z-dimension. Figure 4-5 illustrates the layer buildup process outlined above. This model takes into account penetration of PAH into the microgels, as discussed in Chapter 3.

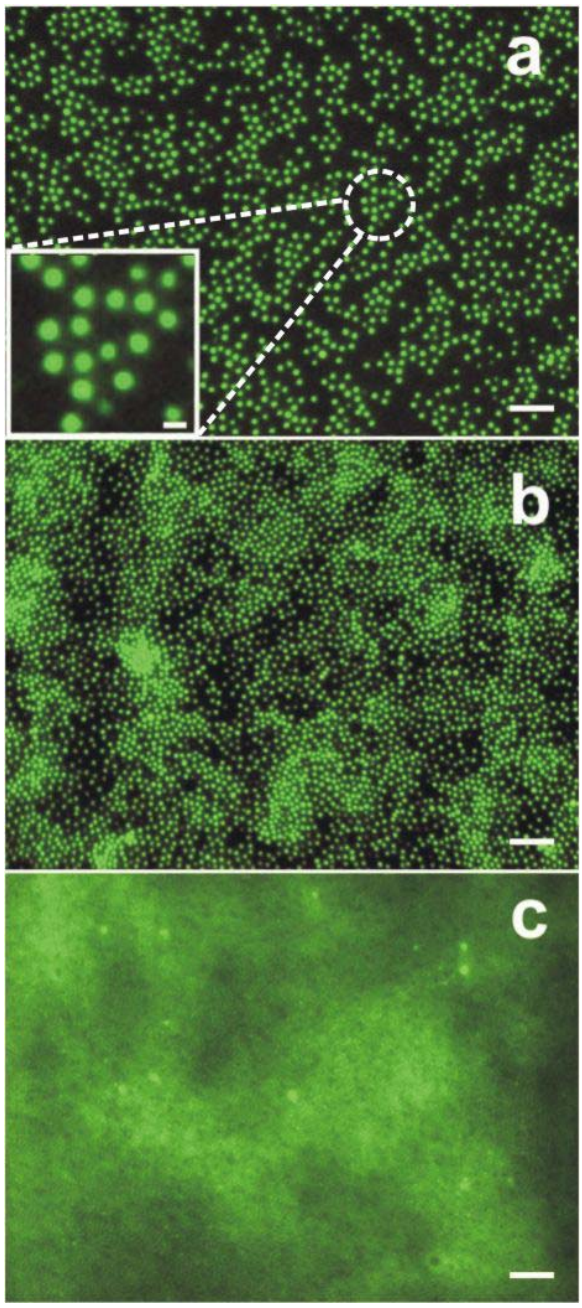

Figure 4-4. Fluorescence microscope images taken of (a) 1, (b) 3, and (c) 5 microgel layer films, which were deposited at ~25 °C, scale bar is 5 μm. From the pictures it can be noted that as the microgel layer number increases the microgel density increases indicating a multilayer buildup mechanism. Inset shows a expanded view of a region on the 1 layer film where the scale bar is 1 μm.

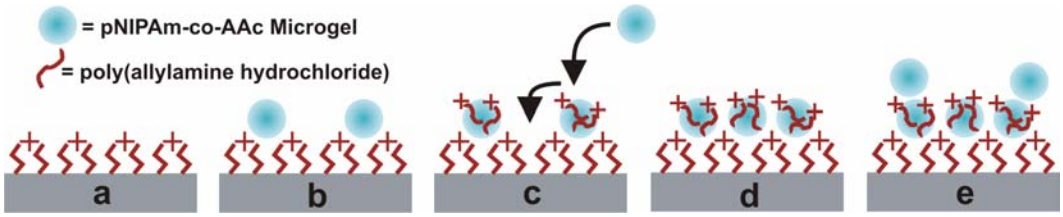

Figure 4-5. Schematic of the proposed microgel thin film buildup mechanism. (a), blank, APTMS functionalized, glass substrate surface, (b), one layer of microgel added to the substrate in a self-regulated fashion (c), addition of PAH to the microgel layer results in charge neutralization/reversal on the microgel surface, which allows microgels to again access the surface and electrostatically attach (d), subsequent addition of PAH to the microgel surface followed by (e), attachment of another microgel layer in a self regulated fashion. PAH and microgel not drawn to scale.

High Temperature Deposition Shown in Figure 4-6 is a series of fluorescence microscope images of films after alternate layer deposition of the microgels at ~60 °C. Film construction under these conditions is expected to follow a different pathway than the films deposited at room temperature. This difference is expected because at temperatures above the VPT, the microgels will be deswollen (see Figure 4-3). Deswollen microgels will have an increased diffusion rate as well as a higher propensity to aggregate due to hydrophobic interactions. Because of these hydrophobic interactions at high temperatures these films are expected to be less homogenous than the films assembled at room temperature. From the images in Figure 4-6 it can be seen that the 1 microgel layer film deposited at high temperature looks very similar the 1 microgel layer film deposited at room temperature. It is interesting to note the size differences between the microgels deposited at room and high temperatures, as seen in the insets of Figures 4-4 and 4-6, where the microgels deposited at high temperature seem to be smaller in diameter than the microgels deposited at room temperature. This result is to be expected if it is assumed that the microgels are attaching to the surface deswollen and becoming

pinned in the deswollen state due to their attachment to the surface. Microgel layer number 3 again shows an increase in microgel coverage, with respect to the 1 microgel layer. It is also interesting to note the film morphology differences between the 3 layer films deposited at room temperature and high temperature. The films deposited at high temperature seem to be less homogenous than the films deposited at room temperature. This is most likely due to the microgels aggregating on the surface due to particle-particle hydrophobic interactions. Microgel layer number 5 still shows no film homogenation, due to particle-particle aggregation, even though the microgel density has increased.

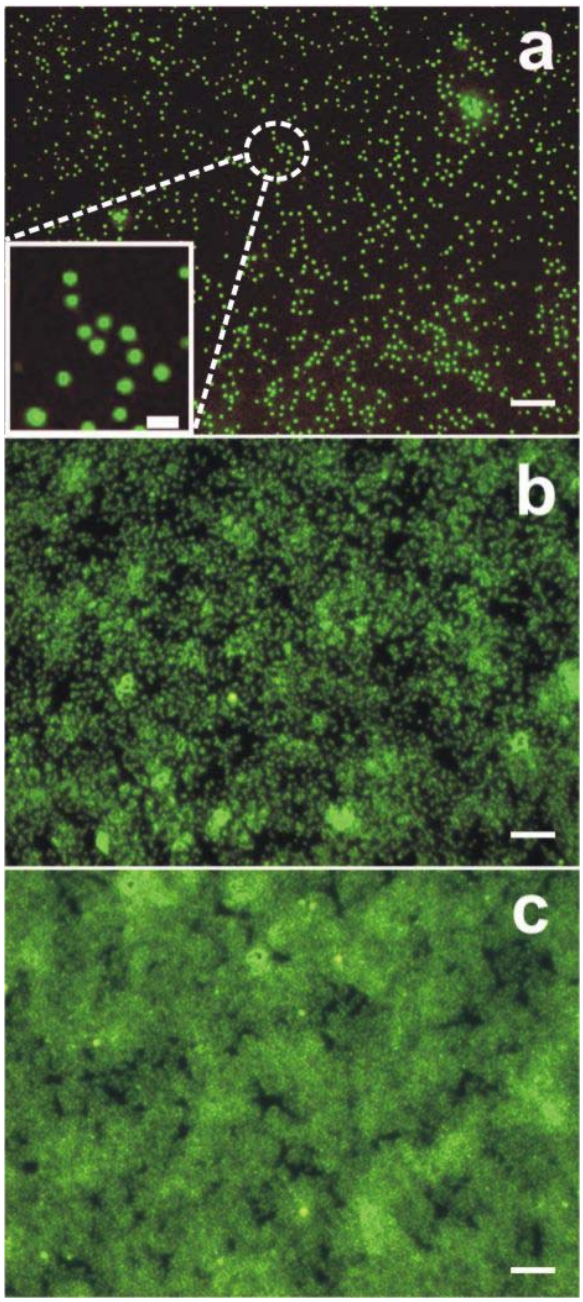

Figure 4-6. Fluorescence microscope images taken of (a) 1, (b) 3, and (c) 5 microgel layer films, which were deposited at ~60 °C, scale bar is 5 μm. From the pictures it can be noted that as the microgel layer number increases the microgel density increases indicating a multilayer buildup mechanism. From these pictures in can also be seen that the films are much less homogenous than the films deposited at 25 ºC, which is most likely due to microgel aggregation at high temperatures. Inset shows an expanded view of a region on the 1 layer film where the scale bar is 1 μm.

Film Thermoresponsivity Another important feature of these films is their ability to swell and deswell in response to temperature. Figure 4-7 shows fluorescence microscope images of a 3 layer film which was oscillated in temperature between ~25 °C and ~45 °C and held at each temperature for 1.5 hrs. It is important to note from these images that as the temperature is increased to temperatures above the LCST of the microgels, 45 °C, the microgel size seems to decrease as should be expected. From the images it can also be seen that the films do not significantly restructure, which illustrates the structural integrity of the films to multiple temperature oscillations. This film strength may be attributed to enforced AAc/PAH binding as the microgels deswell and expose more AAc groups for binding.[17,18] Others have shown that similar pNIPAm-AAc microgels display a high surface charge in the deswollen state due to the phase separation of the hydrophilic acid groups to the particle surface upon pNIPAm collapse.[17,18] It is reasonable to assume, therefore, that the particle attachment to the film will not be significantly weakened by thermal cycling.

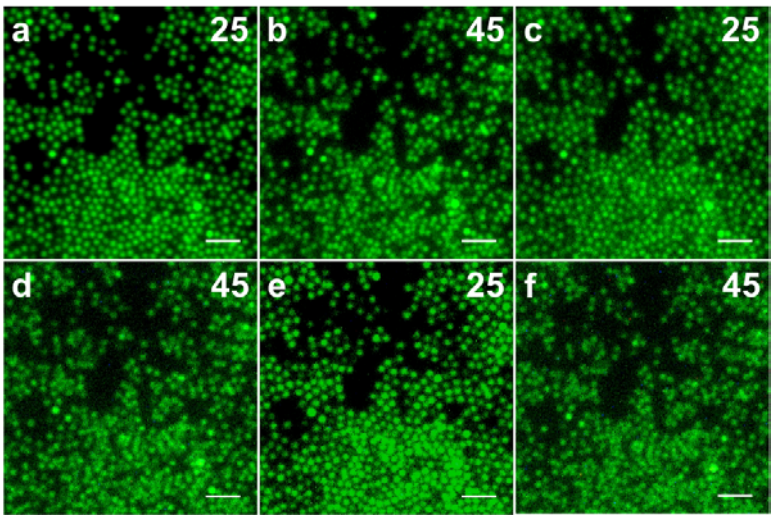

Figure 4-7. Fluorescence microscope images taken of a 3 layer film which was oscillated in temperature between ~25 °C and ~45 °C in chronological order beginning with ~25 °C (a) and ending at ~45 °C (f). The images show that the microgel size appears smaller at ~45 °C which is consistent with the microgels deswelling above their LCST. From the images it can also be seen that the film does not significantly restructure, illustrating its structural integrity in response to temperature. Scale bar is 5 μm.

Figure 4-8 shows the thermoresponsivity of the 3 and 7 layer microgel films in pH 3.0 and 6.5 solutions deposited at ~25 °C and ~60 °C. These measurements were made using scattering data obtained from fluorometry, as described above, where each point represents either the average value of the equilibrated scattering intensity over the final 30 minutes of equilibration or the maximum number of points that could be obtained if the film was not equilibrated over the last 30 minutes of the measurement. Figure 4-8 shows that each film, regardless of microgel deposition temperature, was thermoresponsive although all to different degrees. Figure 4-8 (a, b) shows the 3 and 7 layer films deposited at room temperature in pH 3.0 and 6.5 solutions. It should be noted that the films in pH 3.0 solutions exhibit enhanced thermoresponsivity, indicated by the higher scattering intensity, over the same film in pH 6.5 solution. This result was solely

attributed to the negative charge on the microgels at pH 6.5 hindering the deswelling event. This result can also be seen for the films deposited at high temperature in Figure 4-8, panels c and d. A very interesting feature seen from the films deposited at room temperature, and partially from the films deposited at high temperature, is the observation that when the films are exposed to the pH 6.5 solution, the film thermoresponsivity decreases in a stepwise fashion rather than the thermoresponsivity immediately disappearing upon exposure to pH 6.5 solution. This behavior suggests to us a stepwise exchange of solvent from the inside of the microgels that make up the film and will be exploited in a subsequent chapter for small molecule uptake and release.

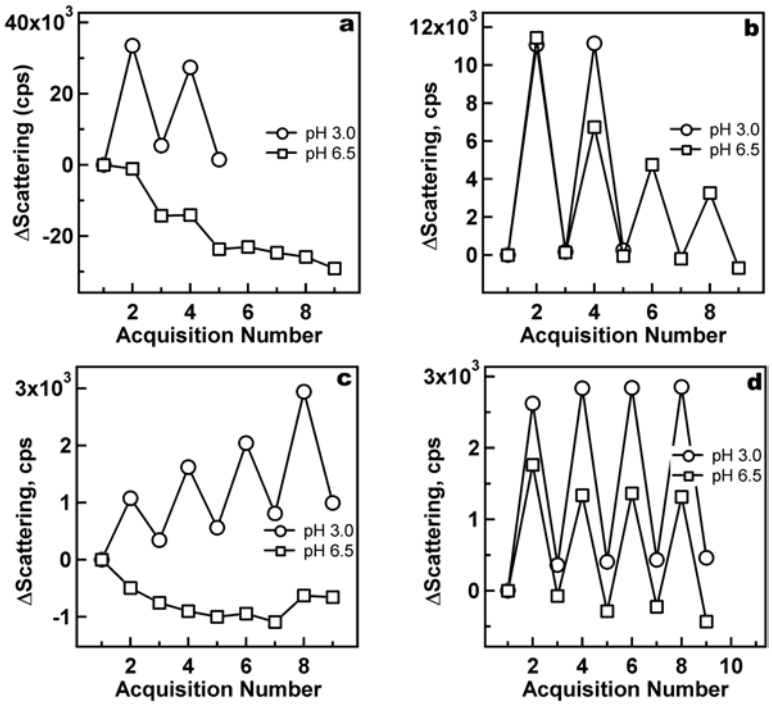

Figure 4-8. Film thermoresponsivity plots made from scattering data obtained from fluorometry experiments of 3 (panels a and c) and 7 (panels b and d) layer microgel films deposited at room temperature (panels a and b) and at high temperature (panels c and d) at pH 3.0 (circles) and pH 6.5 (squares). Each acquisition number corresponds to a specific monitoring temperature, where the odd numbers are 25 ºC and the even numbers are 42 ºC. Each point was normalized for the equilibrated scattering intensity of the film on its first measurement at 25 ºC. The plots show that all of the films at pH 3.0 are thermoresponsive with a decrease in thermoresponsivity when the film is exposed to pH 6.5 solution.

4.4 Conclusions

This chapter described the LbL buildup of thermoresponsive, thin polymeric films using electrostatic interactions between anionic microgels and polycationic PAH. Fluorescence microscopy was used to confirm the buildup mechanism. Particle layer deposition is thought to follow a pseudo-3D mechanism, where the first few particle exposures contribute to saturation of the substrate surface. Further exposures then proceed to build the film up in the z-dimension. Deposition at temperatures above the hydrogel particle deswelling temperature yields films with greater degrees of heterogeneity, perhaps due to hydrophobic aggregation of particles during deposition. Temperature dependent scattering data of as-prepared films verify that the films are strongly thermoresponsive below the AAc pK_a, while that thermoresponsivity decreases in a stepwise fashion upon exposure to pH values above the pK_a.

To a first approximation the pH dependent thermoresponsivity can be explained by just considering the charged state of the microgel, at a specific pH, and correlating that directly to the behavior of the film. For example, the microgels are anionic in solution at pH 6.5 and do not undergo a VPT (Figure 4-3) so likewise the film should not undergo a VPT. This interpretation is not complete and does not take into account the pH dependent ionic interactions that occur on the molecular level between the microgels and PAH. These pH dependent ionic interactions will be discussed in the next chapter.

REFERENCES

(1) Decher, G. *Science* **1997**, *277*, 1232-1237.

(2) Decher, G.; Hong, J. D.; Schmitt, J. *Thin Solid Films* **1992**, *210*, 831-835.

(3) Decher, G.; Hong, J. D. *Ber. Bunsen-Ges. Phys. Chem. Chem. Phys.* **1991**, *95*, 1430-1434.

(4) Serpe, M. J.; Jones, C. D.; Lyon, L. A. *Langmuir* **2003**, *19*, 8759-8764.

(5) Goss, C. A.; Charych, D. H.; Majda, M. *Anal. Chem.* **1991**, *63*, 85-88.

(6) Bruno, A. E.; Barnard, S.; Rouilly, M.; Waldner, A.; Berger, J.; Ehrat, M. *Anal. Chem.* **1997**, *69*, 507-513.

(7) Munkholm, C.; Parkinson, D. R.; Walt, D. R. *J. Am. Chem. Soc.* **1990**, *112*, 2608-2612.

(8) Gan, D.; Lyon, L. A. *J. Am. Chem. Soc.* **2001**, *123*, 7511-7517.

(9) Jones, C. D.; Lyon, L. A. *Macromolecules* **2000**, *33*, 8301-8306.

(10) Grunwell, J. R.; Glass, J. L.; Lacoste, T. D.; Deniz, A. A.; Chemla, D. S.; Schultz, P. G. *J. Am. Chem. Soc.* **2001**, *123*, 4295-4303.

(11) Serizawa, T.; Kamimura, S.; Akashi, M. *Colloid Surf. A-Physicochem. Eng. Asp.* **2000**, *164*, 237-245.

(12) Serizawa, T.; Takeshita, H.; Akashi, M. *Langmuir* **1998**, *14*, 4088-4094.

(13) Fulda, K. U.; Kampes, A.; Krasemann, L.; Tieke, B. *Thin Solid Films* **1998**, *329*, 752-757.

(14) Hu, K.; Brust, M.; Bard, A. J. *Chem. Mat.* **1998**, *10*, 1160-1165.

(15) Jaffar, S.; Nam, K. T.; Khademhosseini, A.; Xing, J.; Langer, R.; Belcher, A. M. *Nano. Lett.* **2004**, *ACS ASAP*.

(16) Mamedov, A. A.; Belov, A.; Giersig, M.; Mamedova, N. N.; Kotov, N. A. *J. Am. Chem. Soc.* **2001**, *123*, 7738-7739.

(17) Daly, E.; Saunders, B. R. *Phys. Chem. Chem. Phys.* **2000**, *2*, 3187-3193.

(18) Makino, K.; Agata, H.; Ohshima, H. *J. Colloid Interface Sci.* **2000**, *230*, 128-134.

CHAPTER 5

pH-DEPENDENT SWELLING BEHAVIOR OF MICROGEL THIN FILMS

5.1 Introduction

This chapter describes the complex, pH dependent ionic interactions between poly(*N*-isopropylacrylamide-*co*-acrylic acid) (pNIPAm-co-AAc) microgels and poly(allylamine hydrochloride) (PAH) in multilayer thin films.[1] These interactions were monitored using quartz crystal impedance (QCI) analysis and surface plasmon resonance spectroscopy (SPR). Unlike the films in Chapter 4, which were assembled using passive polyelectrolyte adsorption, the films in this chapter were assembled using spin coating Layer-by-Layer (scLbL)[2-5] assembly by alternatively exposing 2-mercaptoethylamine (MEA) functionalized Au QCI and SPR substrates to polyanionic pNIPAm-co-AAc microgels and polycationic poly(allylamine hydrochloride) (PAH), where both polyelectrolytes were deposited at pH 6.5. The scLbL process was followed by QCI analysis, which displays a linear decrease in resonant frequency, i.e. increase in mass, as a function of microgel layer number. The swelling behavior of an assembled film in response to acidic (pH ~ 3.0) and neutral (pH ~ 6.5) solution conditions was monitored using QCI. Exposure of a microgel thin film to acidic solution results in a dramatic decrease in resonant frequency and an increase in motional resistance. When this same film was exposed to a neutral pH solution, the resonant frequency and resistance of the quartz again decrease and increase, respectively, but with the changes being more dramatic than the film in acidic solution. This behavior is believed to be due to the film transitioning from a highly solvent swollen state under acidic conditions to a less swollen

state near neutral pH. To confirm this interpretation, SPR measurements were performed, which suggest that the film is less optically dense under acidic conditions, i.e. is more solvent swollen, than the same film at pH ~6.5. This differential solvation behavior is highly reversible, with the solvation/desolvation rates being dependent on the number of microgel layers in the film.

5.2 Experimental Section

Materials All reagents were purchased from Sigma-Aldrich unless otherwise specified. *N*-Isopropylacrylamide (NIPAm) was re-crystallized from hexanes (J.T. Baker) and dried under vacuum prior to use. Acrylic acid (AAc) was distilled under reduced pressure. *N*,*N*'-Methylene(bisacrylamide) (BIS) and ammonium persulfate (APS) were used as received. Poly(allylamine hydrochloride) (PAH), MW 70 000, was used as received. 2-Mercaptoethylamine (MEA) was used as received and stored at 4 °C. 5.0 MHz AT-cut, polished quartz crystals were purchased from International Crystal Manufacturing (Oklahoma City, OK). Cuvettes used were obtained from VWR. 99.999% pure Au was obtained from Alfa Aesar. Glass substrates were 24 x 24 mm Fisher Finest brand cover glass obtained from Fisher Scientific. 95% and absolute ethanol was used for various purposes in this chapter. All water was house distilled and then deionized to a resistance of at least 18 MΩ (Barnstead Thermolyne E-Pure system) and then filtered through a 0.2 μm filter for further purification.

Quartz Crystal Impedance Measurements and Thin Film Deposition 5 MHz AT-cut quartz crystals were used with a standard keyhole electrode configuration. The electrode area of 0.0951 cm^2 gives a mass sensitivity of 1.68 ng/Hz, as calculated using

the Sauerbrey equation (Eq. 1), where Δf_p is the measured frequency shift, f_{p_0} is the frequency of the quartz crystal prior to mass addition, Δm is mass change, A is the electrode area, and μ_q and ρ_q are the shear modulus and density of quartz, respectively. Before polyelectrolyte deposition, the Au electrodes were rendered positively charged using well known thiol self-assembly methods.[6] Specifically, the substrates were immersed in a 1.0 mM ethanolic MEA solution (95% ethanol) for 24 hrs. Following MEA functionalization the substrates were rinsed and stored in ethanol and were used within 7 days. Prior to alternate layer deposition, the substrates were rinsed with DI H_2O and dried under a stream of N_2 gas.

$$\Delta f_p = -2 f_{p_0}^2 \Delta m / A(\mu_q \rho_q)^{1/2} \qquad (1)$$

Impedance analysis was performed as previously described.[7-10] The network parameters of a MEA functionalized quartz crystal were analyzed using a Hewlett Packard E5100A network analyzer in impedance-reflection mode. The network parameters of the crystals were measured by scanning 800 points over the frequency range of 5.0 MHz ± 100 kHz. The admittance (Y) and the phase angle (θ) of the quartz crystal were monitored and used to calculate the series resistance (R_1), capacitance (C_1), inductance (L_1), and frequency (f_s), as well as the parallel frequency (f_p), and capacitance (C_o) as previously described.[9] Figure 5-1 shows the four component equivalent circuit representation of the piezoelectric element used in these studies. These data points were collected over time by acquiring values at a rate of 1 measurement/second using a program written in-house in the LabVIEW 5.0 environment. Following characterization

of the MEA functionalized quartz crystal, the substrate was removed from the measurement fixture and securely attached to a glass coverslip, via double sided tape contacting the non-metallized regions of the crystal (see Appendix A for further description). This assembly was then placed on the vacuum chuck of a spin coater (Specialty Coating Systems, Model P6700), and spun at 3 000 RPM. 10 drops of an aqueous, pH 6.5, 10 % (v/v) microgel solution was added to the metallized region of the crystal. The substrate was allowed to spin for 15 seconds following microgel addition. The spinning substrate was then rinsed copiously with DI water and allowed to spin for an additional 15 seconds. Following rinsing, a layer of PAH was deposited by adding 10 drops of an aqueous, pH 6.5, 0.0526 monoM (moles/L monomer) solution followed by an additional 15 seconds of spinning. The substrate was then rinsed with DI water and subsequent polyelectrolyte layers were added, as described above. An idealized schematic depiction of the thin film configuration is shown in Figure 5-2. The quartz crystal can be removed from the tape holding it to the glass substrate at any time to allow for measurement of the network parameters. In all cases, the film was dried under a light stream of N_2 gas prior to measurement. The procedure of removing the crystal from its measurement fixture has been shown not to affect the network parameters of the crystal (data not shown). After the network parameters of the dry film were measured, a 10 μL drop of the desired pH solution, either pH ~3.0 or ~6.5 (1.0 mM ionic strength), was added to the film and the network parameters were re-measured. Evaporation of the pH solution from the metallized region of the quartz crystal is negligible over the time scale of the experiment. The resulting network parameters can then be related to film mechanical properties, as previously described.[11-14]

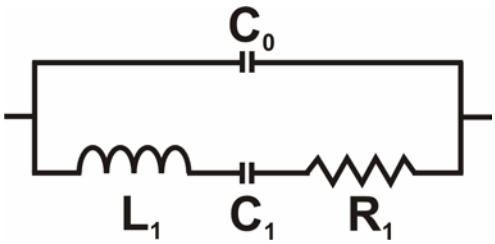

Figure 5-1. Quartz crystal equivalent circuit

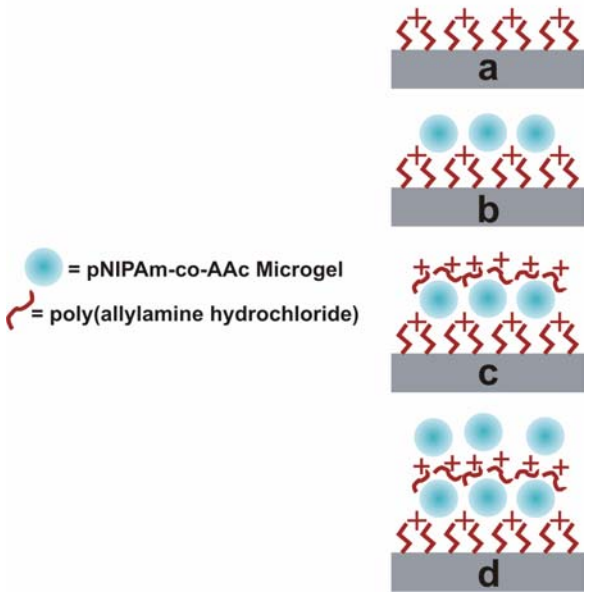

Figure 5-2. Schematic representation of the microgel thin films (not meant to imply order or morphology of the thin film). (a), blank, MEA functionalized, Au substrate surface (b), one layer of microgel added to the substrate (c), addition of one PAH layer to the microgel surface (d), subsequent addition of a microgel layer to the PAH surface. PAH and microgel not drawn to scale.

Surface Plasmon Resonance Spectroscopy Surface plasmon resonance spectra were obtained using an instrument built in-house as part of this project. This scanning angle instrument is equipped with a fiber optic coupled white light source and a fiber optic coupled photodiode array detector (Ocean Optics) for illumination and detection, respectively. Sample excitation and detection angles were controlled using a Newport Corporation motion controller (MM 3000) and rotation stages (495 CC) with 0.01º resolution. A photograph of the instrument can be seen in Figure 5-3. To perform SPR experiments, a 50-nm thick layer of Au was evaporated onto 3-mercaptopropyltrimethoxysilane (MPTMS) functionalized glass cover slips using a Denton Vacuum DV-502A thermal metal evaporator. MPTMS was attached to the

substrates by exposing Ar plasma cleaned glass (Harrick Scientific) to a 1% (v/v) ethanolic (200 proof ethanol) MPTMS solution for 2 hrs. This layer functions as a molecular adhesion layer, thus improving the adhesion of Au to the glass substrate. The Au-coated substrate was then exposed to a 1 mM, ethanolic MEA solution for 24 hrs to render the Au surface positively charged. These substrates were then used for scLbL deposition. To obtain SPR spectra, the uncoated side of the glass substrate was optically coupled to the bottom of a hemispherical prism using a drop of immersion oil and mounted on to a custom made, temperature controlled flow cell. White light was then introduced to the sample over a variety of angles and the reflectance from the sample was monitored as a function of wavelength at a single angle.

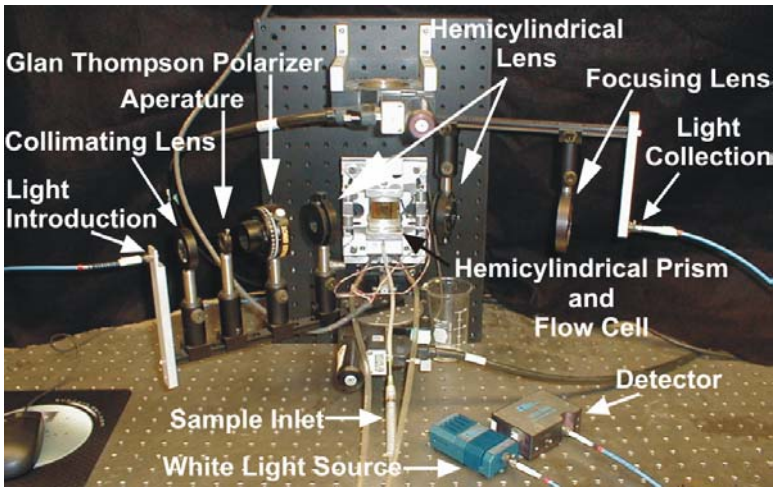

Figure 5-3. Photograph of the SPR setup used for the experiments in this chapter.

Microgel Synthesis The same batch of microgels was used throughout this chapter. The microgels were synthesized exactly as outlined in Chapter 4 with the only difference being that these microgels do not contain 0.1% 4-acrylamidofluorescein. Since this synthesis was explained in the previous chapter it will not be explained here. Following synthesis, the particles were purified by centrifuging the particle solution, decanting the supernatant solution and resuspending in fresh H_2O. This process was repeated 7 times.

Photon Correlation Spectroscopy The temperature and pH responsivity of the pNIPAm-co-AAc microgels was confirmed by photon correlation spectroscopy (PCS, Protein Solutions Inc.) prior to their use for thin film fabrication. This technique has been described in Chapter 3. For these measurements, each sample was allowed to equilibrate at each temperature for 20 min. At each temperature, 5 consecutive runs were performed where each run was composed of 15 individual radius measurements using a 30 s integration time for each measurement.

5.3 Results

Figure 5-4 shows temperature dependent PCS data for the microgels used in this chapter at acidic (~3.0) and approximately neutral (~6.5) pH values. From the figure it can be seen that under acidic conditions ($pH<pK_a$), the microgels have an average R_h of ~260 nm. Since the AAc groups are almost fully protonated at this pH, the microgels undergo a continuous VPT over a ~6 ºC range, with a lower critical solution temperature (LCST) of ~31ºC. From Figure 5-4 it is observed that at pH~6.5 ($pH>pK_a$), the microgels have an average R_h of ~375 nm. The swelling of the microgels at this pH is expected due

to deprotonation of the majority of the AAc groups, which introduces charge-charge repulsion and increased osmotic pressure in the network. Furthermore, as the microgels are heated in pH 6.5 solution, they are unable to deswell to the same minimum R_h observed at pH 3.0, and the VPT temperature is much higher, again due to the charged nature of the microgel network.

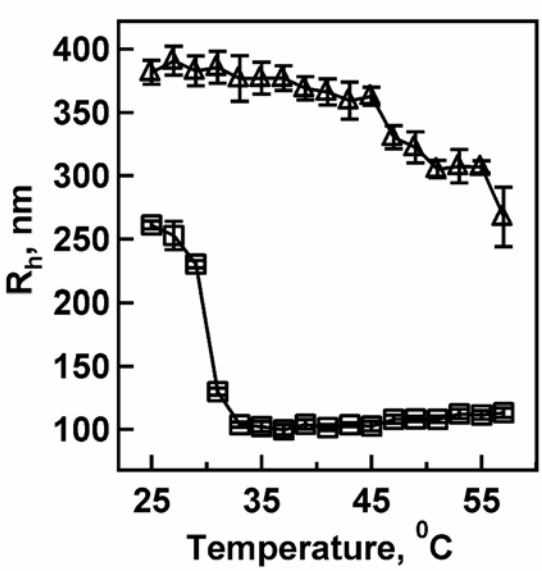

Figure 5-4. Volume phase transition curves taken from PCS measurements for the pNIPAm-AAc microgels used in this chapter, at pH 3.0 (squares) and pH 6.5 (triangles). Error bars represent one standard deviation about the average of five measurements.

Since the microgels are negatively charged at pH 6.5, scLbL was performed at this pH. This ensures the strongest polyelectrolyte interactions during layer buildup, and should result in a denser film. Cryo-scanning electron microscopy (cryo-SEM) micrographs of the assembled microgel thin films can be seen in Figure 5-5.[15] This technique is able to show sample morphology in the solvated state by cryo-freezing samples in liquid ethane followed by ice "etching" techniques and chromium coating.

These experiments were performed with Dr. Robert Apkarian at the Emory University Integrated Microscopy and Microanalytical Facility in Atlanta, GA. From the micrographs it can be seen that films are being assembled using scLbL assembly resulting in highly porous films that are highly interpenetrating within a layer but appear layered along the film thickness.

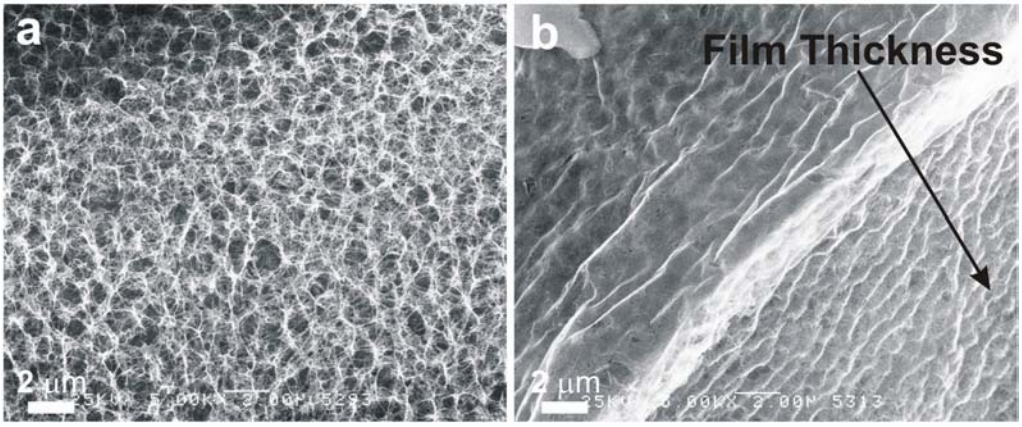

Figure 5-5. Cryo-SEM micrographs of the top (a) and cross-section of a 20 layer film assembled as described above, taken at 25 kV acceleration voltage. The films appear to be highly interpenetrated within a layer as can be seen from the image of the top of the film but appear layered in the cross-section view.

Layer buildup was also monitored via QCI. These measurements were performed by measuring the initial network parameters of the MEA functionalized quartz crystal in air. Following this measurement, the crystal was removed from its measurement fixture and 5 layers of microgel/4 layers PAH were spun onto the crystal in an alternating fashion, as described in the experimental section. The crystal was then dried under a stream of N_2 gas and placed back in the measurement fixture to allow the new network parameters to be measured. This process was repeated for every 5 microgel layers.

Shown in Figure 5-6 is a plot of the change in resonant frequency of the crystal oscillating in air (Δf_p) as a function of microgel layer number; the resonant frequency decreases linearly with increasing film thickness. Figure 5-6 also shows the corresponding changes in mass as calculated from Δf_p values using Eq. 1. The Sauerbrey equation relates mass changes directly to Δf_p assuming the microgel thin film is behaving as a rigidly attached overlayer. This assumption is valid considering that the QCI crystal R_1 value does not significantly increase with layer number, indicative of low losses in crystal oscillation (see Appendix A). Using this simple formalism, the total frequency change following the addition of 45 microgel layers corresponds to ~4.0 μg of added mass, or 0.44 μg per 5 microgel/4 PAH layers. We estimate that ~0.299 μg should be added to the crystal surface for each microgel layer, assuming deposition of a close packed monolayer of microgels (~84 % surface is covered by microgel), where each microgel is assumed to have a polymer content of 5% by mass and a density of ~ 1.45. This corresponds to 1.495 μg added mass for every 5 microgel layers, without considering the mass of the PAH added for each layer. The discrepancy between the experimental results and the predicted values is most likely due to the lack of truly close packed microgel layers.

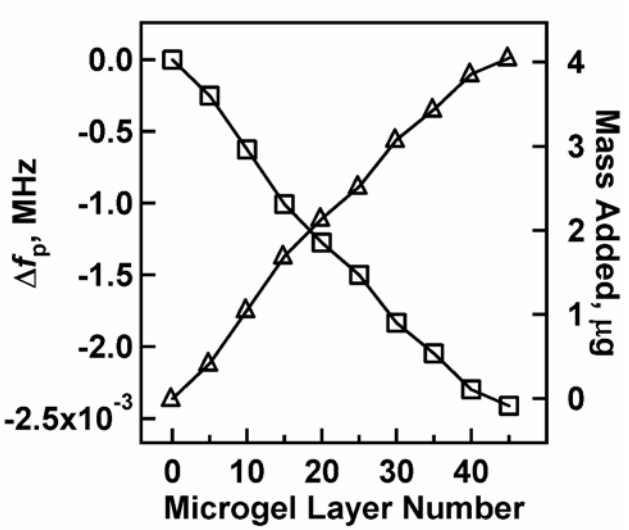

Figure 5-6. Δf_p (squares) and added mass (triangles) values as a function of microgel layer number obtained from QCI measurements.

Another way to represent these data is by showing the full impedance spectra obtained during the frequency sweep. Figure 5-7 shows plots of phase angle (θ) and the logarithm of the admittance (Log Y) as a function of frequency for a crystal functionalized with MEA only, as well as a 10 and 40 layer film. These curves were obtained in air. Plots of Y vs. frequency are included in Appendix A. The shifts to lower frequency with added mass that are observed for both sets of curves again indicates a decrease in resonant frequency. Also, the curve shapes do not change significantly with layer addition, suggesting little or no dampening of the crystal oscillation. However, if a blank, MEA functionalized crystal is exposed to pH 3.0 and 6.5 solution, the crystal's θ and Log (Y) behavior are observed to become dramatically different. Figure 5-8 shows these data, where it can be seen that the crystal oscillation becomes extremely dampened as indicated by the very broad θ and Log (Y) curves (for Y vs. frequency plots see Appendix A). Note that this behavior is pH independent.

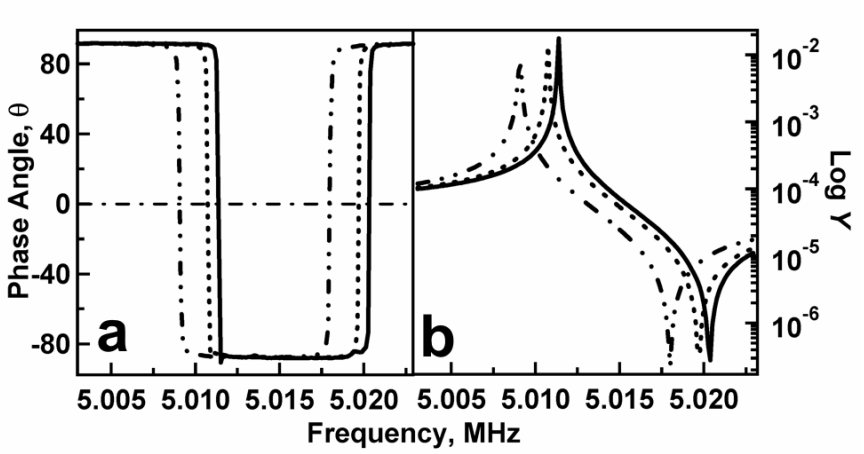

Figure 5-7. Quartz crystal θ (a) and Log (Y) (b) behavior for a MEA functionalized crystal (solid) and a 10 (dotted line) and 40 (dot-dash line) microgel layer thin films.

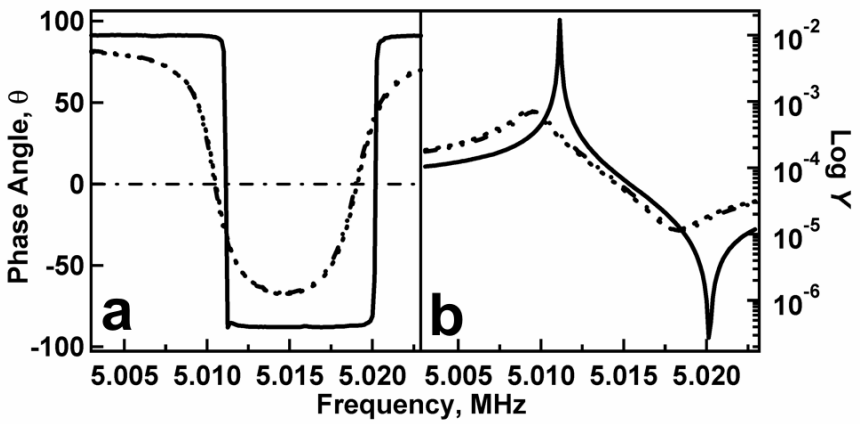

Figure 5-8. Quartz crystal θ (a) and Log (Y) (b) behavior as 10 μL of pH 3.0 (dotted line) and 6.5 (dot-dash line) solution is added to a blank, MEA functionalized quartz crystal surface (solid line = air oscillation).

Figure 5-9 shows the pH-dependent phase angle and admittance spectra for the 10 and 40 layer microgel thin films (for *Y* vs. frequency plots see Appendix A). In panel (a) we see that the θ curve for the 10 layer film in air is very similar in shape to the spectrum obtained from the blank crystal in air (Figures 5-7 and 5-8). As in the case of the MEA-functionalized crystal, when the microgel films are exposed to pH 3.0 and 6.5 solutions, the curves become very broad due to dampening of the oscillation. The dampening of the crystal oscillation is also evident in the admittance spectra shown in panels (b) and (d). From the plots of θ and Log (*Y*) it is difficult to resolve a difference in curve position or shape as a function of pH, but the shift in the position of the curves relative to the respective film in air is quite obvious. From Figure 5-9(a,c) it is observed that the 10 layer film is more sensitive to solution addition relative to the 40 layer film, as evidenced by a larger negative frequency shift in θ. Indeed, the frequency at which the phase angle crosses zero is almost unchanged during solution addition in the case of the 40 layer film.

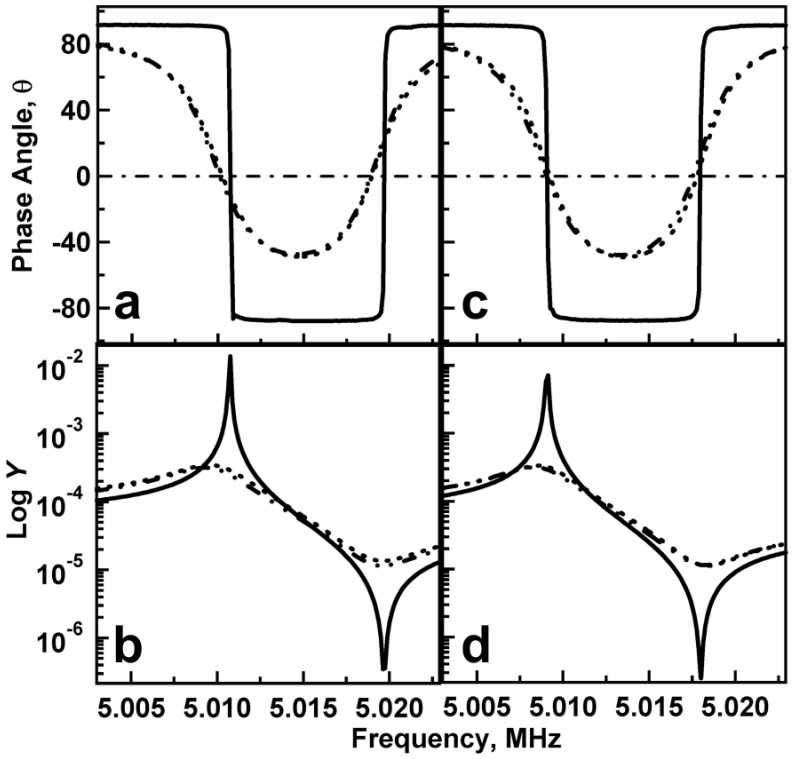

Figure 5-9. Quartz crystal θ (a,c) and Log (Y) (b,d) behavior as 10 μL of pH 3.0 (dotted line) and 6.5 (dot-dash line) solution was added to a 10 (a,b) and 40 (c,d) layer microgel thin film (solid line = air oscillation).

The dependence of f_p and the resonant resistance (R_1) on layer number and pH are shown in Figure 5-10. The figure shows that the magnitude of f_p decreases as a function of layer number and plateaus at ~20 microgel layers while R_1 increases over the whole range. This behavior is indicative of a film that is becoming more viscous, i.e. less swollen, with layer number.[8,16-19] Furthermore, the values of f_p and R_1 are lower and higher, respectively, at pH 6.5 relative to pH 3.0. Table 5-1 lists the differences in network parameter values for films exposed to pH 3.0 and 6.5 solutions, compared to their respective network parameters in air. These data show that the f_p and R_1 values are

shifted more when the films are exposed to pH 6.5, as compared to pH 3.0. Table 5-1 also includes values of Q calculated using Eq 2.[13] Q is a general figure of merit for the quality factor of an oscillator, with larger values indicating less dampened (narrower frequency response) oscillation. The numbers used in this calculation come from the equivalent circuit model presented in Figure 5-1 and the corresponding network values, which are tabulated in Table 5-2. Using this formalism, we find that Q is significantly lower at pH 6.5 for the 20 and 30 layer films, again suggesting a more viscous, or dampening layer.

$$Q = 1/R_1 \sqrt{L_1 / C_1} \qquad (2)$$

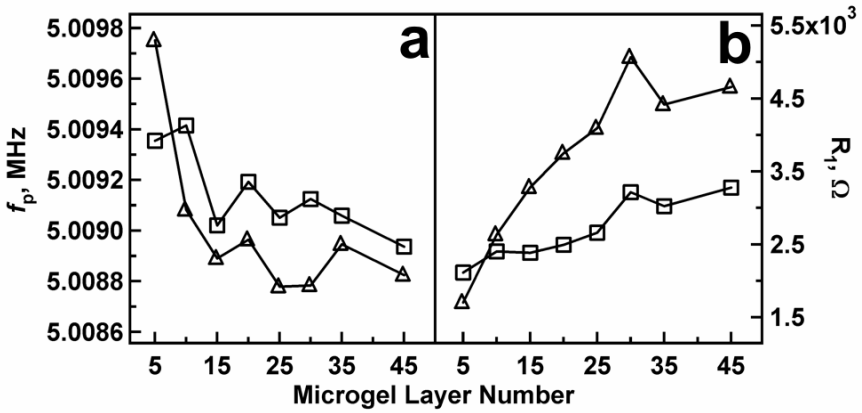

Figure 5-10. Quartz crystal network parameters f_p (a) and R_1 (b) as a function of microgel layer number at pH 3.0 (squares) and 6.5 (triangles).

Table 5-1: Network parameters for microgel films exposed to pH solutions

Microgel Layer	Δf_p, MHz pH 3.0/6.5[a]	ΔR_1, Ω pH 3.0/6.5[a]	Q pH 3.0/6.5[b]
10	-0.00122/-0.00155	2324/2555	1726/1778
20	-0.00081/-0.00104	2294/3550	1630/1178
30	-0.00038/ -0.00073	2995/4845	1148/864

[a] Values calculated by subtracting f_p for the respective microgel films in air from f_p obtained by exposing each film to pH 3.0 or 6.5 solution.

[b] Calculated using Eq. 2 from the absolute values for R_1, C_1, and L_1 (Supporting Information).

Table 5-2: Absolute values for the network parameters for microgel films exposed to pH solutions

Microgel Layer	R_1, Ω pH 3.0/6.5	L_1, H pH 3.0/6.5	C_1, fF pH 3.0/6.5[b]
10	2402.547/2634.196	0.131761/0.148893	7.66/6.78
20	2495.014/3751.063	0.129256/0.14046	7.81/7.19
30	3215.759/5066.544	0.117359/0.13913	8.60/7.26

A plot of the calculated *Q* values for all the films as a function of pH can be seen in 5-11(a). From the figure it can be observed that the value of *Q* generally decreases as a function of layer number indicating an increasing viscosity. Also the *Q* values for the films at pH 6.5 are lower than the films at pH 3.0 with exception to the 5 and 10 layer film. As stated above *Q* and viscosity are inversely related. From this relation Eq. 3 can be derived, which relates a solution of high viscosity (η_2) and low viscosity (η_1) to their calculated *Q* values. Using this equation it is possible to calculate the viscosity of a solution from its calculated *Q* value as long as the *Q* value is known for that crystal in contact with a solution of known viscosity.

$$\eta_1 / \eta_2 = k(Q_2 / Q_1) \qquad (3)$$

Using Eq. 3 the viscosities for all the films in contact with pH 3.0 and 6.5 solutions were calculated, where η_2 is the combined viscosity of given film in contact with a pH solution

(pH 3.0 or 6.5), η_1 is the viscosity of a pH solution (~1.0) in contact with a blank, MEA functionalized crystal, Q_1 and Q_2 are the respective calculated Q values, and k is a proportionality constant calculated to be .415 by plugging in published values of Q and η into Eq. 3 and solving for k.[18] The calculated film viscosities are plotted in Figure 5-11(b). The figure shows that the films generally increase in viscosity with layer number and are higher at pH 6.5 than at pH 3.0. These values also correspond very nicely with viscosities, published by Richtering and coworkers, for pNIPAm microgels in solution.[20,21]

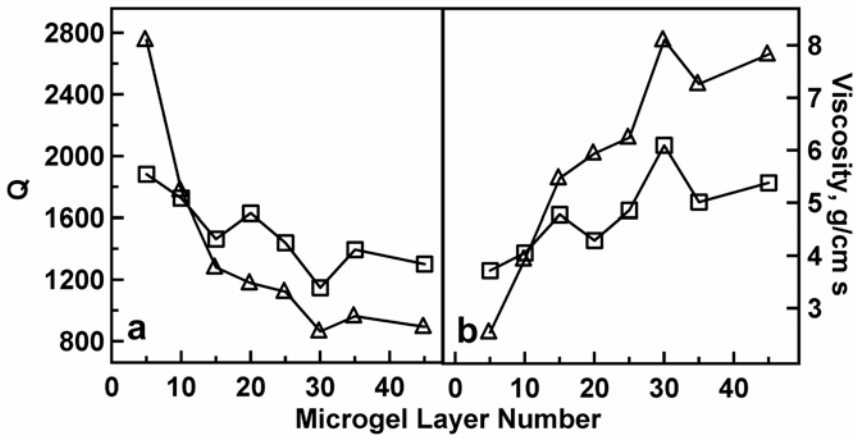

Figure 5-11. Plots of the calculated Q (a) and viscosities (b) values using Eqs. 2 and 3. From the plots it can be seen that decreasing Q values corresponds to increasing film viscosity.

Surface plasmon resonance analysis performed on similar films as above displayed similar behavior. Figure 5-12 shows plots of the SPR reflectance wavelength minimum (λ_{min}) and percent reflectance values as a function of microgel layer number at pH 3.0 and 6.5. For these experiments all films were assembled on MEA functionalized, Au

coated, glass substrates similar to the substrates used for QCI experiments. Following assembly of a given number of microgel layers, the substrate was attached to a hemispherical prism and coupled to the temperature controlled, fluid flow cell of the SPR instrument. The experiments were conducted at room temperature while monitoring the reflectance spectrum from the substrate in contact with either pH 3.0 or 6.5 solution. During the experiment, the light excitation and detection arms were held constant at 73º relative to the prism normal. Full reflectance spectra as a function of layer number and pH can be seen in Appendix A. Figure 5-12(a) shows that when a 10 layer microgel film is exposed to pH 3.0 solution, the λ_{min} increases by ~90 nm compared to a blank substrate exposed to a pH 3.0 solution. If pH 6.5 solution is introduced to the same 10 layer film via the fluid flow cell, λ_{min} further increases by ~20 nm. Figure 5-12(b) shows that the percent reflectance from the 10 layer film increases from ~2.8% to ~4.5% upon pH 3.0 and 6.5 exposure, respectively. As the number of microgel layers is increased from 10 to 20, the λ_{min} of the film at pH 3.0 increases by ~5 nm, while the same film exposed to pH 6.5 solution changes λ_{min} by ~20 nm. If the percent reflectance of the film at pH 3.0 and 6.5 are compared, it can be seen that the film at pH 6.5 displays a higher percent reflectance that the film at pH 3.0, indicating that the film at pH 6.5 scatters more light, or is more lossy than the film at pH 3.0. Similar SPR behavior is also observed for a 30 layer microgel thin film.

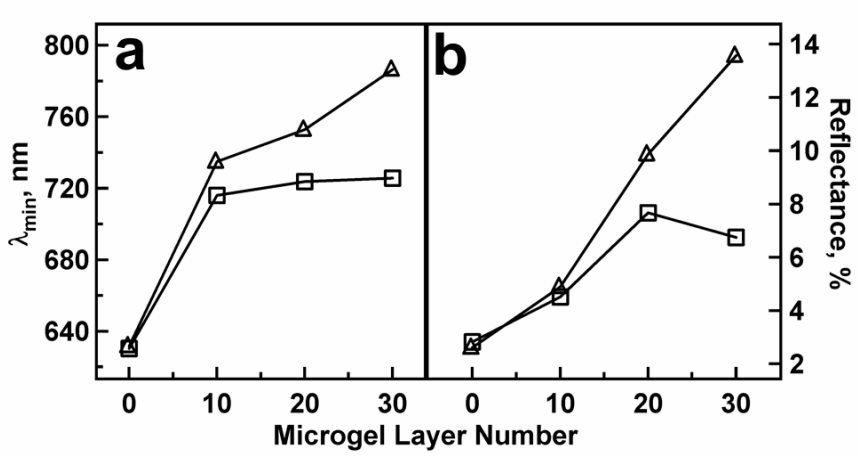

Figure 5-12. Plots of λ_{min} (a) and percent reflectance (b) as a function of microgel layer number in response to pH 3.0 (squares) and 6.5 (triangles) solutions.

The results of repeated pH cycling on the film optical properties are shown in Figure 5-13. For a 10 layer film, the shift in λ_{min} was ~20 nm upon changing the solution pH from 3.0 to 6.5 while the percent reflectance increased by ~1%. Conversely, the 30 layer film λ_{min} shifts by ~60 nm while the percent reflectance changes by ~7% as the solution pH is changed from 3.0 to 6.5. The shifts observed for the 30 layer film are not as reproducible as in the 10 layer case.

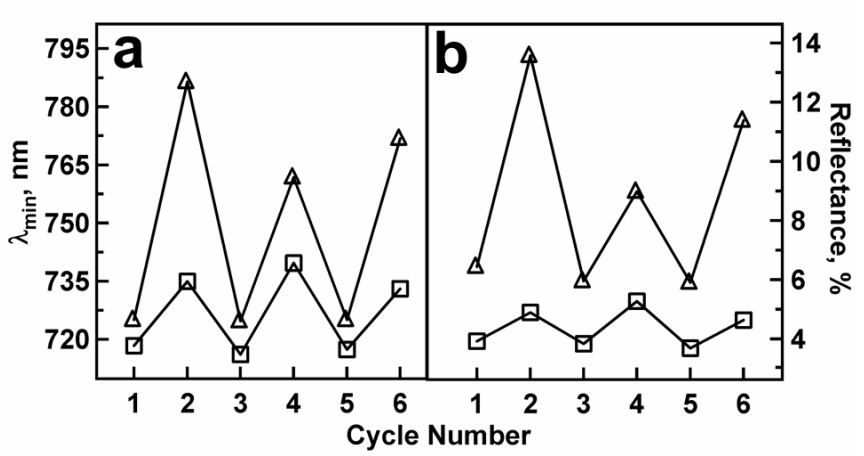

Figure 5-13. Plots of λ_{min} (a) and percent reflectance (b) values as a 10 (squares) and 30 (triangles) layer microgel film is alternatively exposed to pH 3.0 (odd numbers) and 6.5 (even numbers) solution.

To investigate the kinetics of film equilibration during pH changes, λ_{min} was measured as a function of time following the pH switch. These data are presented in Figure 5-14. Panel (a) illustrates that when a 10 layer film is exposed to a pH 6.5 solution, λ_{min} reaches its equilibrium value of ~740 nm in ~5 sec. When the solution pH is changed to 3.0, λ_{min} decreases to its equilibrium value of ~715 nm again in ~5 sec. However, for a 20 layer film to reach its equilibrium value of ~760 nm at pH 6.5, ~75 sec of equilibration time is required. The equilibrium value of ~720 nm is reached in less than 40 sec upon pH 3.0 solution addition. Figure 5-14(c) shows that when a 30 layer film is exposed to pH 6.5, λ_{min} increases quickly within the first 20 sec, followed by a slow component, ultimately reaching its equilibrium value of ~785 nm in ~300 sec. When this film is exposed to pH 3.0, the λ_{min} decreases and reaches its equilibrium value of ~725 nm in less than 10 seconds. Qualitatively, these data indicate that the film kinetics are roughly independent of layer number (fast kinetics) when going from pH 6.5 to pH

3.0. However, the kinetics appear to become more sluggish with increasing layer number for switches from pH 3.0 to 6.5.

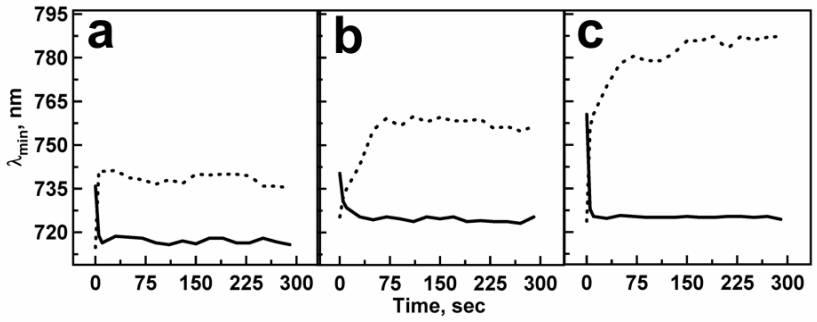

Figure 5-14. Plots of λ_{min} over time for 10 (a), 20 (b), and 30 (c) layer microgel thin films upon introduction of pH 3.0 (solid line) and 6.5 (dotted line) solutions.

5.4 Discussion

QCI crystals, with their Au electrodes functionalized with MEA, were used to monitor scLbL deposition as microgel layers were added to the crystal. Figure 5-6 shows that the mass added to the QCI crystal increased linearly as microgel layers are added to the substrate surface. This data is indicative of a reproducible buildup mechanism that is expected for layers assembled using LbL assembly techniques. If scLbL deposition did not result in consistent particle density per layer for these thin films, the linear behavior seen in Figure 5-6 would not be observed. The θ and Log (Y) behavior of a QCI crystal as a function of microgel layer number shown in Figure 5-7(a,b) illustrates that the blank QCI crystal exhibits the expected sharp resonance behavior indicative of a crystal that is experiencing very low losses, with typical Q values of ~35 000. It can also be seen from Figure 5-7(a) that as microgel layers are added to the QCI crystal the phase behavior

remains fairly sharp, i.e. low losses are experienced, but are shifted to lower frequency indicative of mass loading. The Log (Y) plots, Figure 5-7(b), for a microgel thin film loaded QCI crystal showed curves that are also shifted to low frequency and have a slight decrease in amplitude of Y, while still maintaining high Q values (~25 000).

As expected, crystal oscillation in solution results in dampened oscillation, as seen in Figure 5-8. This behavior is a well known effect of oscillation dampening/energy loss of a QCI crystal in contact with a solution and has been explained by researchers such as Kanazawa, Buttry and Ward to be due to viscous loading of the liquid on the crystal.[8-10,17] Viscous loading has been shown to affect the QCI crystal resonant oscillation frequency in a solution viscosity dependent fashion, i.e. more viscous solutions are able to shift the resonant frequency to lower values than a less viscous solution.[8,17] From the figure it is also important to note that the curves for the crystal in contact with pH 3.0 and 6.5 solutions are overlapped indicating that the response of the blank quartz crystal is not pH sensitive.

These viscous loading effects become more prevalent when the crystal is coated with microgel multilayers. Figure 5-9 shows the θ and Y response of a crystal composed of 10 and 40 microgel layers as a function of pH solution addition. From Figure 5-9(a,b) it can be seen that the θ and Y behavior of a dry, 10 layer film in air is similar to a blank, MEA functionalized crystal in air with a characteristic high Q factor (~35 000) but shifted to lower frequency. However, immersion of the films in aqueous media results in significant damping, as evidenced by the broadening of both the θ and Y response. If the network parameters f_p and R_1 are plotted as a function of layer number upon exposure of the films to pH 3.0 and 6.5 solutions (Figure 5-10) the difference in crystal behavior

becomes apparent. As can be seen from the figure, and as outlined in Table 5-1, the values of f_p and R_1 are shifted more for a film at pH 6.5 for almost every layer number. For example, f_p is shifted to a lower frequency for a film exposed to a solution of pH 6.5 versus 3.0 while the crystal oscillation is more resistive at pH 6.5 versus pH 3.0. This behavior can be understood by taking into account the differential ionization of weak polyelectrolytes AAc and PAH as a function of pH.[22-25] At pH 3.0 the AAc groups on the microgel will be almost fully protonated as will be the PAH. This should decrease the interaction between the now neutral particle and cationic PAH, which results in film swelling. If on the other hand a pH 6.5 solution is added to the film, the AAc groups become almost fully charged while the PAH stays mostly ionized (pK_a~9.0),[26] thereby enforcing the PAH-AAc complexation. A more highly complexed film results in a more viscous film as indicated by the measured resonant frequency and resistance values. This hypothesis can be verified from the calculated Q values as a function of layer number and pH as seen in Table 5-1 and Figure 5-11(a). From this it can be seen that the Q value decreases with layer number and, with exception to the 5 and 10 layer film, is lower at pH 6.5 than at pH 3.0. This trend in the value of Q is indicative of a film that is more viscous with layer number and increasing pH as seen in Figure 5-11(b).[18] A viscosity increase with layer number suggests that the film becomes denser as more layers are added.

This behavior was confirmed by probing the local optical properties of the film in response to pH using SPR, which is a well known and studied technique for probing optical densities and has previously been exploited for similar films.[27-30] The data shown in Figure 5-12(a) reveal the fact that a film exposed to pH 3.0 is less optically dense, i.e.

more water swollen, than the film at pH 6.5 as noted by a smaller shift in λ_{min} for a film exposed to pH 3.0 solution. The differential solvation behavior is also evident in the larger percent reflectance values for a film exposed to a pH 6.5 solution, as opposed to a pH 3.0 solution, indicating that the film is more lossy due to scattering from refractive index heterogeneities. Figure 5-13 shows the reproducibility of the pH dependent film solvation for a 10 and 30 layer film. This behavior is noted by the oscillatory behavior in λ_{min} and percent reflectance indicative of a film that is able to dynamically change solvation in a pH dependent fashion. This behavior is shown to be reproducible over at least 6 pH cycles. The kinetics of film solvation state switching were also monitored via SPR, where it is expected that films of lower layer number should respond to pH switching faster than films composed of more layers. Shown in Figure 5-14 are the data illustrating this point. From Figure 5-14 it can be seen that the films at pH 3.0 all swell very fast compared to film deswelling upon exposure to pH 6.5 solution. By comparing the panels in Figure 5-14, the film thickness dependent swelling kinetics can be observed, where the 10 layer film changes solvation the fastest, followed by the 20 and 30 layer upon pH 6.5 solution introduction. This behavior is expected, at least qualitatively, given the fact that film deswelling is dependent on ion transport, water diffusion, and film reorganization, all of which should increase in time with film thickness. Conversely, film swelling is less dependent on film reorganization, as disruption of the PAH-AAc interactions should be faster than re-formation of the complexes following a pH jump.

5.5 Conclusions

QCM and SPR studies reveal that LbL assembled microgel thin films are pH sensitive materials that switch their solvation state depending on whether the film is exposed to a pH solution where the attractive forces were enforced (pH 6.5) or disrupted (pH 3.0). This behavior scales with layer number, where a film containing more microgel layers is less sensitive to solution addition than a film with fewer layers. It is also shown that a film with a given layer number at pH 6.5 is able to affect the network parameters of a QCI crystal more than a film exposed to pH 3.0 solution, which is indicative of a pH dependent film viscosity. The films are also able to switch their solvation state over at least 6 pH cycles, where the kinetics of swelling/deswelling are dependent on microgel layer number.

From the results presented in this chapter it is apparent why the data interpretation given for pH dependent film thermoresponsivity in Chapter 4 is incomplete. In that chapter only the pH dependent microgel charge was considered and was directly related to film thermoresponsivity. In this chapter the pH dependent ionic interactions between the microgels and PAH were considered. As can be seen from the data in this chapter the microgels do become more charged at high pH but are immediately complexed by the charges on the PAH, neutralizing its structure. Considering these results, film thermoresponsivity cannot be solely attributed to the charged state of the microgel and must be a result of the pH dependent ionic interactions in the films.

REFERENCES

(1) Serpe, M. J.; Lyon, L. A. *Chem. Mater.* **2004**, *submitted*.

(2) Cho, J.; Char, K. *Langmuir* **2004**, *20*, 4011-4016.

(3) Lee, S. S.; Lee, K. B.; Hong, J. D. *Langmuir* **2003**, *19*, 7592-7596.

(4) Chiarelli, P. A.; Johal, M. S.; Holmes, D. J.; Casson, J. L.; Robinson, J. M.; Wang, H. L. *Langmuir* **2002**, *18*, 168-173.

(5) Lee, S. S.; Hong, J. D.; Kim, C. H.; Kim, K.; Koo, J. P.; Lee, K. B. *Macromolecules* **2001**, *34*, 5358-5360.

(6) Palegrosdemange, C.; Simon, E. S.; Prime, K. L.; Whitesides, G. M. *J. Am. Chem. Soc.* **1991**, *113*, 12-20.

(7) Beck, R.; Pittermann, U.; Weil, K. G. *Ber. Bunsen-Ges. Phys. Chem. Chem. Phys.* **1988**, *92*, 1363-1368.

(8) Kanazawa, K. K.; Gordon, J. G. *Anal. Chem.* **1985**, *57*, 1770-1771.

(9) Buttry, D. A.; Ward, M. D. *Chem. Rev.* **1992**, *92*, 1355-1379.

(10) Ward, M. D.; Buttry, D. A. *Science* **1990**, *249*, 1000-1007.

(11) Kanazawa, K. K. *Faraday Discuss.* **1997**, 77-90.

(12) Kim, B.-S.; Vinogradova, O. I. *J. Phys. Chem. B* **2004**, *108*, 8161-8165.

(13) Kim, J. M.; Chang, S. M.; Muramatsu, H. *Polymer* **1999**, *40*, 3291-3299.

(14) Marxer, C. M.; Coen, M. C.; Greber, T.; Greber, U. F.; Schlapbach, L. *Anal. Bioanal. Chem.* **2003**, *377*, 578-586.

(15) Apkarian, R. P.; Wright, E. R.; Seredyuk, V. A.; Eustis, S.; Lyon, L. A.; Conticello, V. P.; Menger, F. M. *Microsc. Microanal.* **2003**, *9*, 286-295.

(16) Kanazawa, K. K.; Melroy, O. R. *IBM J. Res. Dev.* **1993**, *37*, 157-171.

(17) Kanazawa, K. K.; Gordon, J. G. *Anal. Chim. Acta* **1985**, *175*, 99-105.

(18) Martin, S. J.; Granstaff, V. E.; Frye, G. C. *Anal. Chem.* **1991**, *63*, 2272-2281.

(19) Lee, S. W.; Hinsberg, W. D. *Anal. Chem.* **2002**, *74*, 125-131.

(20) Senff, H.; Richtering, W. *J. Chem. Phys.* **1999**, *111*, 1705-1711.

(21) Senff, H.; Richtering, W.; Norhausen, C.; Weiss, A.; Ballauff, M. *Langmuir* **1999**, *15*, 102-106.

(22) Tanchak, O. M.; Barrett, C. J. *Chem. Mater.* **2004**, ACS ASAP.

(23) Hiller, J.; Rubner, M. F. *Macromolecules* **2003**, *36*, 4078-4083.

(24) Yang, S. Y.; Rubner, M. F. *J. Am. Chem. Soc.* **2002**, *124*, 2100-2101.

(25) Rmaile, H. H.; Schlenoff, J. B. *Langmuir* **2002**, *18*, 8263-8265.

(26) Ochiai, H.; Anabuki, Y.; Kojima, O.; Tominaga, K.; Murakami, I. *J. Polym. Sci. Pt. B-Polym. Phys.* **1990**, *28*, 233-240.

(27) Harmon, M. E.; Kuckling, D.; Pareek, P.; Frank, C. W. *Langmuir* **2003**, *19*, 10947-10956.

(28) Harmon, M. E.; Kuckling, D.; Frank, C. W. *Macromolecules* **2003**, *36*, 162-172.

(29) Harmon, M. E.; Jakob, T. A. M.; Knoll, W.; Frank, C. W. *Macromolecules* **2002**, *35*, 5999-6004.

(30) Kuckling, D.; Harmon, M. E.; Frank, C. W. *Macromolecules* **2002**, *35*, 6377-6383.

CHAPTER 6

SMALL MOLECULE UPTAKE AND RELEASE FROM MICROGEL THIN FILMS

6.1 Introduction

The previous chapters of this dissertation have focused on studying the fundamentals of microgel/polyelectrolyte interactions, using these interactions to buildup films in a LbL fashion and studying their resulting behavior. This chapter is more applications-based and describes the use of microgel thin films for thermally regulated uptake and release of small molecules in solution.[1,2] In Chapter 1, controlled release from hydrogel thin films or nanoparticles was mentioned.[3-8] These studies relied on the application of an external stimulus to alter the solvation behavior of the material to release its drug. For example, Needham and coworkers developed lipid coated hydrogel microparticles capable of releasing the chemotherapeutic drug agent doxorubicin in response to solution pH and ionic strength changes.[9-12] Multilayer thin films have also been used to achieve similar goals.[13-16] This chapter first describes some preliminary results for the thermally regulated uptake and release of fluorescein-5-isothiocyanate (FITC). Based on those results we used microgel thin films to load and release doxorubicin (DX).

Spin coating, layer-by-layer (scLbL) assembly was used to prepare thin films composed of thermoresponsive poly(*N*-isopropylacrylamide-*co*-acrylic acid) (pNIPAm-co-AAc) microgels by alternatively exposing 3-aminopropyltrimethoxysilane (APTMS) functionalized glass substrates, to polyanionic pNIPAm-AAc microgels and polycationic

poly(allylamine hydrochloride) (PAH).[17-20] The films were subsequently loaded with FITC or DX by cycling the temperature of the loading solution between 25 and 50 ºC. Release characteristics were then examined using uv-vis spectroscopy, which illustrated temperature dependent pulsatile release.

6.2 Experimental

Materials All reagents were purchased from Sigma-Aldrich unless otherwise specified. *N*-Isopropylacrylamide (NIPAm) was re-crystallized from hexanes (J.T. Baker) and dried under vacuum prior to use. Acrylic acid (AAc) was distilled under reduced pressure. *N*,*N*'-Methylene(bisacrylamide) (BIS) and ammonium persulfate (APS) were used as received. Poly(allylamine hydrochloride) (PAH), MW 70 000, was used as received. 2-Mercaptoethylamine (MEA) was used as received and stored at 4 °C. 5.0 MHz AT-cut, polished quartz crystals were purchased from International Crystal Manufacturing (Oklahoma City, OK). 3-Aminopropyltrimethoxysilane (APTMS) was used as received (United Chemical Technologies). Cuvettes used for PCS were from VWR. Glass substrates were 24 x 24 mm Fisher Finest brand cover glass obtained from Fisher Scientific. 95% and absolute ethanol was used for various purposes in this investigation. Doxorubicin hydrochloride (DX) was used as received. Fluorescein-5-isothiocyanate (FITC) was used as received obtained from Molecular Probes. pH 3.0 and 7.0 buffers were obtained from Fisher Scientific. All water used throughout this investigation was distilled and deionized to a resistance of at least 18 MΩ (Barnstead Thermolyne E-Pure system) and then filtered through a 0.2 μm filter for further purification.

Microgel Synthesis The same batch of microgels was used throughout this chapter. The microgels were synthesized exactly as outlined in Chapter 5 and will not be explained here. Following synthesis, the particles were purified by centrifuging the particle solution, decanting the supernatant solution and resuspending in fresh H_2O. This process was repeated 7 times.

Photon Correlation Spectroscopy The temperature and pH responsivity of the pNIPAm-co-AAc microgels was confirmed by photon correlation spectroscopy (PCS, Protein Solutions Inc.) prior to their use for thin film fabrication. This technique has been described in Chapter 3. For these measurements, each sample was allowed to equilibrate at each temperature for 20 min. At each temperature, 5 consecutive runs were performed where each run was composed of 15 individual radius measurements using a 30 s integration time for each measurement.

Quartz Crystal Microgravimetry The quartz crystals used here are the same as used in Chapter 5. The Sauerbrey equation (Eq. 1) was used to calculate mass addition as microgel layers were deposited on the surface, where Δf_p is the measured frequency shift, f_{p_0} is the frequency of the quartz crystal prior to mass addition, Δm is mass change, A is the electrode area, and μ_q and ρ_q are the shear modulus and density of quartz, respectively. Before polyelectrolyte deposition, the Au electrodes were rendered positively charged using well known thiol self-assembly methods.[21] Specifically, the quartz crystal Au electrodes were gently wiped free of dust using a Kimwipe (Kimberly-Clark). Following this step the substrates were immersed in a 1.0 mM ethanolic MEA solution (95% ethanol) and allowed to react for 24 hrs. Following MEA functionalization the substrates were rinsed and stored in ethanol and were used within 7 days. Prior to

alternate layer deposition, the substrates were rinsed with DI H_2O and dried under a stream of N_2 gas. The resonant frequency for dry microgel thin films was collected over time, using a Hewlett Packard E5100A network analyzer, by acquiring values at a rate of 1 measurement/second using a program written in-house in the LabVIEW 5.0 environment.

$$\Delta f_p = -2 f_{p_0}^2 \Delta m / A(\mu_q \rho_q)^{1/2} \qquad (1)$$

Thin Film Deposition Thin films were assembled on glass substrates by adding a APTMS functionalized glass substrate to the vacuum chuck of a spin coater (Specialty Coating Systems, Model P6700), and spun at 3 000 RPM. Methods for functionalizing glass substrates with APTMS have been previously published and involve exposure of plasma cleaned microscope cover glass to a 1% (v/v) ethanolic APTMS solution for 2 h.[22] To assemble films on QCM substrates, MEA functionalized quartz crystals were removed from the measurement fixture and securely attached to a glass coverslip, via double sided tape contacting the non-metallized regions of the crystal and the assembly added to the vacuum chuck, as described in Chapter 5. Film deposition was performed in an identical fashion regardless of the substrate used. 10 drops of an aqueous, pH 6.5, 10% (v/v) microgel solution was added to spinning substrates and allowed to spin for 15 seconds following addition. The spinning substrate was then rinsed copiously with DI water at pH 6.5 and allowed to spin for an additional 15 seconds. Following rinsing, a layer of PAH was deposited by adding 10 drops of an aqueous, pH 6.5, 0.0526 monoM (moles/L monomer) solution followed by an additional 15 seconds of spinning. The

substrate was then rinsed with DI water at pH 6.5 and subsequent polyelectrolyte layers were added, as described above. For QCM measurements the quartz crystal was removed from the tape holding it to the glass substrate following deposition of 10 layers to allow for measurement of the resonant frequency.

Film Thermoresponsivity Measurements The thermoresponsivity of the thin films in FITC loading solution and in water release medium was determined using a Photon Technologies International fluorometer to detect elastic light scattering from the film, as described in Chapter 4.

Loading and Release of FITC from Thin Films Loading of microgel thin films was accomplished by immersing films in 10 mL of a FITC solution with a concentration of 5.78 x 10^{-5} M. The structure of FITC can be seen in Figure 6-1. The solution temperature was cycled between ~50 and ~25 ºC (room temperature) while holding at each temperature for 1 h for a total of 6 temperature cycles. A typical FITC release experiment was performed by immersing FITC loaded films in 10 mL of release medium (DI water) held at ~25 ºC for 1 h. Following the 1 h cycle all release medium was removed and replaced with fresh medium and release monitored at high temperature (~50 ºC) for 1 h. Once this cycle was complete, all release medium was again removed and completely replaced. This cycle could repeated numerous times until the release of FITC from the film was complete. Uv-vis analysis was performed on the collected sample aliquots where the absorbance of the solutions was monitored at 490 nm (~λ_{max} for FITC)

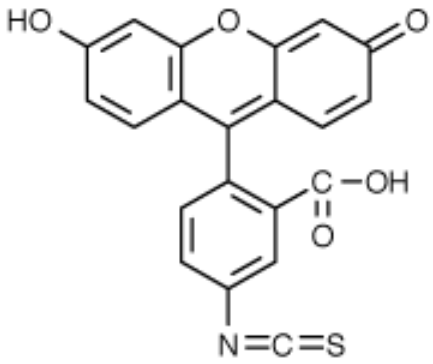

Figure 6-1. Chemical structure of fluorescein-5-isothiocyanate

Loading and Release of DX from Thin Films Loading of microgel thin films was accomplished by immersing films in 10 mL of phosphate buffered DX solution (pH 7.0, 50 mM ionic strength) with a concentration of ~8.0 x 10^{-5} M. The structure of DX can be seen in Figure 6-2. The solution temperature was cycled between ~50 and ~25 ºC (room temperature) while holding at each temperature for 1 h for a total of 6 temperature cycles. A typical release experiment was performed by immersing DX loaded films in 10 mL of release medium (pH 3.0 citrate buffer, 50 mM ionic strength) held at ~50 ºC for 1 h, while removing 3 mL aliquots of release medium at 10 min intervals. 3 mL of fresh release medium was immediately added back to the glass release vessel to maintain a total volume of 10 mL. Following 1 h all release medium was removed from the release vessel and replaced with 10 mL fresh release medium to monitor release from films maintained at room temperature (~25 ºC) for 1 h. In this case the release medium was only sampled at the end of the 1 h cycle. This temperature cycling was typically carried out over ~ 7 hrs, unless otherwise indicated. Uv-vis analysis was performed on each

collected sample aliquot where the absorbance of the solutions was monitored at 490 nm (~λ_{max} for DX). For releases being monitored over time (as for the above release at ~50 ºC) there is the issue of dilution by removal and addition of 3 mL of release medium every 10 min. This dilution was corrected for by addition of a dilution factor into the absorbance measured by uv-vis. For example, the loaded film is immersed in release medium at ~50 ºC and after 10 min a 3 mL aliquot is removed from the release vessel followed by immediate addition of 3 mL of fresh release medium at ~50 ºC. If the film does not release additional DX following the initial 10 minute aliquot removal, the release solution was simply diluted by removal and addition of release medium. In the case of 3 mL serial dilution of a stock DX solution in pH 3.0 buffer at similar concentrations used in this study a dilution factor of 0.269 is obtained. This dilution factor means that serial dilution, in 3.0 mL increments, results in ~26.9% decrease in the initial absorbance value for each dilution. In our case we correct for dilution by measuring the absorbance from the initial 3.0 mL aliquot of removed release medium. From this absorbance value we could calculate the expected absorbance from the diluted release medium if additional DX is not being released from the film after the initial 10 min aliquot removal (serial dilution). After another 10 min has elapsed (total 20 min release) an additional aliquot of release medium is removed from the release vessel and the absorbance value analyzed. If additional DX did not release from the film after the initial aliquot was taken, this absorbance value will be exactly that calculated for 3 mL dilution of the initial DX solution (26.9% less than the initial absorbance). If the film did release DX after the initial aliquot was taken this absorbance value will be greater than that expected for serial dilution. The difference between the measured absorbance value

and the calculated value expected for serial dilution is the absorbance due to additional DX release from the film. This difference is then added to the initial absorbance value to give a cumulative absorbance value.

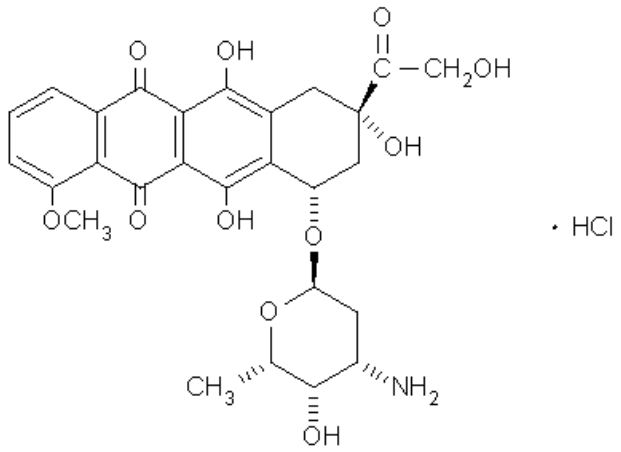

Figure 6-2. Chemical structure of doxorubicin

6.3 Results and Discussion

Shown in Figure 6-3 is the temperature dependent photon correlation spectroscopy (PCS) data for the microgels used in this investigation at pH 3.0 and 6.5. From the figure it can be seen that the microgels at pH 3.0 ($pH<pK_a$), have an average R_h of ~260 nm. Since the AAc groups are almost fully protonated at this pH, the microgels undergo a rather sharp deswelling event over a ~6 ºC range, with a lower critical solution temperature (LCST) of ~31ºC. Figure 6-3 also shows microgels at pH 6.5 ($pH>pK_a$), which have an average R_h of ~375 nm, where the swelling of the microgels at this pH is expected due to AAc deprotonation, which introduces charge-charge repulsion and increased osmotic pressure in the network. Furthermore, as the microgels are heated at

this pH they are unable to deswell to the same minimum R_h observed at pH 3.0, and the VPT temperature is shifted to a much higher temperature, again due to the charged nature of the microgel network.

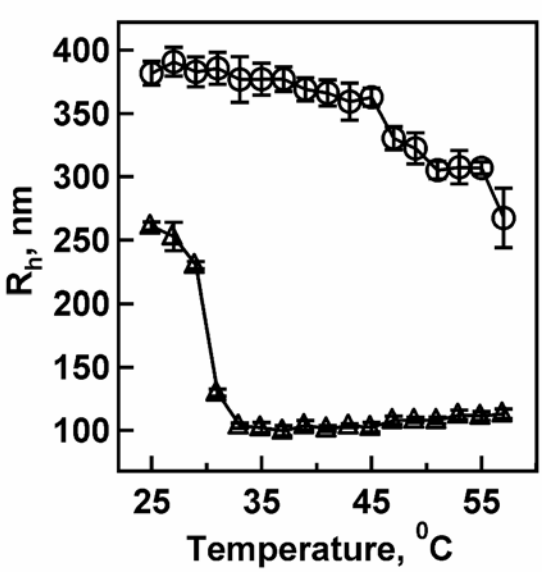

Figure 6-3. Volume phase transition curves taken from PCS measurements for the pNIPAm-AAc microgels used in this chapter, at pH 3.0 (triangles) and pH 6.5 (circles). Error bars represent one standard deviation about the average of five measurements.

Quartz crystal microgravimetry (QCM) was used in this chapter to confirm thin film buildup by monitoring the mass change as poly(*N*-isopropylacrylamide-*co*-acrylic acid) (pNIPAm-co-AAc) microgel and PAH layers were added to the 2-mercaptoethylamine (MEA) functionalized surface.[23] In these studies, we assume that the thin film is rigidly attached to the quartz crystal surface. Figure 6-4 shows a plot of the resonant frequency (Δf_p) as a function of microgel layer number where f_p decreases linearly with increasing layer number. Figure 6-4 also shows the corresponding changes in mass as calculated from Δf_p values using the Sauerbrey equation (Eq. 1), which relates

mass changes directly to Δf_p. From this simple calculation the total frequency change following the addition of 30 microgel layers corresponds to ~3.0 μg of added mass, or 1.0 μg per 10 microgel/9 PAH layers.

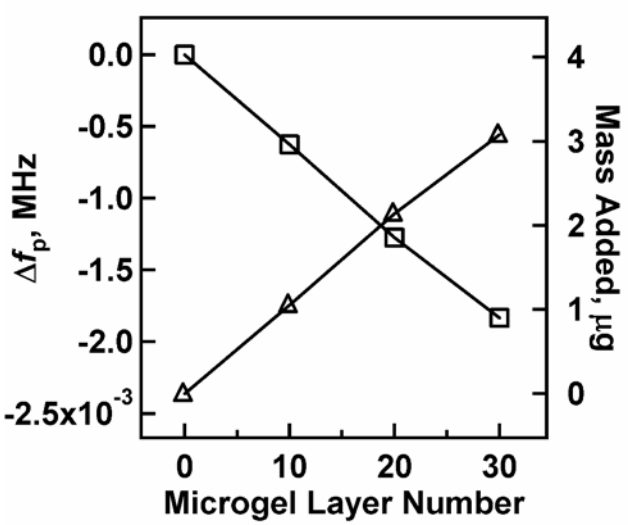

Figure 6-4. Δf_p (squares) and added mass (triangles) values as a function of microgel layer number obtained from QCM.

Since it was verified by QCM that microgel thin films were being built up in a reliable fashion, they were initially used for loading and releasing of FITC. FITC was used as a model drug to test the thin film loading an releasing ability. After this was proven the thin films were used for uptake and release of the chemotherapeutic drug agent doxorubicin (DX). Figure 6-5 shows an idealized schematic depiction of the thin film configuration and the drug loading/release mechanism.

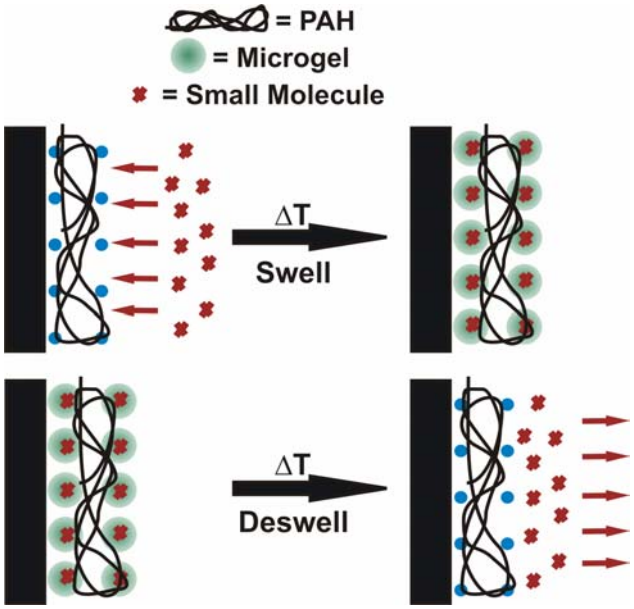

Figure 6-5. Schematic representation of the microgel thin films used in this chapter (not meant to imply order or morphology of the thin film). Films could be loaded by deswelling/swelling the film in a solution containing the molecule of interest. This molecule could be released from the films by deswelling the film upon heating. PAH and microgel not drawn to scale.

To demonstrate thermally regulated loading and release of FITC, microgel thin films composed of 10, 20, and 30 particle layers were constructed on 3-aminopropyltrimethoxysilane (APTMS) functionalized glass substrates, as described above. Before the loading and release experiments were performed the thermoresponsivity of the assembled thin films was confirmed using light scattering, as explained above. The light scattering results for the film immersed in FITC can be seen in Figure 6-6, which show that the film scatters more light at high temperature than at low temperature, indicative of a film that is deswollen and swollen, respectively. When that film is added to the release medium (water) the light scattering was again monitored, which showed similar temperature dependent solvation.

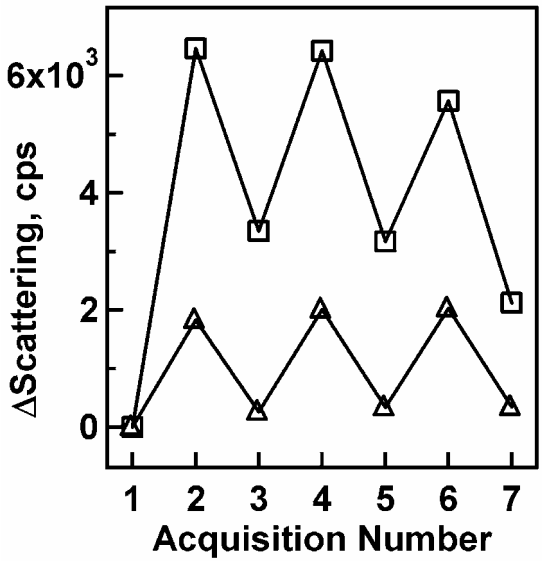

Figure 6-6. Scattering profiles from a 20 layer film in FITC solution for loading (squares) and release medium (triangles). Odd and even acquisition numbers correspond low temperature and high temperature, respectively. The figure shows that the films at high temperature scatter more light indicative of film deswelling.

Since it was determined that the films were thermoresponsive during and after FITC loading, FITC release from the films was monitored using uv-vis. This was done as described in the experimental. Figure 6-7 shows the results for a 10(a) and 30(b) layer film, which show that in each case the films release FITC in a temperature dependent fashion, i.e. the films held at high temperature release FITC as noted by the high absorbance value from the release medium, while the films at low temperature do not as noted by the low absorbance value. This can be correlated to film solvation (Figure 6-6), where the films release only when they are deswollen. This suggest that film deswelling mediates FITC release from the films, possibly following a solvent exchange mechanism. For example, the loaded film is immersed in release medium and heated causing the film

to deswell therefore pushing out a portion of its absorbed FITC. When re-swelled in fresh release medium the absorbed FITC in the film gets diluted. It also can be seen from the figure that the 30 layer film is releasing more than the 10 layer film. From these initial experiments this was expected because a thicker film should be able to load and therefore release more FITC. Further experimentation (as described for DX release) shows that this is not a general trend.

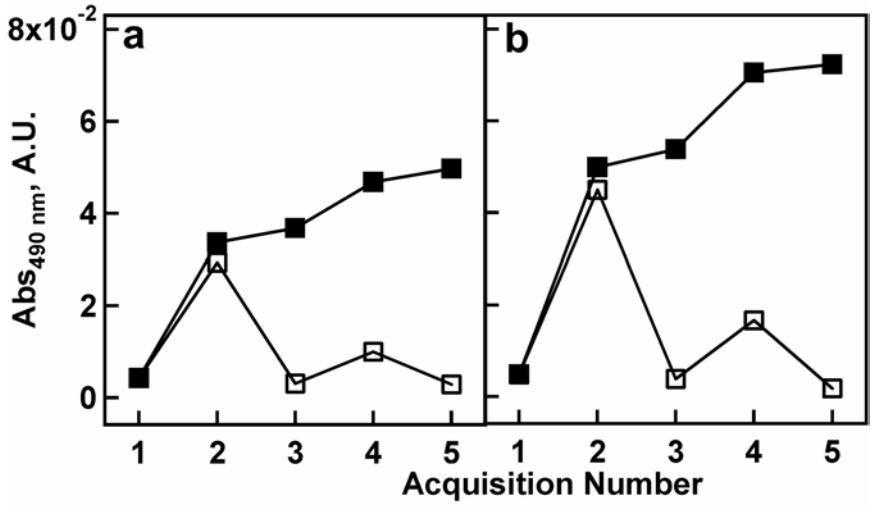

Figure 6-7. Pulsatile (open) and cumulative (solid) release profiles for a 10 (a) and 30 (b) layer thin film where the films were held at 20 ºC (odd numbers on x- axis) and 50 ºC (even numbers on x-axis) for 1 hour intervals. Cumulative release profiles are simply the summation of the absorbance values obtained from pulsatile release. It is observed that the films release significantly more amounts of FITC at high temperature than at low temperature. It can also be seen from the figure that the 30 layer film releases more than the 10 layer film.

Since the films showed thermally regulated release of FITC the next step was to show the release of a bio-relevant molecule. For these experiments the chemotherapeutic drug agent doxorubicin (DX) was used. Again, microgel thin films composed of 10, 20, and 30 particle layers were constructed on 3-aminopropyltrimethoxysilane (APTMS) functionalized glass substrates and used for loading and releasing DX, in a thermally regulated fashion. Loading the films with DX was performed in a similar manner as the above by holding the temperature at ~50 and ~20 ºC for 1 h at each temperature for a total of 6 temperature cycles. For loading, the DX was dissolved in buffered, pH 7.0 (50 mM ionic strength) solution. Loading DX at this pH was more efficient, compared to pH 3.0. This behavior can be understood considering the results discussed in the Chapter 5, which suggests the film is neutral at this pH due to the enforced ionic interactions

between the microgels and PAH.[24] Considering that DX is a weak base it also is mostly neutral at this pH, which should allow for unhindered DX loading into the film. On the other hand, no DX was loaded into films at pH 3.0 presumably due to the positive charge on DX and the film at that pH (observed visually, data not shown). pH dependent loading and release of molecules from similar films has previously been observed.[16] Temperature cycling of the films for loading purposes was also necessary to efficiently load DX into the films as can be inferred by the release profiles seen in Figure 6-8(a). From this figure it can be seen that more DX was released from the film loaded by holding the temperature of the DX solution at ~50 and ~20 ºC for 1 h for a total of 6 temperature cycles, compared to the film simply soaked in DX solution with no temperature cycling for the same amount of time.

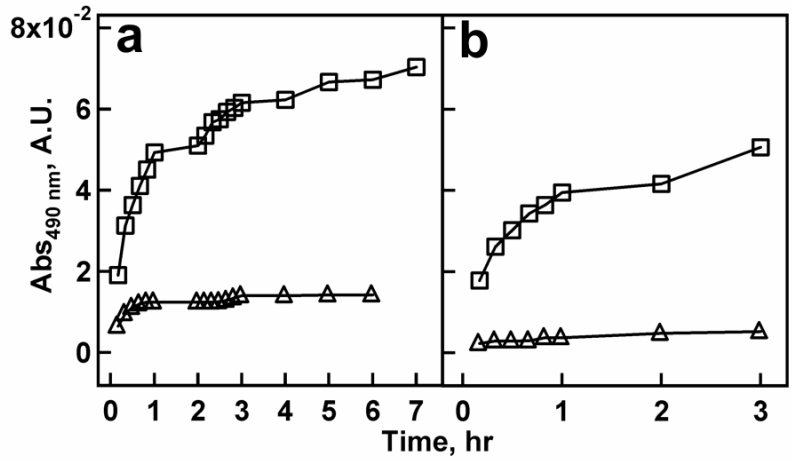

Figure 6-8. (a) Release profiles for 20 layer films loaded with DX obtained by cycling (squares) and not cycling (triangles) the temperature of the loading solution. For this experiment films were initially exposed to release medium at 50 ºC for 1 h followed by 1 h at 20 ºC, which was repeated for 7 h. (b) Release profiles for 10 layer films where the temperature of the release medium was increased to facilitate DX release (squares) and held at room temperature (triangles), which shows minimal release. For this experiment each film was loaded in the same manner, by cycling the temperature of the loading solution between 50 ºC for 1 h followed by 1 h at 20 ºC for 3 cycles.

Once optimal loading conditions were determined, release experiments were performed as a function of microgel layer number. These experiments were conducted by holding the temperature of the release medium (pH 3.0 buffer, 50 mM ionic strength) at ~50 and ~20 ºC for 1 h intervals, while removing aliquots of release medium for analysis at various time intervals. pH 3.0 buffer was chosen because it allowed for the most efficient release of DX from the films (data not shown). This behavior is most likely due to the ionic repulsion between the protonated DX and PAH in the film, where the release is promoted by increasing the temperature of the release medium, thereby causing a deswelling of the microgel thin film.[24] Figure 6-9(a) shows the pulsatile release behavior for the films as a function of temperature and microgel layer number. From the figure it can be seen that all the films release DX in a temperature dependent fashion due to the

films microgel component deswelling at high temperature and presumably "squeezing" DX out of the film. If films were not thermally cycled, the release of DX from the film was greatly reduced, Figure 6-8(b). Figure 6-9(b) shows the cumulative release profiles as a function of time where it can be seen that the 10 layer film releases the least amount of DX. From the figure it can also be seen that the 20 and 30 layer films release approximately the same amount of DX. The exact reason for this observation is not known but could be due to film densification as more layers are added to a film, as described in Chapter 5. Since this is the case a 30 layer film may be denser than the 20 layer film and therefore has less available volume to load DX.[24] Figure 6-10 shows the equilibration time of films loaded in the same manner as above and held at 50 ºC while sampling the release medium over time. From the figure it can be seen that the films take ~12 hrs to equilibrate, illustrating the ability of microgel thin films to release DX over long periods of time.

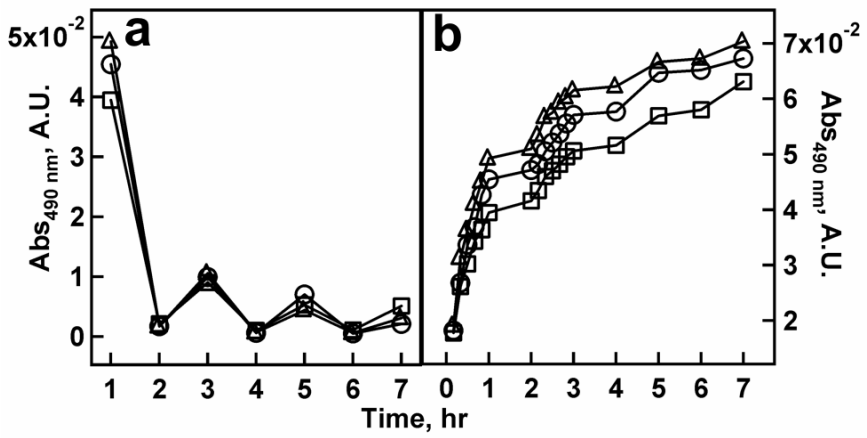

Figure 6-9. (a) Pulsatile release profiles for a 10 (squares), 20 (triangles), and 30 (circles) layer thin film where films were held at 50 ºC and 20 ºC for 1 hour intervals. (b) Cumulative release profiles for a 10 (squares), 20 (triangles), and 30 (circles) layer thin film where the films were held at 50 ºC and 20 ºC while sampling the release medium every 10 minutes for the first two hot cycles. Note, films were initially exposed to release medium at 50 ºC for 1 h followed by a 1 h cycle at 20 ºC. This was repeated for 7 h (a, b).

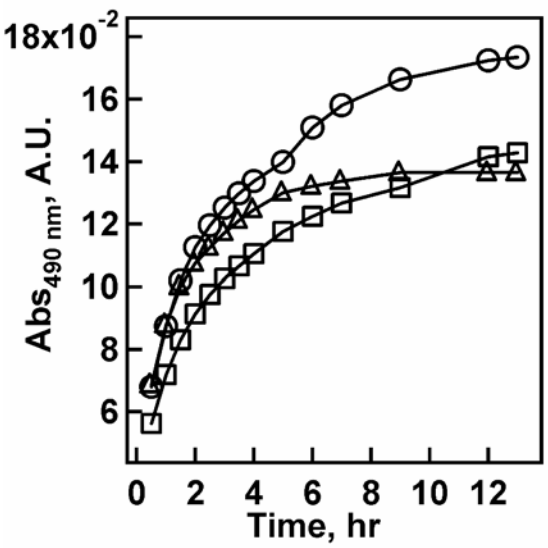

Figure 6-10. Cumulative release profiles for a 10 (squares), 20 (triangles), and 30 (circles) layer thin film held at 50 ºC over time while sampling the release medium at various time intervals.

6.4 Conclusions

This chapter illustrated the ability of scLbL assembled pNIPAm-co-AAc microgel thin films to load and release small molecules such as FITC and DX in a temperature and pH dependent fashion. By cycling the temperature to above the LCST of the microgels comprising the films we could modulate the loading and release behavior, where films that were temperature cycled loaded more efficiently than films not temperature cycled. Also, films at high temperature were able to release in a more efficient fashion than films only soaked in release medium with no temperature increase.

REFERENCES

(1) Nolan, C. M.; Serpe, M. J.; Lyon, L. A. *Biomacromolecules* **2004**, *ACS ASAP*.

(2) Serpe, M. J.; Lyon, L. A. **2004**, *in preparation*.

(3) Gupta, P.; Vermani, K.; Garg, S. *Drug Discov. Today* **2002**, *7*, 569-579.

(4) Peppas, N. A. *Curr. Opin. Colloid Interface Sci.* **1997**, *2*, 531-537.

(5) Kikuchi, A.; Okano, T. *Adv. Drug Deliv. Rev.* **2002**, *54*, 53-77.

(6) Kim, S. W.; Bae, Y. H.; Okano, T. *Pharm. Res.* **1992**, *9*, 283-290.

(7) Qiu, Y.; Park, K. *Adv. Drug Deliv. Rev.* **2001**, *53*, 321-339.

(8) Hoffman, A. S. *Adv. Drug Deliv. Rev.* **2002**, *54*, 3-12.

(9) Kiser, P. F.; Wilson, G.; Needham, D. *J. Control. Release* **2000**, *68*, 9-22.

(10) Eichenbaum, G. M.; Kiser, P. F.; Dobrynin, A. V.; Simon, S. A.; Needham, D. *Macromolecules* **1999**, *32*, 4867-4878.

(11) Eichenbaum, G. M.; Kiser, P. F.; Shah, D.; Simon, S. A.; Needham, D. *Macromolecules* **1999**, *32*, 8996-9006.

(12) Kiser, P. F.; Wilson, G.; Needham, D. *Nature* **1998**, *394*, 459-462.

(13) Chung, A. J.; Rubner, M. F. *Langmuir* **2002**, *18*, 1176-1183.

(14) Quinn, J. F.; Caruso, F. *Langmuir* **2004**, *20*, 20-22.

(15) Vazquez, E.; Dewitt, D. M.; Hammond, P. T.; Lynn, D. M. *J. Am. Chem. Soc.* **2002**, *124*, 13992-13993.

(16) Burke, S. E.; Barrett, C. J. *Macromolecules* **2004**, *37*, 5375-5384.

(17) Chiarelli, P. A.; Johal, M. S.; Holmes, D. J.; Casson, J. L.; Robinson, J. M.; Wang, H. L. *Langmuir* **2002**, *18*, 168-173.

(18) Cho, J.; Char, K. *Langmuir* **2004**, *20*, 4011-4016.

(19) Lee, S. S.; Lee, K. B.; Hong, J. D. *Langmuir* **2003**, *19*, 7592-7596.

(20) Lee, S. S.; Hong, J. D.; Kim, C. H.; Kim, K.; Koo, J. P.; Lee, K. B. *Macromolecules* **2001**, *34*, 5358-5360.

(21) Palegrosdemange, C.; Simon, E. S.; Prime, K. L.; Whitesides, G. M. *J. Am. Chem. Soc.* **1991**, *113*, 12-20.

(22) Serpe, M. J.; Jones, C. D.; Lyon, L. A. *Langmuir* **2003**, *19*, 8759-8764.

(23) Buttry, D. A.; Ward, M. D. *Chem. Rev.* **1992**, *92*, 1355-1379.

(24) Serpe, M. J.; Lyon, L. A. *Chem. Mater.* **2004**, *submitted*.

CHAPTER 7

COLLOIDAL HYDROGEL MICROLENSES

7.1 Introduction

This chapter is divided into three main sections all describing the use of colloidal hydrogels (microgels) as microlens elements. The first section describes the use of microgels as microlens elements in air,[1] the second section describes the use of these microlenses in solution, which show dynamic focal length tunability by taking advantage of the microgel responsivity to changes in solution temperature and pH,[2] and the third section describes the use of microlenses in solution, which show dynamic focal length tunability in response to laser irradiation.[3]

For all the studies presented in this chapter a *monolayer*, as opposed to a *multilayer*, of microgels is used. For all studies poly(*N*-isopropylacrylamide-*co*-acrylic acid) (pNIPAm-co-AAc) microgels were immobilized on glass substrates using previously described electrostatic interactions of microgels with positively charged substrates (Chapters 4 and 6).[4] Because pNIPAm-co-AAc microgels are mechanically soft, it is possible for the attractive forces between the substrate and the microgel to cause the microgel to deform upon attachment and subsequent drying to produce a microgel decorated substrate where the particles are deformed in an anisotropic fashion. As discussed in Chapter 2, pNIPAm-co-AAc microgels are also environmentally responsive,[5,6] allowing the possibility of dynamically tuning the microgel curvature in response to solution temperature and pH changes.

The field of micro-optics (e.g. lenses and mirrors) has been of considerable interest over the past decade, as photonic applications attempt to keep up with the trend of device miniaturization. Microlenses in particular have been applied to such fields as telecommunications, image analysis,[7,8] and photolithography.[9-14] Microlenses and microlens arrays are well know and can be accomplished by a number of routes such as photolithography,[9,11,13,15,16] photothermal patterning,[17] photopolymerization/photo-curing,[18-20] and polymeric particle self-assembly/melting.[21,22] These systems have been studied in detail but often have the shortcoming of requiring multiple fabrication steps resulting in lenses with fixed focal lengths, relatively large diameters and/or slow focal length switching speeds. A self-assembly approach, in which the microlens precursors are synthesized by traditional solution polymerization routes and are then directly assembled on a substrate would be extremely beneficial with respect to the speed of fabrication and the ultimate size limitations of such arrays. Another challenge is to construct true microlens arrays, using self assembly approaches, where the focal length of individual lens elements can be addressed on demand, independent of other array elements. Accomplishment of the above goals would represent an enabling technology for a new class of applications in foveated vision, parallel chemical sensing, and beam steering as well as an expansion of the tools available to current efforts in the field.

7.2 Microlens Elements in Air

7.2.1 Experimental

Materials All reagents were purchased from Sigma-Aldrich unless otherwise specified. *N*-Isopropylacrylamide (NIPAm) was re-crystallized from hexanes (J.T. Baker)

and dried under vacuum prior to use. Acrylic acid (AAc) was distilled under reduced pressure. *N*,*N*'-Methylene(bisacrylamide) (BIS) and ammonium persulfate (APS) were used as received. 3-Aminopropyltrimethoxysilane (APTMS) was purchased from United Chemical Technologies Inc. and was kept in a desiccator for storage. The glass substrates used were 24 x 50 mm Fisher Finest brand cover glass obtained from Fisher Scientific. Sulfuric acid and 30% hydrogen peroxide (J.T. Baker) were used to make Piranha cleaning solutions. 95% and absolute ethanol was used for various purposes in this investigation. All water used throughout this investigation was first house distilled and then deionized to a resistance of at least 18 MΩ (Barnstead Thermolyne E-Pure system) and then filtered through a 0.2 μm filter to remove particulate matter. 3M transparency film for laser printers and a Hewlett Packard LaserJet 4000N printer was used for pattern printing.

Glass Substrate Preparation APTMS functionalized glass cover slips were used throughout this section as positively charged substrates for microgel deposition. Prior to functionalization the glass substrates were cleaned as previously outlined.[23] Glass cover slips were first wiped clean of any dust using a Kimwipe (Kimberly-Clark). Following this step the substrates were immersed in hot Piranha solution, 4:1 H_2SO_4 : H_2O_2, (~70 °C) to remove any organics from the substrate surface (Caution! Piranha solutions react violently in the presence of many organic compounds and should be handled with extreme caution). Next, the substrates were rinsed copiously with H_2O then copiously with 95% ethanol. Following this rinsing procedure the substrates were immersed in an ethanolic (absolute ethanol) 1% APTMS solution for ~2 hrs. After 2 hrs the substrates were removed from the APTMS solution and again rinsed copiously with 95% ethanol.

These substrates were stored in 95% ethanol for no longer than 5 days prior to use. Prior to particle deposition, these substrates were rinsed with H_2O and dried under a stream of nitrogen gas.

Microgel Synthesis The same batch of microgels was used throughout all the experiments presented in this chapter. The microgels had a molar composition of 89.5% NIPAm, 0.5% BIS, and 10% AAc synthesized as outlined in Chapter 4, using 300 mM total monomer concentration. Polymerization was carried out in a three-neck, 200 mL round-bottom flask to which 100 mL of filtered, aqueous solution of NIPAm and BIS was added. This solution was heated to ~70 °C while degassing with N_2 gas and stirring vigorously with a magnetic stir bar for ~1 hr. After 1 hr, 200 μL of AAc was added to the round-bottom flask to bring the total monomer concentration up to 300 mM. Once the additional monomer was added, the reaction was immediately initiated by injection of 1 mL of a hot (~ 70 °C) APS solution (6.13 mM) to bring the solution concentration to 0.0613 mM APS. Within ~1 minute the solution turned turbid indicating successful initiation. This solution was allowed to heat and stir for an additional 4 hours while keeping the reaction under a nitrogen blanket. Following synthesis the particles were purified by dialysis against DI water for ~2 weeks with the water being changed twice per day, using 10 000 MW cut-off dialysis tubing (VWR).

Microscopy Optical and electron microscopies were used throughout this section to confirm microgel shape, size and lensing ability. A Hitachi S800 scanning electron microscope (SEM) was used to determine the shape of microgels attached to the glass substrate. Images were obtained by attaching a dry microgel decorated glass substrate to a SEM peg at a 45˚ angle and placed in the SEM chamber. The substrate was then imaged

with an accelerating voltage of 4 kV and the sample tilted relative to the incoming electrons in order to obtain profile images of the microgels, as previously described.[24] Brightfield transmission, polarized light, and differential image contrast (DIC) optical microscopies were used to confirm the lensing abilities of the microgels attached to the substrate as well as to determine microgel size. An Olympus IX 70 inverted microscope equipped with a high numerical aperture, oil immersion 100X objective (N.A.=1.30) was used to obtain images of the microgels adsorbed to the glass substrate as well as imaging a mask through the microgel to prove the lensing abilities of the microgels. Images were captured using a black and white CCD camera (PixelFly, Cooke Corporation).

7.2.2 Results and Discussion

Microgels that are approximately 2 μm in diameter in their water-swollen state were used to fabricate microlenses. A differential image contrast (DIC) microscope image of the microgels adsorbed to a glass substrate is shown in Figure 7-1(a). Microgels were adsorbed to an APTMS functionalized glass substrate by exposing the glass substrate to a 10% (v/v) aqueous microgel solution for approximately 1 hr. The substrate was then rinsed with deionized H_2O and air dried for approximately 1 day prior to imaging. Because these microgels are soft/deformable materials it should be the case that when the microgel dries on a surface it does so in an anisotropic fashion (one dimension deswells more than the other) under conditions where the surface/microgel adhesion is strong. This anisotropic drying behavior is seen in the SEM image of the microgels in Figure 7-1(b) where it is observed that the microgels de-swell in the z-dimension more than they do in the x-y dimension. This type of microgel behavior has been reported previously by other investigators.[24]

From Figure 7-1(b) it is apparent that the microgels do resemble traditional plano-convex lenses but it is not intuitive that this type of material can actually be used as an optical element. To evaluate the optical properties of the deformed microgels, an inverted optical microscope (Scheme 7-1) was used and the particles were imaged through crossed polarizers. When a microscope is set up in crossed polars, where the polarization directions for the polarizer and analyzer are perpendicular, a characteristic "cross" pattern arising from optical interference is visible in the objective back focal plane. This cross pattern can be seen by looking down the eyepiece tube of the microscope after the eyepiece has been removed or if an optical element, such as a long focal length Bertrand lens, is inserted into the imaging system. To determine if microgels can act as microlenses we inserted the substrate containing dried microgels onto the microscope and imaged in a standard brightfield transmission configuration, Figure 7-1(a). The polarizer/analyzer pair was then inserted into the microscope such that their polarization directions were perpendicular, as determined by observing the characteristic cross pattern upon removal of the microscope eyepiece. The eyepiece was then replaced and the microgels were observed under crossed polars with slight defocusing of the objective. Upon defocusing, characteristic cross patterns, as seen in the top right inset of Figure 7-2, could be observed through each microgel attached to the substrate. Normally, if a Bertrand lens was inserted into a microscope under crossed polars, the observer would see one large cross pattern through the eyepiece. The fact that a cross pattern is visible through each microgel is indicative of the microgels all acting as independent lenses.

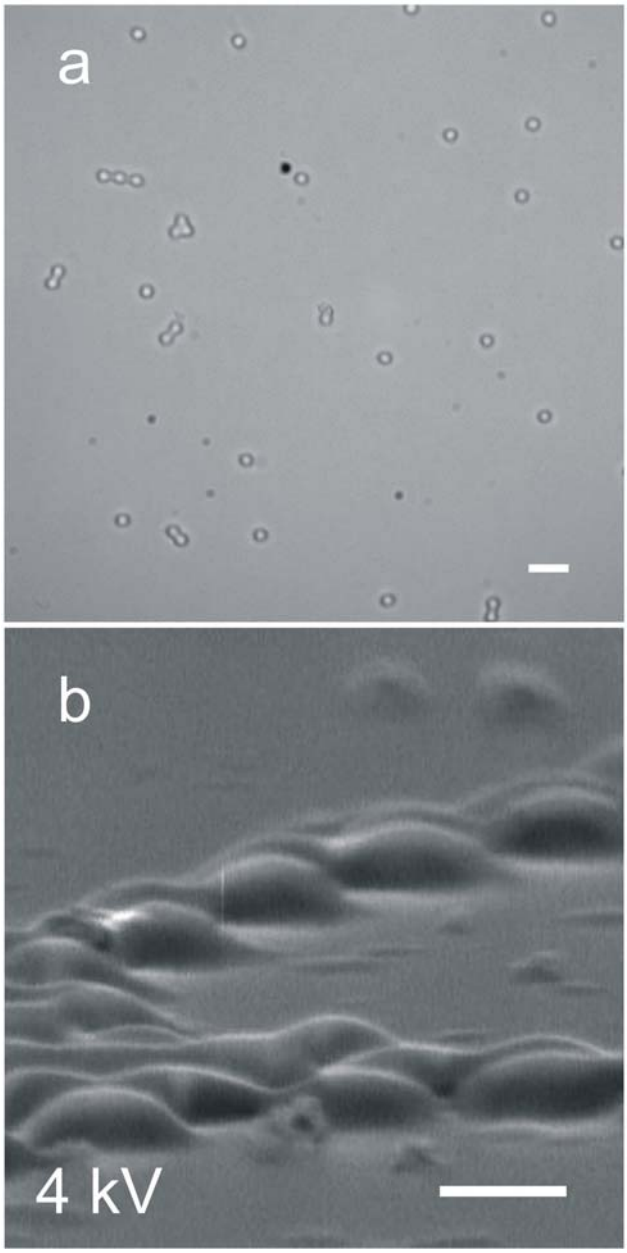

Figure 7-1. (a) DIC image of microgels used throughout this section, scale bar is 5 μm. (b) SEM image of the microgels imaged at a grazing angle relative to the substrate. As can be seen from the image, the microgels have a plano-convex shape. Scale bar for the SEM is 1 μm.

Scheme 7-1. Inverted light microscopy setup used for imaging experiments in this section

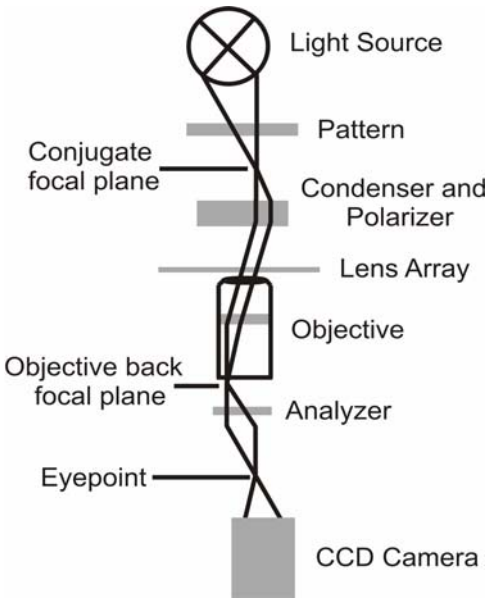

From this observation it seems that the microgels are acting as independent microlenses. To test their ability to reconstruct and project a real-space image, a photomask made by printing a GT pattern on a standard transparency slide using a standard laser printer, was inserted near a conjugate plane to the back focal plane of the objective. The mask is shown in the top left inset of Figure 7-2. The appropriate conjugate plane lies at or near the filament of the halogen bulb used for bright field illumination. The pattern was inserted into the microscope as close to the bulb as possible (at the aperture stop) so that the light passed through the GT pattern before being projected upon the lenses. The same substrate used to show the cross patterns was used here as well. If the microgels were indeed acting as microlenses the microgels should be able to independently project the GT pattern upon defocusing of the objective. Slight defocusing is necessary since it is impossible to place the pattern exactly at the true

conjugate focal plane. Shown in Figure 7-2 is an image of the microgels with the pattern GT projected through each microgel attached to the substrate. The interesting feature of these microlenses is their ability to project the GT pattern with high pattern integrity, despite the fact that these optical elements were prepared by simple solution polymer chemistry. Another interesting observation was the fact that not every microgel brings the GT into focus at the same exact point, which illustrates that our microgels have a variety of different focal lengths (i.e. curvature). Altering the surface chemistry or the softness of the microgels by varying their crosslink density presumably can control this.

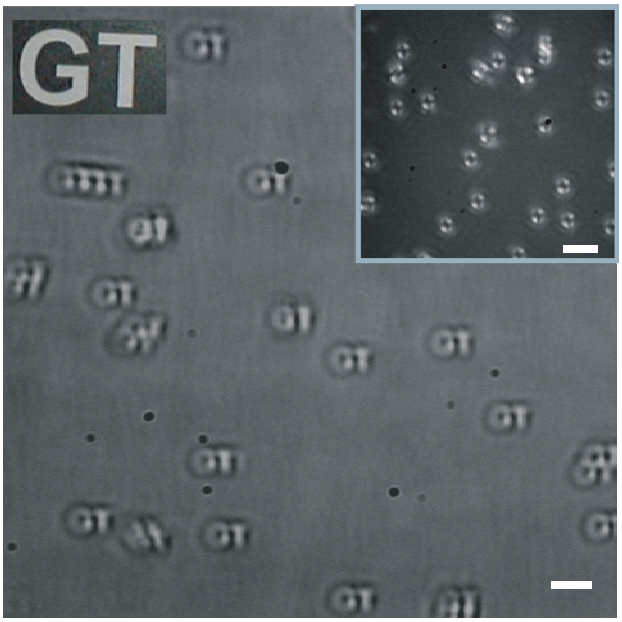

Figure 7-2. Microscope image of the substrate supported microgels from Figure 1(a) illustrating the microgels' ability to project a pattern that has been placed at the illumination aperture stop. The scale bar is 5 μm. Top left inset shows the photomask used for the GT projection onto the microgel array. Top right inset shows that each microgel on the substrate is displaying the characteristic cross pattern, which is visible under crossed polars when a Bertrand lens is inserted into the microscope, through every microgel attached to the substrate. The scale bar is 10 μm.

Thus far we have demonstrated the construction of microlenses from soft colloidal precursors arranged on a substrate in a random fashion. To further illustrate the usefulness of this microlens fabrication process ordered microlens arrays were assembled following the same procedure as outlined above but instead of rinsing the substrate with H_2O after one hour the microgel solution was allowed to completely dry on the substrate without rinsing, which took about 4-5 hours on average. Light microscopy images of a select region of the arrays are shown in Figure 7-3 (a, c). The images show that the microgels self-assemble into ordered arrays spontaneously upon drying which results in

very few defects. Next, we showed that these arrays were useful for pattern projection as shown in Figure 7-3 (b, d) for a triangle pattern and a cross pattern, respectively. It was also shown that more complex patterns could be obtained from the simple patterns used by defocusing the patterns to the point that the images overlap, as seen in the top right insets of Figure 7-3 (b, d).

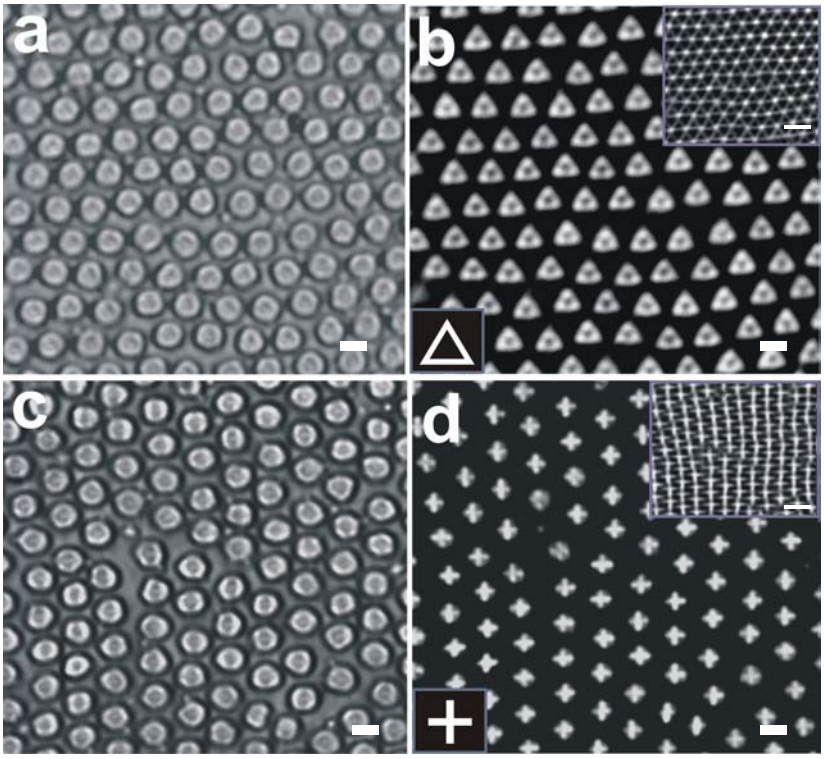

Figure 7-3. Microscope image of a portion (~25 μm x 25 μm) of the substrate supported microgels in an ordered array. Panels (a, c) show the microscope image of the microgels dried on the substrate while panels (b, d) show the image projection of the pattern, shown in the bottom left insets of panels (b, d). The scale bar is 2 μm. The above images show that the microgels exhibit the ability to project patterns in an ordered array. Shown in the top right insets of panels (b, d) are projections of the patterns in a defocused state illustrating the ability of the array to form connected features, which allows for the formation of more complex patterns. The scale bar is 5 μm.

7.2.3 Section Conclusions

This section has demonstrated the ability of pNIPAm-co-AAc microgels to act as microlenses. This was accomplished by assembling the microgels onto substrates through electrostatic interactions, which restricts the dimensional changes of the particles in the x-y plane, thus causing the particle to adopt a plano-convex shape following drying. The lensing ability of these particles has been illustrated by observing their ability to bring an image present in the back focal plane of an optical microscope into the image plane. This

effect indicates that the substrate-supported microgels are capable of acting as independent optical elements. It was also illustrated that ordered microlens arrays could be easily obtained by following a simple drying procedure. The next section describes the use of the above microlens arrays in solution, which show focal length tunability dependent on solution conditions.

7.3 Microlens Elements in Solution

7.3.1 Experimental

Materials All reagents were purchased from Sigma-Aldrich unless otherwise specified. *N*-Isopropylacrylamide(NIPAm) was re-crystallized from hexanes (J.T. Baker) prior to use. Acrylic acid(AAc) was distilled under reduced pressure. *N*,*N*'-Methylene(bisacrylamide) (BIS) and ammonium persulfate (APS) were used without further purification. 3-Aminopropyltrimethoxysilane (APTMS) was purchased from United Chemical Technologies Inc. The glass substrates used were 24 x 50 mm Fisher Finest brand cover glass obtained from Fisher Scientific. 95% and absolute ethanol was used for various purposes in this investigation. Water was distilled and then deionized (DI) to a resistance of at least 18 MΩ. (Barnstead Thermolyne E-Pure system) and then filtered through a 0.2 μm filter to remove particulate matter. 3M transparency film for laser printers and a Hewlett Packard LaserJet 4000N printer was used for pattern printing.

Microgel Synthesis The same batch of microgels was used throughout these experiments and were the exact same microgels used in the previous section.

Microlens Substrate Preparation Glass substrates were cleaned in an Ar plasma (Harrick Scientific) for 30 min to remove organics from the substrate surface. The

substrates were immersed in an ethanolic (absolute ethanol) 1% APTMS solution for ~2 hrs. After 2 hrs the substrates were removed from the APTMS solution and again rinsed copiously with 95% ethanol. These substrates were stored in 95% ethanol for no longer than 5 days prior to use. Prior to assembly, these substrates were rinsed with DI water and dried under a stream of N_2 gas. The substrate was then exposed to an aqueous 10% (v/v) microgel solution at pH 6.5 (~0.001 M ionic strength) and allowed to completely dry on the substrate (~24 hrs). The substrate was subsequently immersed in DI water for 2 hrs, then rinsed with DI water, and dried with N_2 gas to leave behind only microgels strongly attached to the substrate by electrostatic interaction. Under these conditions, we find that the glass substrate is largely covered with a close-packed monolayer of particles. The thickness of this film is somewhat less than the swollen particle diameter, as the particles spread and flatten on the substrate, as shown in Figure 7-4. Decreasing the particle concentration results in a sparser coverage. While the details of why ordered monolayers arise from this procedure are still a matter of investigation, it is clear that by correctly balancing the particle concentration, particle-surface attraction, particle-particle repulsion, and capillary forces from the solvent, ordered arrays can be obtained. Dynamic tunability of the microlenses in response to pH was illustrated by introducing different pH solutions (~0.001 M ionic strength) into the void space in a microlens array/silicone gasket/coverslip sandwich assembly (Scheme 7-2) using syringes inserted through the wall of the gasket.

Scheme 7-2. Inverted light microscopy setup used for imaging experiments in this section

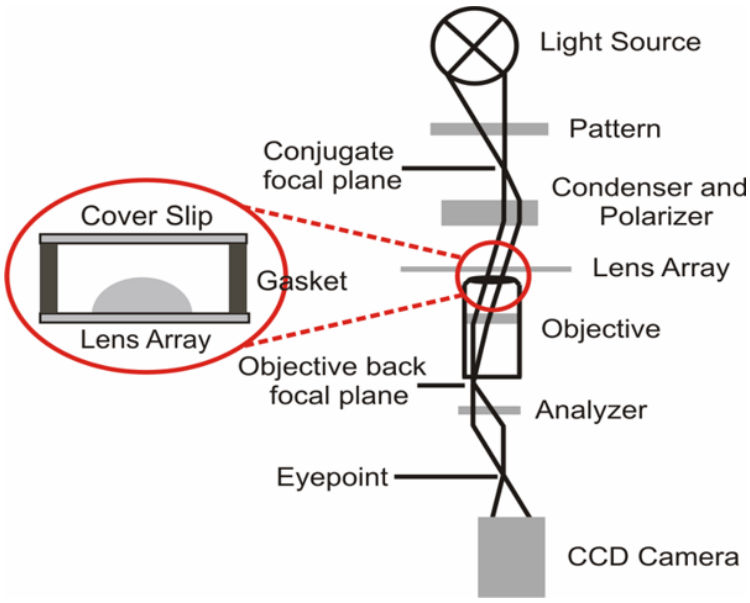

Microscopy Optical and electron microscopies were used to confirm microgel shape, size and lensing ability. A Hitachi S800 scanning electron microscope (SEM) was used to determine the shape of microgels attached to the glass substrate in the dried state. SEM images were obtained by attaching a dry microgel decorated glass substrate to a SEM peg and placed in the SEM chamber. The substrate was then imaged with an accelerating voltage of 15 kV with the sample tilted relative to the incoming electrons in order to obtain profile images of the microgels. Brightfield transmission, and differential image contrast (DIC) optical microscopies were used to confirm the lensing abilities of the microgels attached to the substrate. An Olympus IX70 inverted microscope equipped with a high numerical aperture, oil immersion100X objective (N.A.=1.30), a microscope objective heater and a Peltier-based temperature stage was used for imaging the pattern

under various conditions. Images were captured using a black and white CCD camera (PixelFly, Cooke Corporation) as a function of pH and temperature.

7.3.2 Results and Discussion

Microgels that are approximately 2 μm in diameter in their water-swollen state were used to fabricate microlens arrays, as described above. A SEM image of the microgels adsorbed to a glass substrate is shown in Figure 7-4. Figure 7-5 shows the focal length tunability of a microlens in response to pH at 25 °C. The differential interference contrast (DIC) images in panels (a) and (b) show that the substrate bound microgel is compact at pH 3.0 and swollen at pH 6.5, respectively. This behavior is again due to the AAc groups within the microgel network becoming negatively charged (pK_a~4.25) at pH 6.5, which in turn causes gel swelling due to Coulombic repulsion and osmotic effects.[5,6] Since the diameter, and presumably the curvature of the substrate-bound microgels are tunable in response to pH, the lens power should be similarly tunable. This lens power tunability is illustrated in Figure 7-5 (c, d) at pH 3.0 and 6.5, respectively. This figure is made by zooming in on a single particle from an array, as seen in Figure 7-6. Figure 7-5 (c) shows that the microgel at pH 3.0 brings into focus a cross pattern placed conjugate to the objective back focal plane (Scheme 7-2),[1] while Figure 7-5 (d) shows that the same microgel at pH 6.5 is not able to focus the cross pattern at the same focal point. This focal length tunability can be understood by considering the microgels to be more optically dense at pH 3.0 than at pH 6.5. Taking into account the fact that focal lengths are dependent upon the ratio of the refractive index (RI) between the lens material and the surrounding medium, where a higher RI difference gives a lens with a shorter focal

length (higher lensing power), it is clear why the cross-like pattern is visible through the microlens at pH 3.0 and is not focused at pH 6.5.

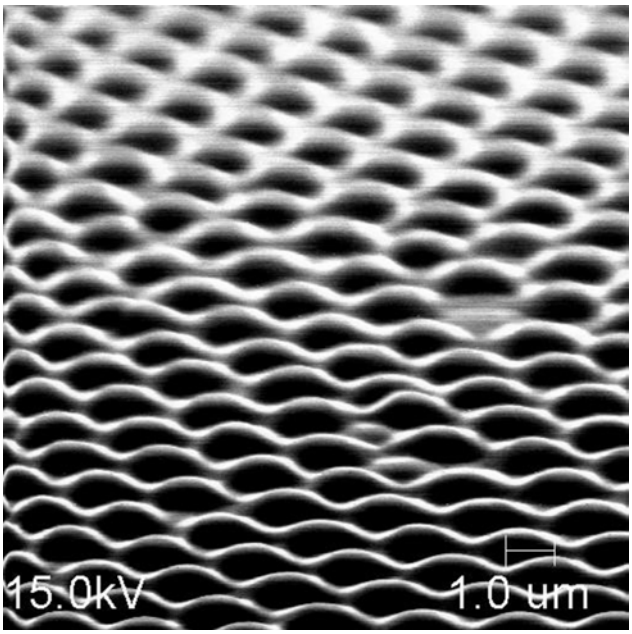

Figure 7-4. SEM image of a microlens array imaged at a grazing angle with respect to the substrate. The microgels have formed an ordered array of plano-convex shapes.

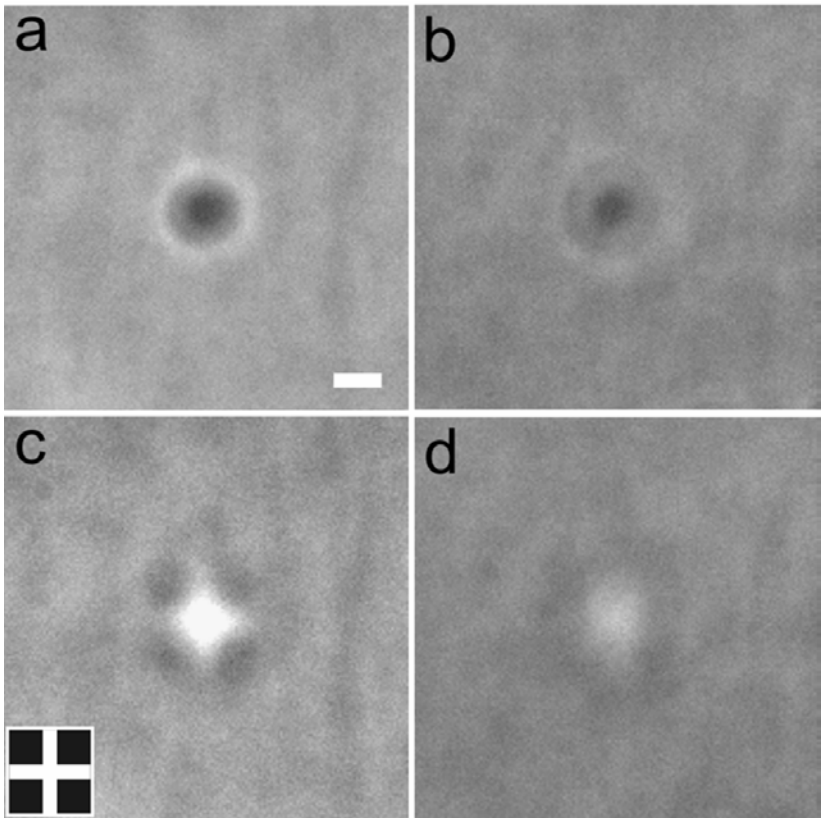

Figure 7-5. Panels (a) and (b) show the DIC microscopy images of a substrate-bound microgel at pH 3.0 and 6.5, respectively, at 25 °C. Panels (c) and (d) show the projection of the cross pattern (inset) through the microgel at the respective pH values. The scale bar is 1 μm.

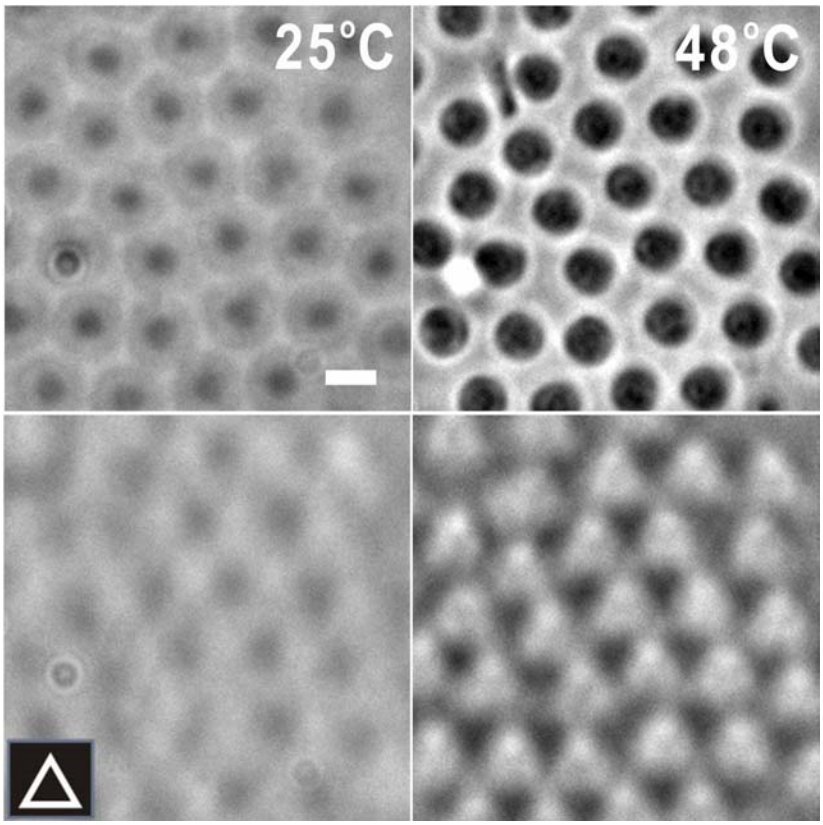

Figure 7-6. DIC and pattern projection images of particle arrays in water at pH 6.5 showing homogeneous image quality from lens to lens. The scale bar is 1 μm and the triangle pattern used is shown in the inset.

Since pNIPAm-co-AAc microgels are thermoresponsive at pH 3.0 but significantly less so at pH 6.5, the microlenses should display a pH dependent thermal tunability. Figures 7-7 and 7-8 show the responsivity of the substrate bound microgels and their resulting lensing ability as a function of temperature at pH 3.0 and 6.5, respectively. The DIC microscopy images in Figure 7-7(top) show that the microgels respond to increases in temperature by decreasing in size. This shrinking results in an increase in RI contrast with respect to water, which should result in an improved microlens structure. Figure 7-7(bottom), illustrates that this is the case. As the

temperature is increased from 25 °C to 40 °C the microlens focuses the cross-like pattern with higher fidelity. It is also interesting to note that the hydrogel undergoes a sharp transition at ~31 °C,[25-27] which is the same point at which the microlens drastically changes its lensing ability. Figure 7-8(top) shows the DIC images of the substrate bound microgel at pH 6.5 as a function of temperature. In contrast to the behavior at pH 3.0, the higher pH results in a microgel that is not responsive to heating over the same temperature range. It is not until 48 °C that the microgel undergoes a transition, which is consistent with previous studies of gel swelling.[25] As expected, the lensing ability, which is shown in Figure 7-8(bottom), is unaffected until the transition temperature of 48 °C, at which point the optical properties drastically change.

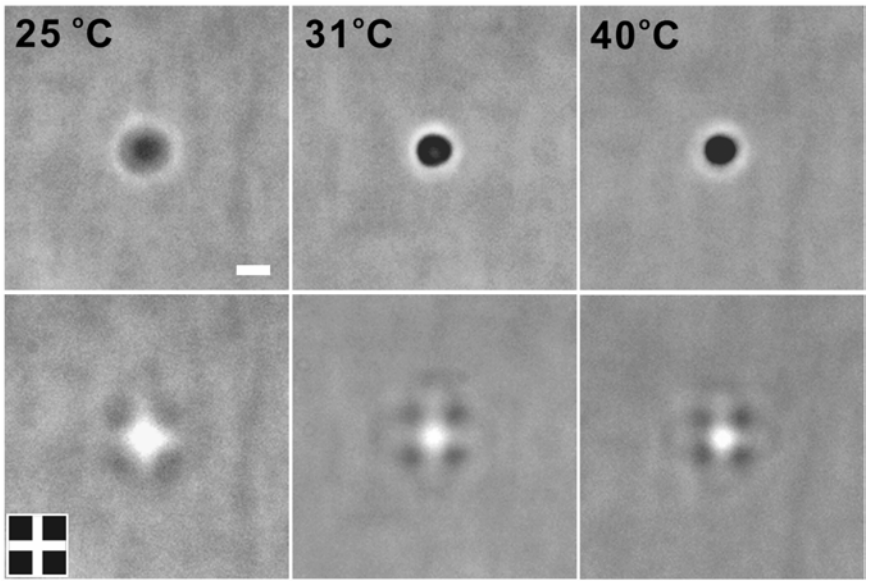

Figure 7-7. (Top) DIC microscopy of a substrate bound microgel in pH 3.0 solution as a function of temperature. (Bottom) Projection of the cross pattern (inset) through the microgel at the indicated temperatures. The scale bar is 1 μm.

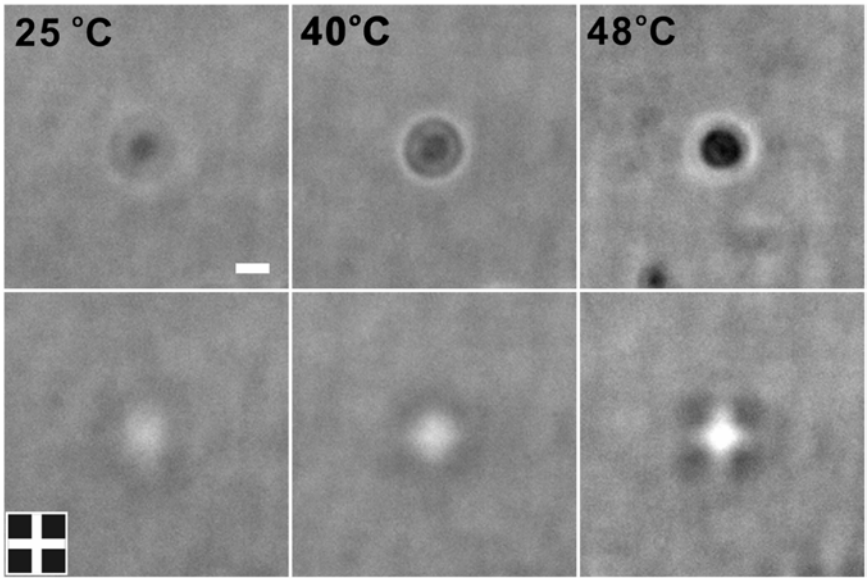

Figure 7-8. (Top) DIC microscopy of a substrate bound microgel in pH 6.5 solution as a function of temperature. (Bottom) Projection of the cross pattern (inset) through the microgel at the indicated temperatures. The scale bar is 1 μm.

7.3.3 Section Conclusions

To conclude this section, optical microscopy was used to show that substrate supported, stimuli-responsive pNIPAm-co-AAc microgels form dynamically tunable microlenses. The lenses are produced via simple aqueous phase polymerization and the arrays are fabricated without the need for photolithographic or micromolding processes. These characteristics make this system attractive for rapid construction of lens arrays with wet chemical methods. Furthermore, these structures have been shown to be tunable as a function of temperature and pH, where the water content of the microgel has a profound effect on lensing ability due to changes in refractive index contrast with the medium. Given the intrinsically fast (sub-millisecond) shrinking rates of microgels, the ultimate tuning rates of such arrays could be similarly rapid, which is the topic of

discussion of the next section. This section represents the first demonstration of dynamically tunable microlenses that are truly scalable to high-density array formats.

7.4 Microlenses in Solution with Phototunable Focal Lengths

7.4.1 Experimental

Materials All reagents were purchased from Sigma-Aldrich unless otherwise specified. Poly(allylamine hydrochloride) (PAH), MW 70 000, was used as received. *N*-Isopropylacrylamide (NIPAm) was re-crystallized from hexanes (J.T. Baker) and dried under vacuum prior to use. Acrylic acid (AAc) was distilled under reduced pressure. *N*,*N*'-Methylene(bisacrylamide) (BIS) and ammonium persulfate (APS) were used as received. 3-Aminopropyltrimethoxysilane (APTMS) was purchased from United Chemical Technologies Inc. and was kept in a desiccator for storage. The glass substrates used were 24 x 50 mm Fisher Finest brand cover glass from Fisher Scientific. 95% and absolute ethanol (200 proof) was used for various purposes in this investigation. All water used throughout this investigation was first distilled and then deionized (DI) to a resistance of at least 18 MΩ (Barnstead Thermolyne E-Pure system) and then filtered through a 0.2 μm filter to remove particulate matter. 3M transparency film for laser printers and a Hewlett Packard LaserJet 4000N printer was used for pattern printing.

Microgel Synthesis The same batch of microgels was used throughout these experiments and were the exact same microgels used in the previous sections.

Au Nanoparticle Synthesis 250 mL of 1.0 mM $HAuCl_4$ solution was stirred while heating to a vigorous boil. 25 mL of a 38.8 mM sodium citrate was then rapidly added to the above solution producing a pale yellow solution, which quickly became a deep

burgundy. The solution was allowed boil for an additional 10 min following the color change. The heat source was then removed and stirring was allowed to proceed for 15 min. The particle diameter determined by transmission electron microscopy (TEM, JEOL 1210 Analytical TEM) was 16±1.6 nm.[28]

Microlens Array Substrate Preparation The glass substrates were cleaned and functionalized with APTMS exactly as outline in the previous section. These substrates were stored in 95% ethanol for no longer than 5 days prior to use. Prior to assembly, each substrate was rinsed with DI H_2O and dried under a stream of nitrogen gas. A concentrated solution of 16±1.6 nm gold nanoparticles was allowed to electrostatically assemble onto the APTMS functionalized glass substrate for 30 min. This substrate was then exposed to a 0.0053 monoM (moles/L monomer) solution of the linear polyelectrolyte PAH, MW 70 000, for 30 min, thereby allowing for electrostatic adsorption of a monolayer of the polymer. After each deposition step, the substrate was rinsed copiously with DI water and dried under a stream of nitrogen gas. The substrate was then exposed to an aqueous 10% (v/v) microgel solution at pH ~6.5, which was allowed to completely dry on the substrate (~24 hrs). At this pH, the microgels are anionic, resulting in good adhesion to the cationic substrate, as well as a high surface coverage. The substrate was subsequently immersed in DI water for 2 hrs, rinsed with DI water, and dried with nitrogen gas to leave behind microgels that are strongly attached to the substrate by electrostatic interactions.

Microscopy Optical and electron microscopies were used to confirm microgel shape, size and lensing ability. A Hitachi S800 scanning electron microscope (SEM) was used to determine the shape of the substrate bound microgels. This was accomplished by

attaching a dry microgel decorated glass substrate to a SEM peg, followed by imaging with an accelerating voltage of 25 kV with the sample tilted relative to the incoming electrons in order to obtain profile images of the microgels. Brightfield transmission and differential image contrast (DIC) optical microscopies were used to confirm the tunability of the micro-optical elements attached to the substrate. An Olympus IX 70 inverted microscope equipped with a high numerical aperture, oil immersion 100X objective (N.A.=1.30), a microscope objective heater and a Peltier-based temperature stage was used for imaging the pattern under various conditions. The experimental setup is shown in Scheme 7-3. Images were captured using a black and white CCD camera (PixelFly, Cooke Corporation) as a function of laser intensity, which was adjusted by neutral density filters, (10.22 $mW/\mu m^2$ ~ 184.97 $mW/\mu m^2$). An Itronx Imaging Technologies FASTCAM DVR CCD camera was used to determine the time scale of the laser induced optical switching at a rate of 2000 frames per second (FPS).

7.4.2 Results and Discussion

This section describes the first demonstration of microlens arrays comprised of fast-responding, reversible, photo-tunable lens elements, which are prepared using simple wet chemical methods. As described above, the arrays are fabricated by exposing 3-aminopropyltrimethoxysilane (APTMS) functionalized glass substrates to citrate stabilized Au nanoparticles (16±1.6 nm), which attach to the glass substrate via electrostatic interactions.[29] The presence of Au nanoparticles on the surface allows for local heating of the sample through excitation of surface plasmon modes on the Au nanoparticles with a frequency-doubled Nd:YAG laser (λ=532 nm).[17,28] Plasmon excitation results in energy transfer to the environment in the form of thermal dissipation

through electron-phonon and phonon-phonon coupling.[30] This Au nanoparticle-coated substrate is subsequently rendered positively charged by exposure to the cationic polyelectrolyte poly(allylamine hydrochloride) (PAH). PNIPAm-co-AAc microgels are attached to the substrate by adding a drop of an aqueous 10% (v/v) microgel solution at pH 6.5 to the APTMS/Au/PAH modified glass substrate. In this fashion, the microgel particles coat the nanoparticle-modified glass substrate via electrostatic self-assembly. At this pH, the microgels are anionic, allowing for good adhesion to the cationic substrate. After the substrate is dried for 24 hrs, it is immersed in and rinsed with deionized water to leave behind only the microgels strongly attached to the substrate by electrostatic interactions. Figure 7-9 shows a schematic depiction and a scanning electron microscopy (SEM) image of this structure. For lens tuning studies, the microlens array was then exposed to various pH solutions by introduction of the appropriate solution into the void space of a microlens array/silicone gasket/coverslip sandwich assembly. Optical microscopy measurements were performed on this assembly to explore the photo-tuning of the microlens array in response to laser excitation. An Olympus IX-70 inverted optical microscope equipped with a 1.30 N.A. oil immersion 100X objective, a microscope objective heater, a Peltier-based temperature stage and a black and white CCD camera (PixelFly, Cooke Corporation) was used for imaging the pattern under CW laser irradiation, and an Itronx Imaging Technologies FASTCAM DVR CCD camera was used to image the lenses exposed to pulsed laser excitation. In this arrangement, we take advantage of the conjugate focal planes in the microscope by placing a pattern near a plane conjugate to the back focal plane of the objective. When the microgels act as lens elements, they change the effective focal length of the microscope, bringing the back

focal plane of the objective near the eyepoint. This is observed as a projection of the pattern through each active element in the lens array. A diagram of the microscopy setup is Shown in Scheme 7-3.

Scheme 7-3 Inverted light microscopy setup used for imaging experiments in this section

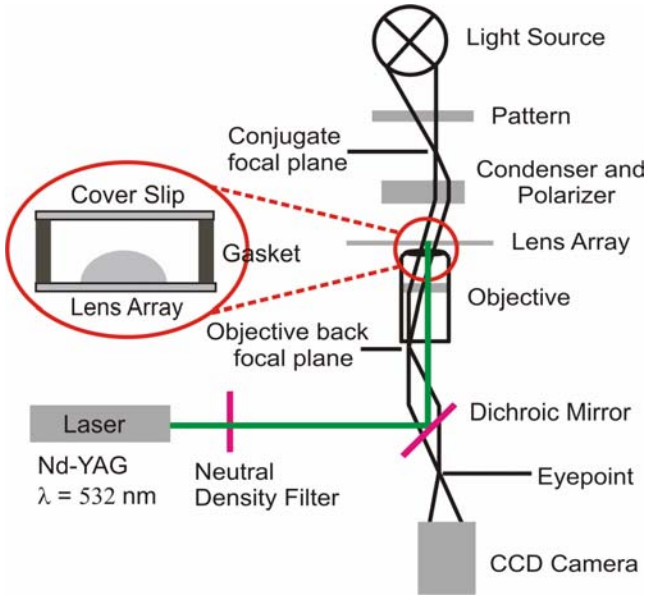

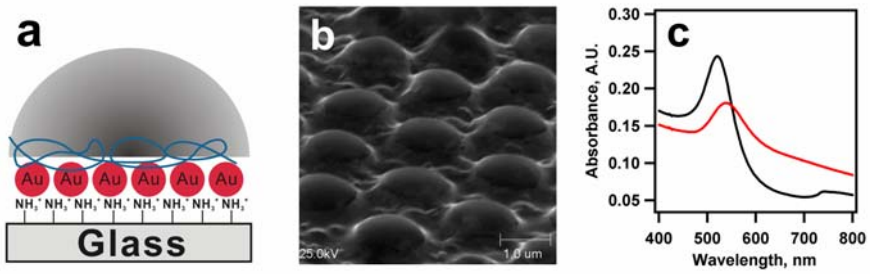

Figure 7-9 (a) Schematic depiction of the multicomponent film used to create photoswitchable microlens arrays. (b) SEM image of the constructed microlens array at grazing angle. (c) UV-vis spectra for Au nanoparticles in solution (black) and a bound to substrate (red).

The key characteristics of this construct with respect to photo-tuning relate to the optical properties of the colloidal Au array, and the thermoresponsivity of the microgel lens elements. UV-vis spectroscopy was used to confirm the presence of Au nanoparticles on the glass substrate following assembly. Figure 7-9c shows the spectra for Au nanoparticles in aqueous solution and an Au nanoparticle functionalized substrate coated with a microlens array. The absorption spectrum for the substrate-bound Au nanoparticles is shifted to slightly higher wavelengths than that of the Au nanoparticle solution. A long-wavelength shoulder is also apparent in the spectrum of the lens array. The long-wavelength shoulder is most likely due to slight Au nanoparticle aggregation on the substrate during assembly, while the plasmon resonance shift results from the microlens array. The deswollen microlenses present a higher local refractive index to the Au nanoparticles surface, thereby shifting the plasmon resonance to lower energy.

The photoresponsivity of the microlens arrays was initially investigated by monitoring the projection of a triangle pattern through the lenses while exposed to a pH 3.0 solution, in response to various laser powers and bath temperatures (Figure 7-10).

Panels (a) and (b) show the focal length tunability of the microlens arrays at a bath temperature of 25 °C upon laser exposure. Each lens is capable of projecting the triangle image only in the region of laser light excitation, where the effective temperature is higher than the microgel LCST. The number of lenses that display a high quality image is also tunable by varying the laser power, as seen in Figure 7-11. Similarly, Figure 7-10 (c, d) show the focal length tunability of the microlens arrays at a bath temperature of 10 °C upon laser exposure. A smaller area of the array is switched under these conditions, as the bath temperature is further from the 31 °C LCST of pNIPAm. Note that the same laser power is impingent on the array in panels (b) and (c). Since a fixed laser power induces a fixed temperature jump, moving the bath temperature far below the LCST results in photo-induced temperature excursion that is now below the polymer LCST (Figure 7-10(c)). It is also theoretically possible to control single lens elements of the array by this method. Since the laser spot is essentially diffraction limited in size (~266 nm diameter) under these illumination conditions, it is in fact smaller than an individual lens. By controlling the bath temperature and the laser intensity one can therefore interrogate a single lens element as seen in Figure 7-11(b, f).

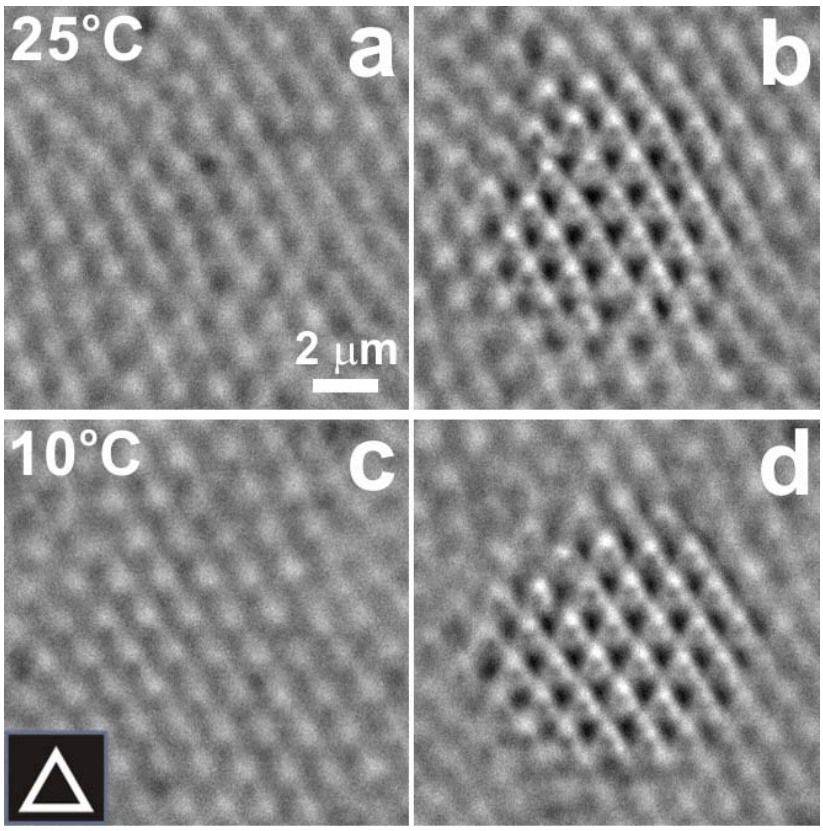

Figure 7-10 Photo-switching of microlens arrays as a function of laser power and solution temperature at pH 3.0. Arrays at 25 °C (a, b) and 10 °C (c, d) show laser power dependent optical properties by projecting a triangle pattern (bottom left) only when the laser power is sufficient to produce the necessary temperature jump to above the microgel LCST. Laser powers are 10.22 mW/μm^2 (a), 38.45 mW/μm^2 (b, c), and 88.90 mW/μm^2 (d). From the figure it can also be seen that each lens is capable of projecting an image only in the region surrounding the incident laser light excitation.

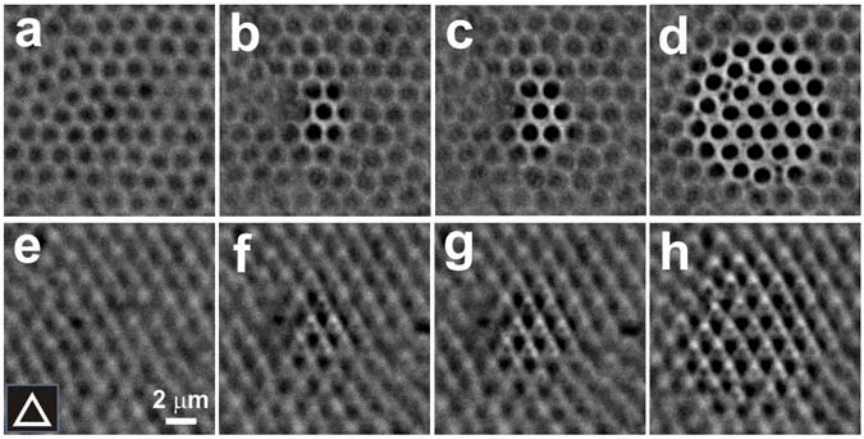

Figure 7-11. (Top) DIC microscopy images of substrate bound microgels in pH 3.0 solution at 25 °C as a function of laser power. (Bottom) Projection of a triangle pattern (inset bottom left) through the microgel at different laser powers. As the laser power increases, the modulated region of the microlens array increases. The laser intensities at the microlens array surface are 10.22 mW/μm^2 (a,e), 20.14 mW/μm^2 (b,f), 24.66 mW/μm^2 (c,g), 38.45 mW/μm^2 (d,h).

Figures 7-12(a) and (b) show images projected through the microlens array at 25 °C and pH 6.5 as a function of laser power. Comparing Figures 7-10(b) and 7-12(a), where the laser powers are identical, suggests that the microlens array at pH 6.5 is less sensitive to laser irradiation than at pH 3.0. This behavior is due to the higher LCST of the microgels at this pH, caused by AAc deprotonation within the microgel network at pH values above the pKa (pK_a~4.25).[25] As expected, the lensing ability of the microlens is unaffected by temperature up to the transition temperature of ~48 °C as observed by the bulk heating experiments seen in Figure 7-8 in the previous section. Figure 7-12 (b,d) illustrates that the microlens array is again extremely sensitive to the bath temperature, as indicated by a decrease in the area of the modulated region at low temperature. This effect can also be confirmed by comparing the modulated area in Figure 7-10(d) to Figure

7-12(d). This effect is due to the lower LCST of the microgels at pH 3.0, which are therefore able to respond to smaller temperature jumps than the microgels at pH 6.5.

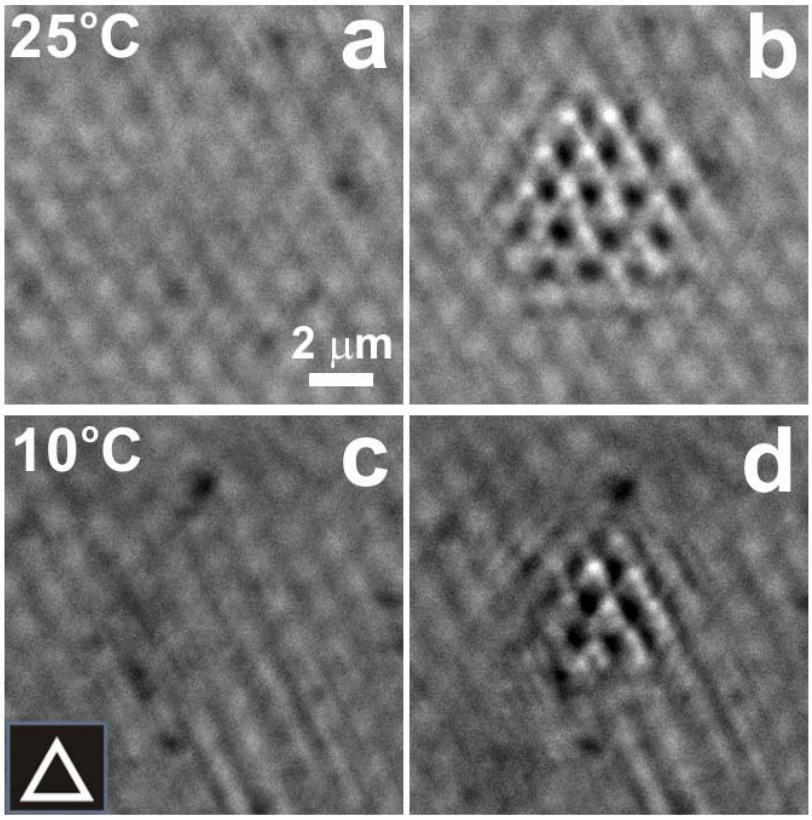

Figure 7-12 Photo-switching of microlens arrays as a function of laser power and solution temperature at pH 6.5. Again it can be seen that the arrays at 25 °C (a, b) and 10 °C (c, d) show laser power dependent optical properties by projecting a triangle pattern (bottom left) only when the laser power is sufficient to produce the necessary temperature jump to above the microgel LCST. Laser powers are 38.45 mW/μm^2 (a), 88.90 mW/μm^2 (b, d), and 48.56 mW/μm^2 (c). By comparison to Figure 7-10 it can be seen that more laser power is required to modulate the micro-optical array at this pH.

The reversibility and response rate of the microlens array are shown in Figure 7-13. The laser modulation frequency was controlled by passing it through an optical chopper. Row (a) shows that the optical properties of the microlens array can be fully modulated, in a completely reversible fashion, using 10 ms laser pulses. This experiment was performed without the projection of a pattern through the array, as the camera was not sensitive enough to detect the projected image while acquiring images at 2000 frames per second. It should be pointed out that the apparent response time of microlenses in the array was measured at <500 μs, as we cannot resolve intermediate stages of microgel deswelling at 2000 frames per second under the conditions presented in Figure 7-13. In other words, individual lens elements go from a non-lensing to a lensing state within one frame at this image capture rate as can be seen in Figure 7-14. Literature reports place microgel deswelling rates on the timescale of tens to hundreds of microseconds, depending on the network density and particle size.[31] Figure 7-13 (b,c) also shows that this reversibility is diminished upon increasing the laser repetition frequency from 200 to 500 Hz. This is due to the fact that while microgel *deswelling* is caused by fast thermal dissipation from the laser-excited Au nanoparticles to the microlenses, the *reswelling* of the microgel is limited by the slow dissipation of heat away from the substrate. Thus, the microlens array appears totally deswollen at 500 Hz, as the pulsing frequency is faster than the microgel reswelling rate.

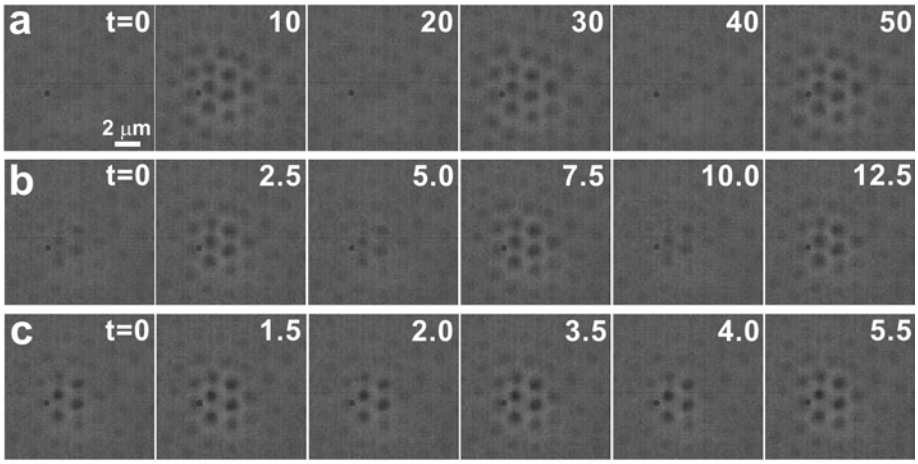

Figure 7-13 Images captured with a fastcam DVR CCD camera at 2000 FPS while chopping the Nd:YAG laser source at 50 Hz (a), 200 Hz (b), and 500 Hz (c) in pH 6.5 solution at 15 °C. The optical properties of the array can be reversibly modulated in phase with laser pulses of 50 Hz (a). However, once the laser modulation frequency exceeds the rate of thermal diffusion from the microgels, the modulation of the microlens array diminishes (b,c). The laser intensity at the array surface is 184.97 mW/μm^2. The numbers at the top right of each image indicate the Δt in milliseconds.

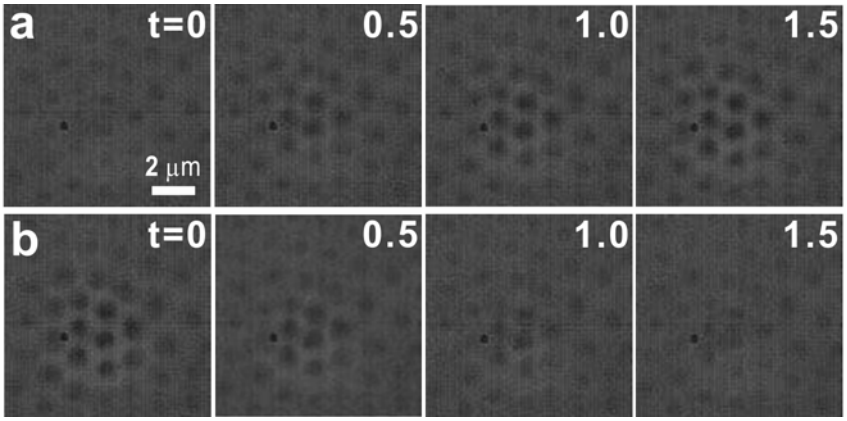

Figure 7-14. Images captured with a fastcam DVR CCD camera at 2000 FPS while chopping a Nd:YAG laser source at a frequency of 50 Hz in pH 6.5 solution at 15 °C. The time required for lenses to switch completely on (a) and off (b) is on the order ~1.5 msec. From the figure it can also be seen that it takes ~.5 msec for the lenses to respond to laser irradiation. The laser intensity at the microlens array surface is 184.97 mW/μm^2. The numbers at the top right indicate Δt in milliseconds.

7.4.3 Section Conclusions

In conclusion, we have fabricated, using simple wet-chemical methods, a high-density micro-lens array that can be tuned or switched by an external laser source. The fabrication technology is inexpensive, scalable, and rapid, in contrast to traditional micromolding or photolithographic approaches. The unique characteristics of the micro optics include the ability to confine the tunable region to the single microlens scale, fast response rate (~10-fold faster than video rate), and highly reversible behavior under pulsed laser control. These characteristics make this system an attractive enabling technology for the future development of agile micro-optical components.

7.5 Chapter Conclusions

This chapter described the fabrication of microlens arrays via wet chemical methods using a facile and inexpensive technique that is easily scalable to coat large

surfaces. These arrays were shown to operate effectively in air and solution and were shown to have dynamically tunable focal lengths controlled by solution temperature and pH. By using laser irradiation to excite surface plasmons on surface attached Au nanoparticles, it was possible to locally heat the solution, which allowed the number of lens elements that focused a pattern to be controlled on the single lens scale. This technology is the first of its kind and has the potential to be used for a variety of applications, which will be pursued in the future by our group.

REFERENCES

(1) Serpe, M. J.; Kim, J.; Lyon, L. A. *Adv. Mater.* **2004**, *16*, 184-187.

(2) Kim, J.; Serpe, M. J.; Lyon, L. A. *J. Am. Chem. Soc.* **2004**, *ACS ASAP*.

(3) Kim, J.; Serpe, M. J.; Lyon, L. A. *Angew. Chem.-Int. Edit.* **2004**, *submitted*.

(4) Serpe, M. J.; Jones, C. D.; Lyon, L. A. *Langmuir* **2003**, *19*, 8759-8764.

(5) Pelton, R. *Adv. Colloid. Interface Sci.* **2000**, *85*, 1-33.

(6) Saunders, B. R.; Vincent, B. *Adv. Colloid Interface Sci.* **1999**, *80*, 1-25.

(7) Chen, S. H.; Yi, X. J.; Kong, L. B.; He, M.; Wang, H. C. *Infrared Phys. Technol.* **2002**, *43*, 109-112.

(8) Motamedi, M. E.; Tennant, W. E.; Sankur, H. O.; Melendes, R.; Gluck, N. S.; Park, S.; Arias, J. M.; Bajaj, J.; Pasko, J. G.; McLevige, W. V.; Zandian, M.; Hall, R. L.; Richardson, P. D. *Opt. Eng.* **1997**, *36*, 1374-1381.

(9) Wu, H. K.; Odom, T. W.; Whitesides, G. M. *J. Am. Chem. Soc.* **2002**, *124*, 7288-7289.

(10) Wu, H. K.; Odom, T. W.; Whitesides, G. M. *Anal. Chem.* **2002**, *74*, 3267-3273.

(11) Wu, M. H.; Park, C.; Whitesides, G. M. *Langmuir* **2002**, *18*, 9312-9318.

(12) Wu, M. H.; Paul, K. E.; Yang, J.; Whitesides, G. M. *Appl. Phys. Lett.* **2002**, *80*, 3500-3502.

(13) Wu, M. H.; Whitesides, G. M. *Adv. Mater.* **2002**, *14*, 1502-1506.

(14) Wu, M. H.; Whitesides, G. M. *J. Micromech. Microeng.* **2002**, *12*, 747-758.

(15) Karkkainen, A. H. O.; Tamkin, J. M.; Rogers, J. D.; Neal, D. R.; Hormi, O. E.; Jabbour, G. E.; Rantala, J. T.; Descour, M. R. *Appl. Optics* **2002**, *41*, 3988-3998.

(16) Karkkainen, A. H. O.; Rantala, J. T.; Maaninen, A.; Jabbour, G. E.; Descour, M. R. *Adv. Mater.* **2002**, *14*, 535-540.

(17) Jones, C. D.; Serpe, M. J.; Schroeder, L.; Lyon, L. A. *J. Am. Chem. Soc.* **2003**, *125*, 5292-5293.

(18) Croutxe-Barghorn, C.; Soppera, O.; Lougnot, D. J. *Eur. Phys. J.-Appl. Phys* **2001**, *13*, 31-37.

(19) Croutxe-Barghorn, C.; Soppera, O.; Lougnot, D. J. *Appl. Surf. Sci.* **2000**, *168*, 89-91.

(20) Okamoto, T.; Mori, M.; Karasawa, T.; Hayakawa, S.; Seo, I.; Sato, H. *Appl. Optics* **1999**, *38*, 2991-2996.

(21) Lu, Y.; Yin, Y. D.; Xia, Y. N. *Adv. Mater.* **2001**, *13*, 34-37.

(22) Hirai, T.; Hayashi, S. *Colloid Surf. A-Physicochem. Eng. Asp.* **1999**, *153*, 503-513.

(23) Goss, C. A.; Charych, D. H.; Majda, M. *Anal. Chem.* **1991**, *63*, 85-88.

(24) Crowther, H. M.; Vincent, B. *Colloid Polym. Sci.* **1998**, *276*, 46-51.

(25) Jones, C. D.; Lyon, L. A. *Macromolecules* **2000**, *33*, 8301-8306.

(26) Gan, D.; Lyon, L. A. *J. Am. Chem. Soc.* **2001**, *123*, 7511-7517.

(27) Tanaka, T.; Fillmore, D. J.; Sun, S.-T.; Nishio, I.; Swislow, G.; Shah, A. *Phys. Rev. Lett.* **1980**, *45*, 1636-1639.

(28) Jones, C. D.; Lyon, L. A. *J. Am. Chem. Soc.* **2003**, *125*, 460-465.

(29) Freeman, R. G.; Grabar, K. C.; Allison, K. J.; Bright, R. M.; Davis, J. A.; Guthrie, A. P.; Hommer, M. B.; Jackson, M. A.; Smith, P. C.; Walter, D. G.; Natan, M. J. *Science* **1995**, *267*, 1629-1632.

(30) Link, S.; El-Sayed, M. A. *Int. Rev. Phys. Chem.* **2000**, *19*, 409-453.

(31) Wang, J.; Gan, D.; Lyon, L. A.; El-Sayed, M. A. *J. Am. Chem. Soc.* **2001**, *123*, 11284-11289.

CHAPTER 8

TEMPERATURE TUNABLE LIGHT DIFFRACTION FROM MICROGEL COLLOIDAL CRYSTALS

8.1 Introduction

The previous chapters of this dissertation have been focused on the electrostatic assembly of microgels on surfaces, which has mostly resulted in disordered arrays (with exception to the microlenses in Chapter 7). While this property does not have negative effects on those experiments they are not useful as light diffracting materials, which is the topic of this chapter. This chapter describes the assembly of microgels into 3-D ordered arrays that, upon stabilization of their crystalline structure via photopolymerization, exhibit temperature dependent light diffraction.

Ordered colloidal assemblies have been of interest since man discovered their beautiful optical properties.[1] A common example of such an ordered material is the gemstone opal.[2,3] The formation of gemstone opals has been studied and it is proposed that the assembly takes place over thousands to hundreds of thousands of years by slow sedimentation and ordering of silica particles in boulders.[4,5] This ordering of the silica particles results in a periodic dielectric constant, which gives rise to reflected light of a given wavelength and their characteristic optical properties. The wavelength of light that is reflected is determined by Bragg's law (Eq. 1). This equation relates the diffracted wavelength (λ) and the diffraction order (m=1,2,3....) to the refractive index of the medium (n), the lattice spacing (d), and the angle of incidence relative to the lattice plane (θ).

$$m\lambda = 2nd\sin(\theta) \qquad (1)$$

In a constant quest to mimic Nature, investigators have been pursuing the ordered assembly of colloidal particles over the past ~50 years.[6,7] These ventures have been quite successful and techniques such as slow sedimentation,[5,8,9] gentle evaporation of solvent[10] or filtration[11,12] are frequently used to achieve such ordered structures. The formation of these structures has offered many opportunities for research in the sciences (physics, chemistry, and mathematics) with a large focus on the use of these materials for omnidirectional photonic bandgap materials.[13-16]

As mentioned above, techniques such as slow sedimentation, gentle evaporation of solvent or filtration are frequently used to achieve ordering of colloidal particles to produce what are called artificial opals or colloidal crystals. Each of these techniques rely on forcing the colloids into close contact enforcing the formation of close-packed (high volume fraction), ordered arrays. These assembly procedures take advantage of the phase behavior of colloids in solution where it has been shown that a volume fraction of ~0.545 to a maximum value of 0.74 give a crystalline phase.[5,17]

These ordered assemblies have been used for various applications such as optical fibers,[18,19] lasers,[20-22] and light-emitting diodes.[23,24] Of interest to the discussion in this chapter is the assembly of colloidal crystals that respond to various stimuli by changing the wavelength of light they diffract. This has been described previously for applications as tunable or fast switching optical materials,[25-29] and sensors.[30-33] For example, Asher and coworkers used such structures for sensing of glucose and creatinine in body fluids

by using a crystalline array of polystyrene beads stabilized by pNIPAm into the voids of the crystal.[30,33] They engineered specific binding sites into this crystalline structure capable of recognizing the presence of these molecules by undergoing a reaction. This reaction caused a change in the crystals local environment, resulting in a change in crystal lattice spacing detected as a shift in the wavelength of light diffraction. Despite how or why the materials were prepared the diffracted wavelength tunability arises from the change in the lattice spacing of the crystal.

This chapter describes the assembly of temperature tunable poly(N-isopropylacrylamide) (pNIPAm) microgel colloidal crystals. Crystallization was accomplished following previously published protocol from our group.[34-38] This involves the centrifugation of microgels down to a volume fraction approximating the optimum for crystal formation, ~ 0.74. The microgels in this state are in a disordered, glassy phase, which can be made crystalline my heating the microgels to above the lower critical solution temperature (LCST) of pNIPAm, ~31 ºC, followed by slow cooling to room temperature. This allows the microgels to transition from a jammed, glassy state to a liquid state (above the LCST) followed by slow microgel reswelling via cooling, which allows the microgels to slowly assemble in a thermodynamically preferred crystalline state. The crystal in the current state can be melted (disordered) by heating followed by fast cooling to transform the crystal back to its disordered, glassy phase. The various phases of the colloidal sample can be seen in Figure 8-1.

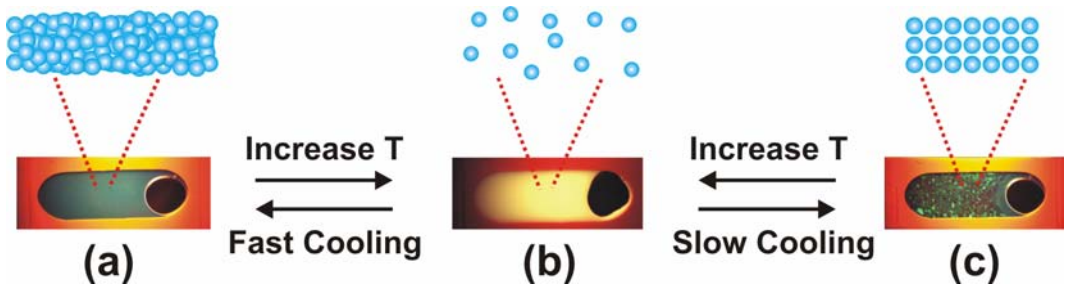

Figure 8-1. Photographs of the various phases a packed colloidal dispersion can be in depending on how the sample is prepared. The glassy phase (a) is reached by heating the sample to above the LCST of the microgels to the liquid phase (b), followed by fast cooling. This process locks the sample in a kinetically trapped, disordered glassy state. If the sample is heated to above the LCST and slowly cooled the crystal phase (c) can be reached due to the microgels arranging in a thermodynamically favored fashion.

The goals of the experiments presented in this chapter are to make a microgel colloidal crystal that is stable to heating, i.e. does not go from crystal to liquid, and upon fast cooling results in the original crystal that was present before heating. The crystal should also show temperature dependent Bragg reflection. For example, when the crystal is heated the original crystalline structure remains but the spacing of the microgels change, Figure 8-2. The first challenge of this project is to find an appropriate way to stabilize the colloidal crystal and once this is found how can this be incorporated into the crystalline samples. The second challenge is to maintain the crystalline structure upon stabilization. The third challenge is to covalently attach the crystal to a substrate upon crystal stabilization. In this chapter microgel colloidal crystals are stabilized using photoinitiated polymerization (photopolymerization) in the crystalline matrix to lock in the crystal structure, which shows temperature dependent Bragg diffraction.

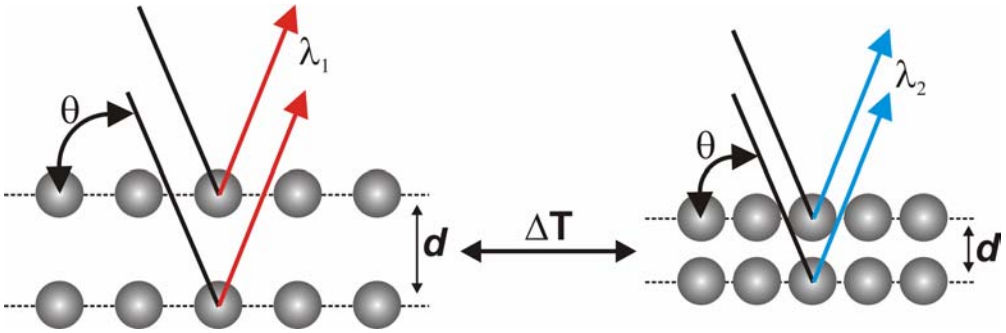

Figure 8-2. The lattice spacing (*d*) of the periodic array dictates the wavelength of light that is diffracted upon exposure to white light. In the case of the experiments presented in this chapter, the lattice spacing can be dynamically tuned with temperature resulting in a dynamically tunable diffraction wavelength.

8.2 Experimental

Materials All reagents were purchased from Sigma-Aldrich unless otherwise specified. *N*-Isopropylacrylamide (NIPAm) was re-crystallized from hexanes (J.T. Baker) and dried under vacuum prior to use. Acrylic acid (AAc) was distilled under reduced pressure. *N*,*N*'-Methylene(bisacrylamide) (BIS), ammonium persulfate (APS) was used as received. 2,2'-diethoxyacetophenone (density of 1.034) was used received and stored at 4 ºC. 3-acryloxypropyltrimethoxysilane (AOPTMS) was obtained from United Chemical Technologies Inc.. CoverWell perfusion chamber gaskets were obtained from Molecular Probes. 29-gauge tipped syringes were obtained from VWR. 24 x 24 mm Fisher Finest brand cover glass obtained from Fisher Scientific. Cuvettes were obtained from VWR. 95% and absolute ethanol was used for various purposes in this investigation. All water used throughout this investigation was first house distilled and then deionized to a resistance of at least 18 MΩ (Barnstead Thermolyne E-Pure system) and then filtered through a 0.2 μm filter for further purification.

pNIPAm-co-AAc Microgel Synthesis. Microgels were synthesized via aqueous free-radical precipitation polymerization, as described in Chapter 3. These microgels had a molar composition of 94% NIPAm, 2% BIS, 4% AAc using 70 mM total monomer concentration. Polymerization was performed in a three-neck, 200 mL round-bottom flask (RBF) containing a magnetic stir bar. To this reactor, 100 mL of a filtered (0.2 μm filter, Pall Gelman Metricel), aqueous solution of NIPAm, BIS, and the surfactant SDS (1 mM) was added. This solution was heated to ~70 °C while degassing with N_2 and stirring vigorously for ~1 hr. After 1 hr, AAc was added to the flask in order to bring the total monomer concentration up to 70 mM. Once the AAc was added, polymerization was immediately initiated by injection of 1.0 mL of a hot (~70°C), APS solution (0.3 mmol). The solution immediately turned turbid indicating successful initiation. This solution was allowed to heat and stir for an additional 5 hours while under a constant flow of N_2 gas. Following synthesis the particles were purified by dialysis against water for ~2 weeks with the water being changed twice per day, using 10 000 MW cut-off dialysis tubing (VWR).

Photon Correlation Spectroscopy The thermoresponsive behavior of the microgels was confirmed by photon correlation spectroscopy (PCS, Protein Solutions Inc.) prior to their assembly. This technique was explained in Chapter 3 so an explanation of the technique will not be given here. For these measurements, each sample was allowed to equilibrate at each temperature for 20 min. At each temperature 5 consecutive runs were performed where each run was composed of 15 individual radius measurements using a 15 sec integration time for each measurement.

Glass Substrate Preparation AOPTMS functionalized glass cover slips were used as monomer functionalized substrates for crystal adhesion during photopolymerization. Prior to functionalization the glass substrates were cleaned in an Ar plasma for ~ 20 min. Following cleaning the substrates were immersed in an ethanolic (absolute ethanol) 1% AOPTMS solution for ~2 hrs. After 2 hrs the substrates were removed from the AOPTMS solution and again rinsed copiously with 95% ethanol. These substrates were stored in 95% ethanol for no longer than 5 days prior to use. Prior to crystallization these substrates were rinsed with H_2O and dried under a stream of nitrogen gas.

Microgel Colloidal Crystal Preparation ~10 mL of the microgel solution prepared above was added to a centrifuge tube and added to an Eppendorf 5804R temperature controlled centrifuge. The microgels were spun down at a relative centrifugal force of 15 557 *g* at 26 ºC into a concentrated plug at the bottom of the centrifuge tube. This process typically took ~2-3 h but could take more time depending on the microgels being spun down. If done correctly, a clear, colorless supernatant solution will be observed, if not, the sample must be centrifuged further. Once the supernatant solution is observed to be clear and colorless it can be removed from the tube leaving behind the microgel pellet at the bottom of the tube. The microgels were then re-suspended in ~8 mL of a 700 mM monomer solution containing 95% NIPAm and 5% BIS. The microgels were re-suspended in the monomer solution a total of 3 times. For the last re-suspension the microgels were spun down, at the same conditions outlined above, being careful not to over pack the microgels at the bottom of the tube by over centrifugation. If this occurs the microgels will not crystallize. It can also be the case that the microgel solution is not spun down enough, which will also result in a sample that will not crystallize. The exact

point at which the centrifugation is stopped is a matter of trial and error but can be estimated when a dense microgel layer (dense white cloud) appears above the concentrated microgel pellet.

Once a microgel/monomer pellet is obtained, that is able to be crystallized, photoinitiator can be added. This was typically done by pipetting 200 μL of the pellet, at ~50 ºC, into a separate eppendorf tube. Heating was necessary to convert the viscous pellet into a liquid-like form. This 200 μL pellet was allowed to cool to the viscous form (room temperature). Various concentrations of the photoinitiator 2,2'-diethoxyacetophenone (PI) with and without ethanol (EtOH) was added to this pellet with the best concentration found to be ~0.0124 M with 1.5 μL added EtOH. Other PI/EtOH combinations that were found to work were 0.0124 M/1.0 μL EtOH, and 0.0062 M/ 1.0 μL EtOH. The general trend was that more PI resulted in crystals that would not crystallize and the addition of EtOH resulted in crystals that polymerized better. This pellet that contained the concentrated microgels, monomers and photoinitiator was then heated to ~50 ºC and injected into a crystallization cell, as seen in Figure 8-3. Following solution injection the cell was allowed to heat for an additional 5 min on a hotplate held at ~50 ºC and the air bubbles trapped in the cell removed by inverting the sample 2-3 times. After 5 min the hotplate was turned off and a cover added to the hot plate to result in slow cooling to room temperature at a rate of ~0.2 ºC/min. This slow cooling gave crystalline samples in ~ 5-8 h.

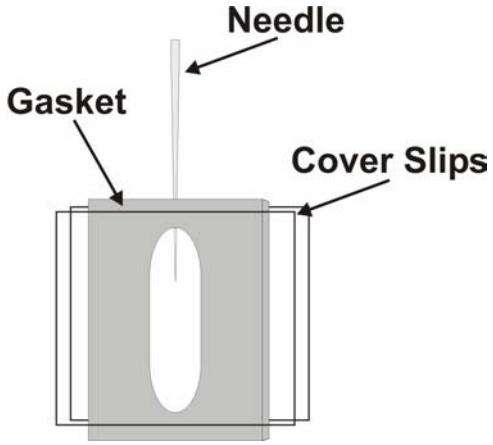

Figure 8-3. Typical cell used for crystallization. Needle is carefully pierced through the gasket and into the cell. Hot, concentrated particle solution is injected into the cell and the needle removed.

After crystallization was complete the crystals could be polymerized. This was done by transferring the cell containing the crystal from the hotplate to an Al metal plate that was buried in ice, taking care not to heat the crystal. The crystal was then exposed to 365 nm light from a Blak-Ray UV lamp (VWR) for 15 min on each side for a total of 45 min with the functionalized side of the cell exposed to the light for two of the three cycles. Following polymerization the unfunctionalized slide of the cell could be removed. The polymerized crystal attached to the functionalized slide was then submersed in deionized water for 24 h prior to use.

Crystal Reflectance Measurements A fiber optic reflectance probe coupled to a white light source and a fiber optic coupled photodiode array detector (Ocean Optics) was used to monitor temperature dependent reflectance spectra from crystalline samples, immersed in deionized water. This was accomplished by immersing the crystalline films, with one side uncovered, in ~ 10 mL of water. This volume will depend on the vessel used to perform the experiment the key being that the top of the crystal is covered with

minimal amount of water but enough to prevent crystal exposure to air upon water evaporation at high temperature. This vessel was placed on a hotplate for heating. The reflectance probe was placed as close to the water surface as possible, without immersing the probe, over a nicely crystalline region of the sample. The measurements were performed by introducing white light to the crystal, at normal incidence, while monitoring the light reflected back into the probe using Ocean Optics provided software (OOIBase32). Using this technique, full reflectance spectra were obtained as a function of temperature over the range of ~25 - 45 ºC

8.3 Results and Discussion

In this chapter the assembly and photopolymerization of microgel colloidal crystals was demonstrated. Before microgel assembly, PCS was performed to confirm the microgel size and pH responsivity. The results can be seen in Figure 8-4. From the figure it can be seen that the microgels at pH 3.0 initially have a hydrodynamic radius (R_h) of ~120 nm and deswell to ~60 nm upon heating. Initially the microgels at pH 6.5 have a larger R_h than the microgels at pH 3.0 but deswell to approximately the same R_h upon heating. It can also be noted that the microgels at pH 6.5 require more heat to deswell, than at pH 3.0, due to Coulombic repulsion from the deprotonated acid groups in the microgel network. Following PCS the microgels were assembled and photopolymerized, as outlined above. A photograph of a polymerized crystal can be seen in Figure 8-5. These pictures show that the crystals are highly diffractive, as evidenced by their color, and have structural integrity. The structural integrity of the crystals arise from photopolymerization, which forms a pNIPAm polymer network in the crystalline matrix

locking in the structure. If the photopolymerization did not work when one slide of the cell is removed the crystals would be completely destroyed.

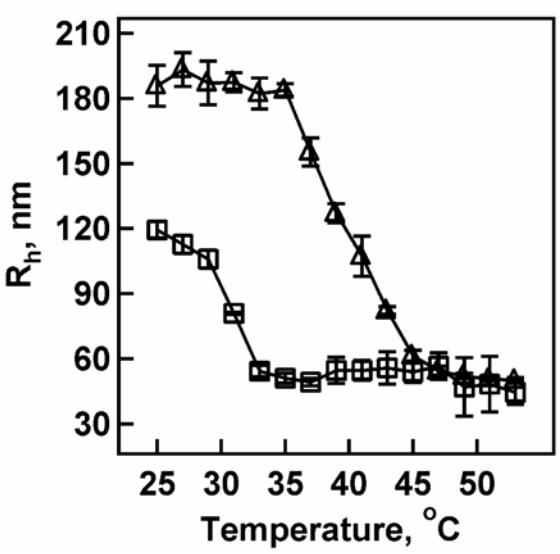

Figure 8-4. Volume phase transition curves for the pNIPAm-co-AAc microgels used in this chapter at pH 3.0 (squares) and pH 6.5 (triangles). As the pH is increased above the pK_a of the AAc groups, the microgels swell and the phase transition is shifted to high temperature due to Coulombic repulsion. Error bars represent one standard deviation about the average of five measurements.

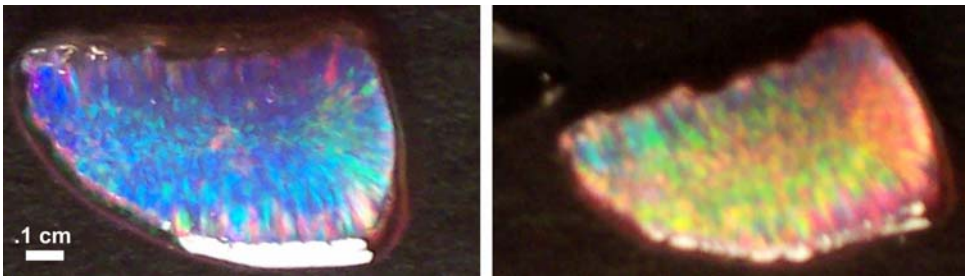

Figure 8-5. Photographs of a photopolymerized microgel colloidal crystal. The images show that the structures are highly diffractive due to periodicity of the microgels in the structure. It can also be seen from the pictures that structure are stable. The crystal appears different colors because the photographs were taken at different angles.

Once it was determined that stable crystal structures were being formed from photopolymerization, the next step was to show that the diffraction wavelength could be tuned by temperature. This temperature responsive Bragg diffraction should be possible since thermoresponsive pNIPAm makes up the crystal matrix as well as the microgels composing the periodic array. Therefore, increases in temperature above the LCST of pNIPAm should deswell the individual microgels plus the matrix resulting in microgels that are closer to one another and effectively decreasing the crystal lattice spacing. This decrease in lattice spacing should result in a shift in the Bragg peak to shorter wavelength, as outlined in Figure 8-2. The results of these experiments can be seen in Figures 8-6 and 8-7. These figures show that a crystal which has Bragg diffraction at long wavelengths can be tuned to short wavelengths just by increasing the temperature of the water that it is immersed in. This wavelength dependent Bragg diffraction is exactly what was predicted, i.e. the peak shifted to shorter wavelength with increasing temperature presumably due to the lattice constant decreasing as a result of temperature induced contraction of the crystal matrix. It is interesting to note from the figures that the Bragg

reflection can be tuned over almost the whole visible spectrum. It should also be noted that the crystalline structure was recovered upon cooling to room temperature (data not shown).

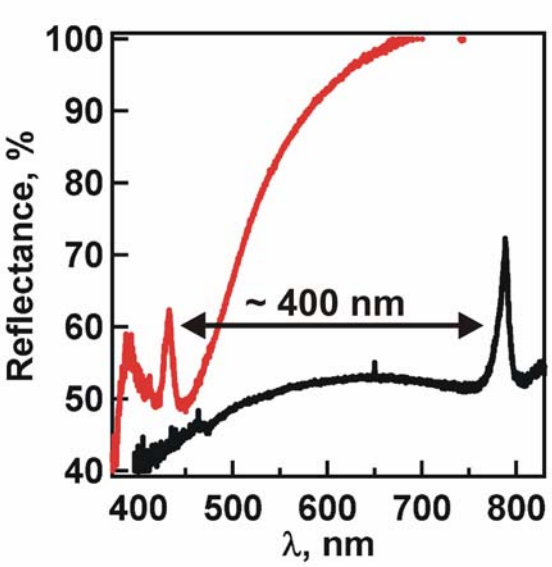

Figure 8-6. Reflectance curves for a photopolymerized colloidal crystal at a bath temperature of 25 (black) and at 35 ºC (red). It can be seen that crystal diffraction is highly dependent on bath temperature as noted by the shift of the diffracted wavelength across the whole visible region of the light spectrum from a 10 ºC increase in bath temperature.

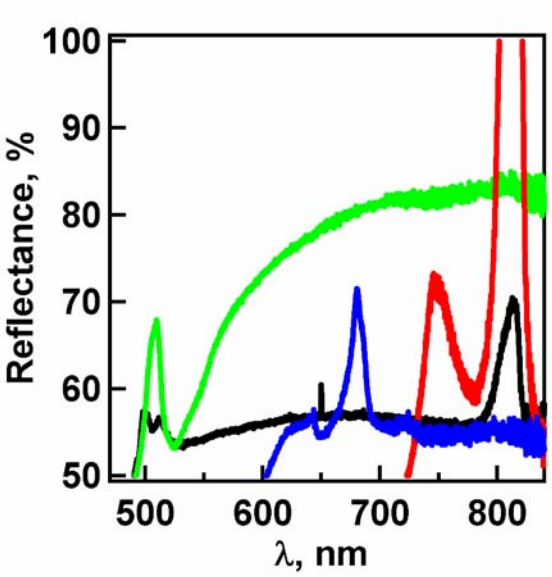

Figure 8-7. Reflectance curves for a photopolymerized colloidal crystal at a bath temperature of 25 (black), 30 (red), 33 (blue) and 35 ºC(green). It can be seen again that crystal diffraction is highly dependent on bath temperature as noted by the shift of the diffracted wavelength across the whole visible region of the light spectrum from a 10 ºC increase in bath temperature.

8.4 Conclusions

This chapter has described the fabrication of microgel colloidal crystals that respond to increases in temperature by decreasing their lattice spacing resulting in a shifting of their Bragg diffraction peak to shorter wavelengths. The work in this chapter represents some initial results and further details of the photopolymerization and temperature responsivity will be investigated in the future. This stable microgel colloidal crystal construct opens the door for future research that could not be pursued using the traditional microgel colloidal crystals (unphotopolymerized). One such opportunity is doping the crystal structure with small particles that will increase the refractive index of the crystal resulting in crystals that diffract more intense light. Preliminary results have been obtained, which show that TiO_2 has such an effect, i.e. crystals that were soaked in

TiO_2 reflected much more intense light than the crystal that were not soaked in TiO_2. This is most likely due to the TiO_2 particles partitioning into the crystalline matrix to interact with the AAc groups on the microgels resulting in an increase in the refractive index of the microgels, which will result in more efficient light diffraction. Experiments have also been conducted which show the partitioning of Au nanoparticles into the crystal. This partitioning has similar effects on crystal diffraction as TiO_2.

REFERENCES

(1) Vukusic, P.; Sambles, J. R. *Nature* **2003**, *424*, 852-855.

(2) Darragh, P. J.; Gaskin, A. J.; Terrell, B. C.; Sanders, J. V. *Nature* **1966**, *209*, 13-16.

(3) Jones, J. B.; Segnit, E. R.; Sanders, J. V. *Nature* **1964**, *204*, 990-991.

(4) Iler, R. K. *Nature* **1965**, *207*, 472-473.

(5) Pieranski, P. *Contemp. Phys.* **1983**, *24*, 25-73.

(6) Alfrey, T.; Bradford, E. B.; Vanderhoff, J. W.; Oster, G. *J. Opt. Soc. Am.* **1954**, *44*, 603-609.

(7) Luck, W.; Klier, M.; Wesslau, H. *Ber. Bunsen-Gesellschaft* **1963**, *67*, 75-83.

(8) Lee, W. M.; Pruzinsky, S. A.; Braun, P. V. *Adv. Mater.* **2002**, *14*, 271-274.

(9) Ackerson, B. J.; Paulin, S. E.; Johnson, B.; van Megen, W.; Underwood, S. *Phys. Rev. E* **1999**, *59*, 6903-6913.

(10) Jiang, P.; Bertone, J. F.; Hwang, K. S.; Colvin, V. L. *Chem. Mat.* **1999**, *11*, 2132-2140.

(11) Holland, B. T.; Blanford, C. F.; Do, T.; Stein, A. *Chem. Mat.* **1999**, *11*, 795-805.

(12) Holland, B. T.; Blanford, C. F.; Stein, A. *Science* **1998**, *281*, 538-540.

(13) Yablonovitch, E. *Sci.Am.* **2001**, *285*, 46-55.

(14) Yablonovitch, E. *Phys. Rev. Lett.* **1987**, *58*, 2059-2062.

(15) Johnson, S. G.; Joannopoulos, J. D. *Appl. Phys. Lett.* **2000**, *77*, 3490-3492.

(16) Nishimura, S.; Shishido, A.; Abrams, N.; Mallouk, T. E. *Appl. Phys. Lett.* **2002**, *81*, 4532-4534.

(17) Pusey, P. N.; van Megan, W. *Nature* **1986**, *330*, 340-342.

(18) Benoit, G.; Hart, S. D.; Temelkuran, B.; Joannopoulos, J. D.; Fink, Y. *Adv. Mater.* **2003**, *15*, 2053-2056.

(19) Temelkuran, B.; Hart, S. D.; Benoit, G.; Joannopoulos, J. D.; Fink, Y. *Nature* **2002**, *420*, 650-653.

(20) Bewley, W. W.; Kim, C. S.; Kim, M.; Canedy, C. L.; Lindle, J. R.; Vurgaftman, I.; Meyer, J. R.; Muller, R. E.; Echternach, P. M.; Kaspi, R. *Appl. Phys. Lett.* **2003**, *83*, 5383-5385.

(21) Cao, J. R.; Kuang, W.; Choi, S. J.; Lee, P. T.; O'Brien, J. D.; Dapkus, P. D. *Appl. Phys. Lett.* **2003**, *83*, 4107-4109.

(22) Colombelli, R.; Srinivasan, K.; Troccoli, M.; Painter, O.; Gmachl, C. F.; Tennant, D. M.; Sergent, A. M.; Sivco, D. L.; Cho, A. Y.; Capasso, F. *Science* **2003**, *302*, 1374-1377.

(23) Ichikawa, H.; Baba, T. *Appl. Phys. Lett.* **2004**, *84*, 457-459.

(24) Matterson, B. J.; Lupton, J. M.; Safonov, A. F.; Salt, M. G.; Barnes, W. L.; Samuel, I. D. W. *Adv. Mater.* **2001**, *13*, 123-127.

(25) Pan, G. S.; Kesavamoorthy, R.; Asher, S. A. *J. Am. Chem. Soc.* **1998**, *120*, 6525-6530.

(26) Reese, C. E.; Mikhonin, A. V.; Kamenjicki, M.; Tikhonov, A.; Asher, S. A. *J. Am. Chem. Soc.* **2004**, *126*, 1493-1496.

(27) Hu, Z. B.; Lu, X. H.; Gao, J. *Adv. Mater.* **2001**, *13*, 1708-1712.

(28) Foulger, S. H.; Jiang, P.; Lattam, A.; Smith, D. W.; Ballato, J.; Dausch, D. E.; Grego, S.; Stoner, B. R. *Adv. Mater.* **2003**, *15*, 685-689.

(29) Foulger, S. H.; Jiang, P.; Ying, Y. R.; Lattam, A. C.; Smith, D. W.; Ballato, J. *Adv. Mater.* **2001**, *13*, 1898-1901.

(30) Alexeev, V. L.; Sharma, A. C.; Goponenko, A. V.; Das, S.; Lednev, I. K.; Wilcox, C. S.; Finegold, D. N.; Asher, S. A. *Anal. Chem.* **2003**, *75*, 2316-2323.

(31) Asher, S. A.; Alexeev, V. L.; Goponenko, A. V.; Sharma, A. C.; Lednev, I. K.; Wilcox, C. S.; Finegold, D. N. *J. Am. Chem. Soc.* **2003**, *125*, 3322-3329.

(32) Holtz, J. H.; Asher, S. A. *Nature* **1997**, *389*, 829-832.

(33) Sharma, A. C.; Jana, T.; Kesavamoorthy, R.; Shi, L. J.; Virji, M. A.; Finegold, D. N.; Asher, S. A. *J. Am. Chem. Soc.* **2004**, *126*, 2971-2977.

(34) Debord, J. D.; Eustis, S.; Debord, S. B.; Lofye, M. T.; Lyon, L. A. *Adv. Mater.* **2002**, *14*, 658-662.

(35) Debord, J. D.; Lyon, L. A. *J. Phys. Chem. B* **2000**, *104*, 6327-6331.

(36) Debord, S. B.; Lyon, L. A. *J. Phys. Chem. B* **2003**, *107*, 2927-2932.

(37) Jones, C. D.; Lyon, L. A. *J. Am. Chem. Soc.* **2003**, *125*, 460-465.

(38) Jones, C. D.; Serpe, M. J.; Schroeder, L.; Lyon, L. A. *J. Am. Chem. Soc.* **2003**, *125*, 5292-5293.

CHAPTER 9

FUTURE DIRECTIONS

Numerous other experiments can be done in order to understand various aspects of the work presented in this dissertation, some of which will be outlined here.

- Polyelectrolyte/microgel interactions, described in Chapter 3, can be used for localizing bio-relevant molecules, such as DNA and/or proteins, in microgels based on electrostatic interactions. This packaging of biomolecules can be used for various drug delivery applications.
- Spin assisted LbL assembly, described in Chapter 5, can be used for the deposition of oppositely charged microgels to produce a microgel film that is totally composed of microgels. This type of films could be used to assemble films with superior thermoresponsivity, compared to the microgel/PAH films or photonic applications if the films are assembled at the correct conditions that allow for ordering of the microgel layers.
- QCM experiments outlined in Chapter 5 can be used for extremely sensitive biosensing. For example, if microgel films can be assembled on a QCM surfaces, where the microgels making up the film are bio-sensitive, then the films can be used for bio-molecule sensing. This sensing motif can be made extremely sensitive by assembling a film, which acts in a non-Sauerbrey fashion in solution, that rigidifies upon bio-molecule binding and switches to a Sauerbrey film. This switch from non-Sauerbrey to Sauerbrey behavior will enhance the sensitivity of

the technique because the binding in no longer being detected based on mass changes.

- The effect on solution ionic strength on microgel thin film behavior can also be investigated using QCI analysis. The general trend that should be observed is a decrease in film viscosity with increased ionic strength due to the weakening of the ionic interactions in the film resulting in a more water swollen film.
- Chapter 6 described the uptake and release of fluorescein and doxorubicin by microgel thin films in a temperature regulated fashion. This technology can be used for the uptake and release of a host of other biomolecules.
- The microlens experiments described in Chapter 7 have enormous possibilities for applications in sensing. For example, molecule binding to a microlens could result in a change in the focal length of that optical element possibly bringing an image into focus to allow for detection. Another way to do this is to look at the change in laser induced focal length changes upon molecule binding. Molecule binding to the microlens could slow the rate at which the microgel can be swollen/deswollen, which can be detected optically.

APPENDIX A

Chapter 5 Supplementary Information for QCI and SPR measurements of pNIPAm-co-AAc/PAH multilayer thin films

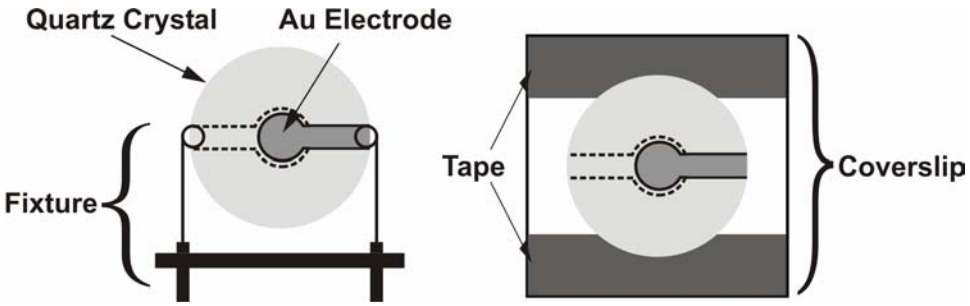

Figure 1-A. Schematic of the QCI measurement fixture used in this chapter (left) and how the QCI crystal is attached to a coverslip for spin coating of thin films (right).

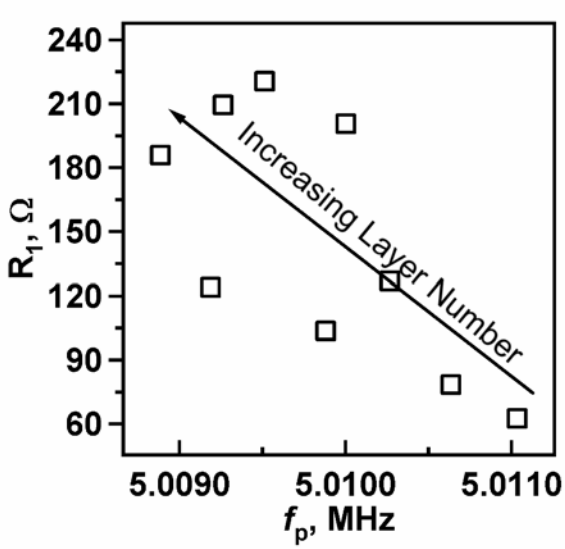

Figure 2-A. Resistance values as a function of resonant frequency as a function of microgel layer number. As can be seen the resistance of the crystal does not significantly increase with layer number indicating low losses and Sauerbrey behavior of the film.

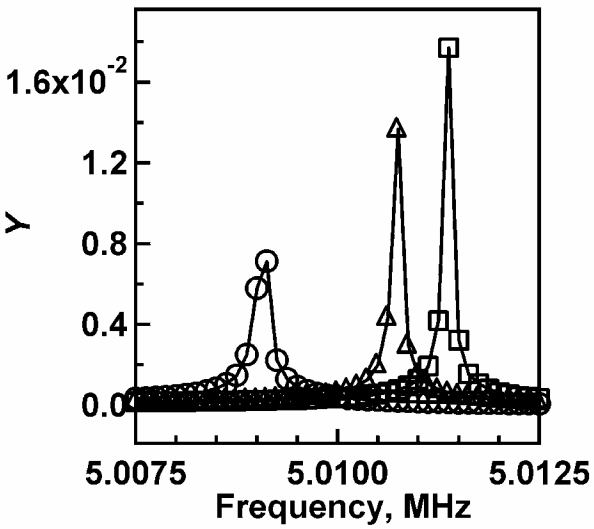

Figure 3-A. Admittance plots for the blank (squares), 10 layer (triangles), and 40 layer (circles) coated QCI crystal from the data in Figure 5-7.

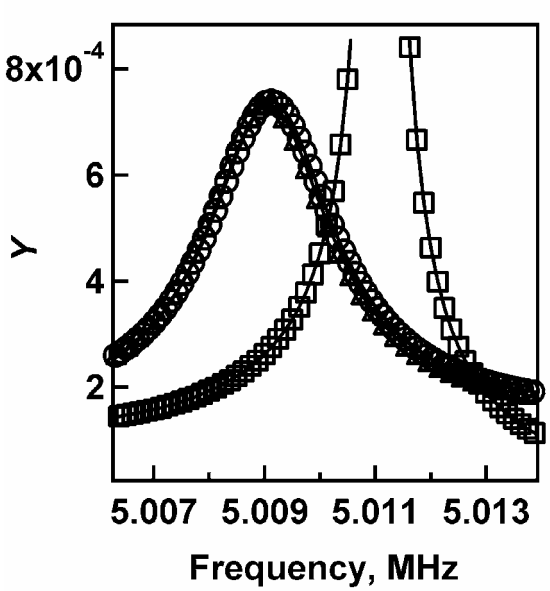

Figure 4-A. Admittance plots for a blank QCI crystal in air (squares), exposed to pH 3.0 (triangles) and pH 6.5 solution (circles) from the data in Figure 5-8.

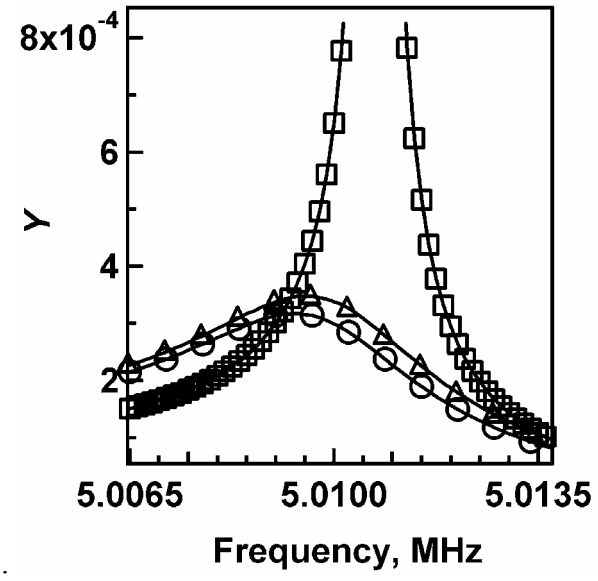

Figure 5-A. Admittance plots for a 10 layer coated QCI crystal in air (squares), exposed to pH 3.0 (triangles) and pH 6.5 solution (circles) from the data in Figure 5-9(a,b).

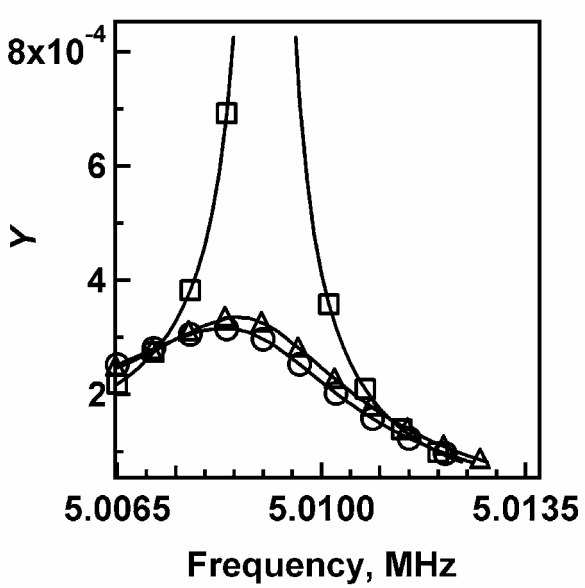

Figure 6-A. Admittance plots for a 40 layer coated QCI crystal in air (squares), exposed to pH 3.0 (triangles) and pH 6.5 solution (circles) from the data in Figure 5-9(c,d).

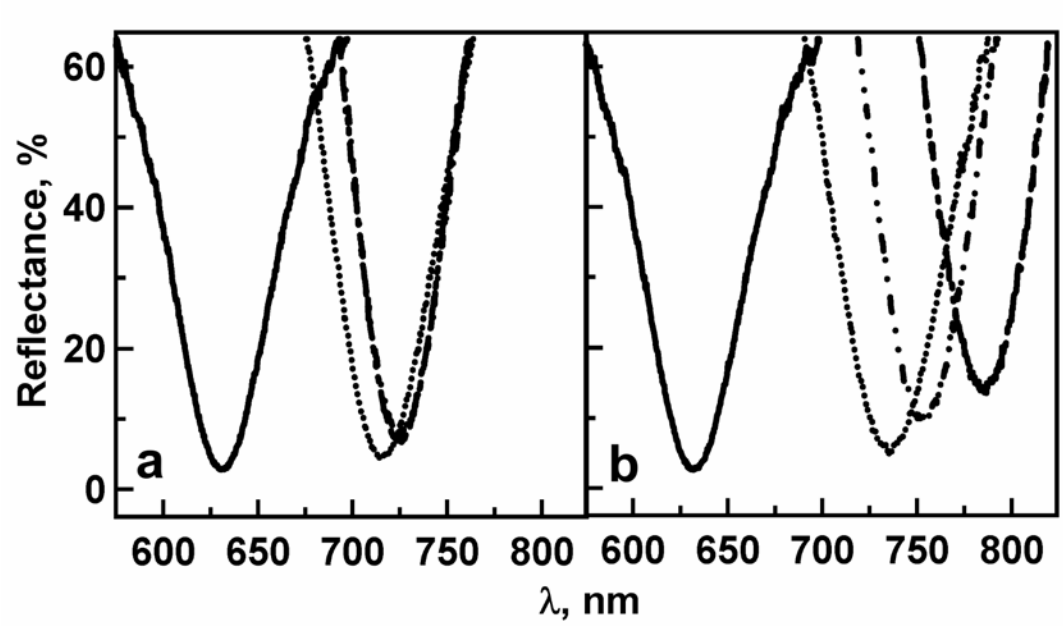

Figure 7-A. Wavelength resolved SPR curves for a blank SPR substrate (solid) and 10 (dots), 20 (dots and dashes), and 30 (dashes) layer microgel thin films at pH 3.0 (a) and 6.5(b). From the figure it can be seen that the SPR was sensitive to the 10 layer film at pH 3.0 but was unable to resolve the curves for the 20 and 30 layer thin films. This behavior was contrary to what was seen for the films exposed to pH 6.5 which showed a layer number dependent λ_{min} and percent reflectance. These are the full curves for the plots in Figure 5-12.